UKAEA-CCFE-PR(22)02

M. R. Hardman, F. I. Parra, C. Chong, T. Adkins, M. S. Anastopoulos-Tzanis, M. Barnes, D. Dickinson, J. F. Parisi, H. Wilson

Extended electron tails in electrostatic microinstabilities and the nonadiabatic response of passing electrons

Extended electron tails in electrostatic microinstabilities and the nonadiabatic response of passing electrons

M. R. Hardman, F. I. Parra, C. Chong, T. Adkins, M. S. Anastopoulos-Tzanis, M. Barnes, D. Dickinson, J. F. Parisi, H. Wilson

This is a preprint of a paper submitted for publication in Plasma Physics and Controlled Fusion

Extended electron tails in electrostatic microinstabilities and the nonadiabatic response of passing electrons

M. R. Hardman[1], F. I. Parra[1], C. Chong[2], T. Adkins[1], M. S. Anastopoulos-Tzanis[3], M. Barnes[1], D. Dickinson[3], J. F. Parisi[4,1], and H. Wilson[3]

[1] Rudolf Peierls Centre for Theoretical Physics, University of Oxford, Oxford, OX1 3PU, UK

[2] Mathematical Institute, University of Oxford, Andrew Wiles Building, Radcliffe Observatory Quarter, Woodstock Road, Oxford, OX2 6GG, UK

[3] York Plasma Institute, Department of Physics, University of York, Heslington, York, YO10 5DD, UK

[4] Culham Centre for Fusion Energy, UKAEA, Abingdon OX14 3DB, UK

E-mail: `michael.hardman@physics.ox.ac.uk`

Abstract.

Ion-gyroradius-scale microinstabilities typically have a frequency comparable to the ion transit frequency. Hence, it is conventionally assumed that passing electrons respond adiabatically in ion-gyroradius-scale modes, due to the small electron-to-ion mass ratio and the large electron transit frequency. However, in gyrokinetic simulations of ion-gyroradius-scale modes, the nonadiabatic response of passing electrons can drive the mode, and generate fluctuations with narrow radial layers, which may have consequences for turbulent transport in a variety of circumstances. In flux tube simulations, in the ballooning representation, these instabilities reveal themselves as modes with extended tails. The small electron-to-ion mass ratio limit of linear gyrokinetics for electrostatic instabilities is presented, including the nonadiabatic response of passing electrons and associated narrow radial layers. This theory reveals the existence of ion-gyroradius-scale modes driven solely by the nonadiabatic passing electron response, and recovers the usual ion-gyroradius-scale modes driven by the response of ions and trapped electrons, where the nonadiabatic response of passing electrons is small. The collisionless and collisional limits of the theory are considered, demonstrating interesting parallels to neoclassical transport theory. The predictions for mass-ratio scaling are tested and verified numerically for a range of collision frequencies. Insights from the small electron-to-ion mass ratio theory may lead to a computationally efficient treatment of extended modes.

Submitted to: *Plasma Phys. Control. Fusion*

1. Introduction

The leading magnetic confinement fusion experiments achieve single particle confinement by exploiting strong magnetic fields that have nested toroidal flux surfaces: the Lorentz force prevents particles crossing the magnetic field in the perpendicular direction, but particles are free to stream along magnetic field lines. Despite this, there are still particle and heat losses from the confined plasma. Neoclassical transport is driven by interparticle Coulomb collisions in toroidal magnetic geometry, and turbulent transport is driven by the free energy available in the equilibrium temperature and density gradients.

Turbulence forms through the nonlinear saturation of microinstabilities. The most important microinstabilities for transport have frequencies ω comparable to the transit frequency of the constituent particle species, and perpendicular wavenumbers $k_\perp$ comparable to the inverse thermal gyroradius of the particles, i.e., $\omega \sim v_{\rm th,s}/a \sim \rho_{*s}\Omega_s \ll \Omega_s$, and $k_\perp \rho_{\rm th,s} \sim 1$, where $v_{\rm th,s} = \sqrt{2T_s/m_s}$ is the thermal speed of the component species s, a is a typical equilibrium length scale, $\Omega_s = Z_s eB/m_s c$ is the cyclotron frequency of the component species s, and $\rho_{*s} = \rho_{\rm th,s}/a \ll 1$, with $\rho_{\rm th,s} = v_{\rm th,s}/\Omega_s$ the thermal gyroradius of the species s. In the above definitions T_s is the species temperature, m_s is the species mass, Z_s is the species charge number, e is the proton charge, B is the magnetic field strength, and c is the speed of light. These microinstabilities are extended along magnetic field lines, with parallel wave numbers such that $k_\| qR \sim 1$, where qR is the "connection length", $q \sim 1$ is the safety factor and $R \sim a$ is the major radius. A diffusive random walk estimate for the heat flux $Q_{\rm s}$ driven by instabilities at the scale $\rho_{\rm th,s}$ gives $Q_{\rm s} \sim Q_{\rm gb,s} = \rho_{*s}^2 n_s T_s v_{\rm th,s}$, with n_s the equilibrium plasma density of species s. To obtain this estimate, we use that the macroscopic profiles have a scale of order a, and that turbulent eddies transport heat by a step length $\rho_{\rm th,s}$ in a timescale $v_{\rm th,s}/a$.

A plasma has multiple particle species: the simplest plasma consists of ions, with charge $Z_{\rm i}e$ and mass $m_{\rm i}$, and electrons, with charge $-e$ and mass $m_{\rm e}$. In a fusion plasma with deuterium ions, the separation between the ion and electron masses has significant consequences for the nature of the turbulence and the underlying instabilities. Since $\sqrt{m_{\rm i}/m_{\rm e}} \approx 60$, we have that $\rho_{\rm th,i} \gg \rho_{\rm th,e}$ and $v_{\rm th,i} \ll v_{\rm th,e}$, i.e., instabilities can be driven over a wide range of space and time scales. Historically, research has largely focused on transport and instabilities driven at the larger scale of the ion gyroradius. This is for the simple reason that the heat flux estimate $Q_{\rm gb,i}$ for $\rho_{\rm th,i}$-scale turbulence dominates the heat flux estimate $Q_{\rm gb,e}$ for $\rho_{\rm th,e}$-scale turbulence by $(m_{\rm i}/m_{\rm e})^{1/2} \gg 1$. However, it is important not to discount the $\rho_{\rm th,e}$ scales for several reasons. It is known that $\rho_{\rm th,e}$-scale turbulence can drive experimentally relevant heat fluxes that exceed the $Q_{\rm gb,e}$ estimate by a large order-unity factor [1–4]. Recently, expensive direct numerical simulations (DNS) with realistic electron-to-hydrogen-ion-mass ratio [5, 6] and realistic electron-to-deuterium-ion-mass ratio [6–11] have demonstrated the existence and significance of cross-scale interactions between turbulence at the scales of $\rho_{\rm th,i}$ and $\rho_{\rm th,e}$. Finally, as we will demonstrate in this paper, even familiar long-wavelength modes with binormal wave numbers $k_y\rho_{\rm th,i} \sim 1$ may have narrow radial structures near mode-rational surfaces that satisfy $k_r\rho_{\rm th,e} \sim 1$, with k_r the radial wave number. These structures result from the dynamics of passing electrons [12, 13], and may be important for understanding cross-scale interactions in multiscale DNS, cf. [6]. We will see that there are novel $k_y\rho_{\rm th,i} \sim 1$ modes driven by the electron response to the electron temperature gradient (ETG) in the $k_r\rho_{\rm th,e} \sim 1$ narrow layer, and we will see that even the familiar ion temperature gradient (ITG) mode can exhibit $k_r\rho_{\rm th,e} \sim 1$ features.

Anisotropy between the radial wave number k_r and the binormal wave number k_y arises naturally in linear modes in magnetic geometry because of the presence of magnetic shear $\hat{s}$. In the presence of magnetic shear, linear modes are conveniently described in terms of "ballooning" modes that follow the magnetic field line many times around the torus [14]. Ballooning modes have wave fronts that rotate with position along the magnetic field line. As we shall describe with more precision later, in a ballooning mode the radial wave number k_r satisfies $k_r \propto -k_y\hat{s}\theta$ for large θ, where θ is the extended poloidal angle that is used to describe the position along the field line as it winds around the torus. Therefore, it is possible for $k_y\rho_{\rm th,i} \sim 1$ modes to have extended "ballooning tails" at $\theta \gg 1$ that correspond to $k_r\rho_{\rm th,i} \gg 1$ components. In the real-space picture, modes with extended ballooning tails are modes with significant amplitude in a layer around mode-rational flux surfaces – flux surfaces where the field line winds onto itself after an integer number of toroidal and poloidal turns. With this in mind, we can understand the origin of electron-driven ballooning tails with a simple physical argument. On irrational flux surfaces, where a single field line covers the flux surface, rapidly moving passing electrons can sample the entire flux surface and respond adiabatically. However, on mode-rational flux surfaces, passing electrons can only sample a subset of the flux surface and hence have a nonadiabatic response.

Linear modes with extended ballooning tails have been observed in simulations with a variety of equilibrium conditions, for example, in simulations of electrostatic modes in core tokamak conditions [12, 13] and in the pedestal [15], as well as in electromagnetic simulations of linear micro-tearing modes in spherical and conventional tokamaks [16–18]. Although simulations of linear modes are inexpensive compared to nonlinear simulations of turbulence, simulations of modes with extended ballooning tails can be remarkably costly. The results presented in this paper are intended as a step towards efficient reduced models of this class of mode.

In this paper we will obtain an asymptotic theory, valid in the limit of $(m_{\rm e}/m_{\rm i})^{1/2} \rightarrow 0$, for electrostatic modes that exist at the long wavelengths of the ion gyroradius scale, i.e., $k_y\rho_{\rm th,i} \sim 1$. Reduced models of these modes must provide a reduced treatment of the electron response. In the simplest case, for example, the classical ITG mode calculation [19, 20], the electron response is taken to be adiabatic. More advanced calculations retain the bounce-averaged response due to trapped electrons, see, e.g., [21, 22]. The nonadiabatic response of passing electrons is traditionally neglected, despite evidence from DNS that indicates that the nonadiabatic passing electron response can alter transport in linear modes [12, 13] and fully nonlinear turbulence [6, 13]. In this paper, we will show that, in the $(m_{\rm e}/m_{\rm i})^{1/2} \to 0$ limit, there are in fact two classes of modes existing at $k_y\rho_{\rm th,i} \sim 1$: first, the traditional ITG or ion-response-driven modes; and second, ETG modes that are driven by the electron response in the large θ tail of the ballooning mode. We find the large θ equations that govern the electron response in the tail of the ballooning mode, and we show that the orderings used to derive these equations are satisfied by the numerical solutions of both the ion-response-driven and electron-response-driven modes simulated using the gyrokinetic code `GS2` [23].

The nature of the large θ equations, and the nature of the corresponding electron-driven ballooning tail, depends on the electron self-collision frequency $\nu_{\rm ee}$ and the electron-ion collision frequency $\nu_{\rm ei} \sim \nu_{\rm ee}$. In the "collisionless" limit, where $a\nu_{\rm ee}/v_{\rm th,e} \sim (m_{\rm e}/m_{\rm i})^{1/2} \ll 1$, the extent of the mode is set by a balance of free-streaming, finite orbit width and finite Larmor radius physics. We find that the electron-driven tail extends to $\theta \sim (m_{\rm i}/m_{\rm e})^{1/2}$. In the "collisional" limit, where $a\nu_{\rm ee}/v_{\rm th,e} \sim 1$, the extent of the mode is set by a balance between perpendicular collisional diffusion and parallel collisional diffusion that is set up by gradients in the fluctuations along the magnetic field line. The diffusion arises from both classical and neoclassical collisional mechanisms. As a result of this balance, we find that the electron-driven tail extends to $\theta \sim (m_{\rm i}/m_{\rm e})^{1/4}$, corresponding to $k_r\rho_{\rm th,e} \sim (m_{\rm e}/m_{\rm i})^{1/4}$. We treat the collisionless and collisional asymptotic theories separately, before turning to numerical simulations that support the analytical results.

The remainder of this paper is structured as follows. In section 2, we briefly review the electrostatic gyrokinetic model that is the starting point for this work. In section 3, we identify a convenient form of the gyrokinetic equation that we use to describe electron dynamics. We obtain the asymptotic theory of collisionless modes in section 4, and we obtain the asymptotic theory of collisional modes in section 5. We compare the results of sections 4 and 5 to numerical simulations in section 6. Finally, in section 7, we discuss the implications of these results and possible extensions of the theory. Included in this paper are appendices containing results pertaining to the collisional limit. In Appendix A, we obtain the classical perpendicular flux contributions to the electron mode equations. In Appendix B, we solve the Spitzer problem necessary to obtain the neoclassical parallel and perpendicular flux contributions to the electron mode equations. In Appendix C, we obtain the parallel and perpendicular fluxes for the electron mode equations in the highly collisional (Pfirsh-Schlüter) limit. In Appendix D, we obtain the parallel and perpendicular fluxes for the electron mode equations in the banana regime of collisionality in a small inverse aspect ratio device. Finally, in Appendix E, we give a detailed analysis of the ion nonadiabatic response at large θ.

2. Electrostatic gyrokinetic equations

In this section, we briefly review the linear, electrostatic, δf gyrokinetic model [24] that is the starting point for the analysis in this paper. In gyrokinetic theory, the microinstability mode frequency ω is taken to be much smaller than the cyclotron frequency Ω_s at which particles gyrate around the magnetic field direction $\boldsymbol{b} = \boldsymbol{B}/B$, where $\boldsymbol{B}$ is the magnetic field. The mode frequency ω is taken to be of order the transit frequency $v_{\mathrm{th,s}}/a$. The spatial scale of the fluctuations perpendicular to the magnetic field line is of order the thermal gyroradius $\rho_{\mathrm{th,s}} = v_{\mathrm{th,s}}/\Omega_s$, and the fundamental gyrokinetic expansion parameter is $\rho_{*s} = \rho_{\mathrm{th,s}}/a$. In δf gyrokinetics, the fluctuating distribution function δf_s for each species s is a sum of the nonadiabatic response h_s, and the adiabatic response $-Z_s e\phi F_{0s}/T_s$, i.e.,

$$\delta f_s(\boldsymbol{r}, \boldsymbol{v}, t) = h_s(\boldsymbol{R}, \varepsilon, \lambda, t) - \frac{Z_s e\phi(\boldsymbol{r}, t)}{T_s} F_{0s}, \qquad (1)$$

where ϕ is the fluctuating electrostatic potential, F_{0s} is the equilibrium Maxwellian distribution, $\boldsymbol{r}$ is the particle position, $\boldsymbol{v}$ is the particle velocity, and we have indicated that h_s is a function of guiding centre position $\boldsymbol{R} = \boldsymbol{r} - \boldsymbol{\rho}_s$ (with $\boldsymbol{\rho}_s = \boldsymbol{b} \times \boldsymbol{v}/\Omega_s$), energy $\varepsilon = m_s v^2/2$ (with $v = |\boldsymbol{v}|$), and pitch angle $\lambda = v_\perp^2/v^2 B$ (with $v_\perp = |\boldsymbol{v} - \boldsymbol{b}\boldsymbol{b}\cdot\boldsymbol{v}|$), whereas ϕ is a function of $\boldsymbol{r}$ but not of $\boldsymbol{v}$. In this paper we consider linear theory, and so we make the eikonal ansatz

$$h_s(\boldsymbol{R}, t) = \sum_{\boldsymbol{k}_\perp} h_{s,\boldsymbol{k}_\perp} \exp\left[\mathrm{i}(\boldsymbol{k}_\perp \cdot \boldsymbol{R} - \omega t)\right],$$

$$\phi(\boldsymbol{r}, t) = \sum_{\boldsymbol{k}_\perp} \phi_{\boldsymbol{k}_\perp} \exp\left[\mathrm{i}(\boldsymbol{k}_\perp \cdot \boldsymbol{r} - \omega t)\right], \qquad (2)$$

where $\boldsymbol{k}_\perp$ is the perpendicular-to-the-field wave vector. Henceforth, we drop the $\boldsymbol{k}_\perp$ subscripts on the Fourier coefficients.

2.1. The gyrokinetic equation and quasineutrality

The linear, electrostatic gyrokinetic equation is

$$v_\parallel \boldsymbol{b} \cdot \nabla\theta \frac{\partial h_s}{\partial \theta} + \mathrm{i}(\boldsymbol{k}_\perp \cdot \boldsymbol{v}_{\mathrm{M},s} - \omega) h_s - C_s^{\mathrm{GK}}[h_s] = \mathrm{i}\left(\omega_{*,s} - \omega\right) J_{0s} F_{0s} \frac{Z_s e\phi}{T_s}, \qquad (3)$$

where $v_\parallel = \boldsymbol{b} \cdot \boldsymbol{v}$, θ is the poloidal angle coordinate that measures distance along the magnetic field line,

$$\boldsymbol{v}_{\mathrm{M},s} = \frac{v_\parallel^2}{\Omega_s} \boldsymbol{b} \times \boldsymbol{b} \cdot \nabla \boldsymbol{b} + \frac{v_\perp^2}{2\Omega_s} \boldsymbol{b} \times \frac{\nabla B}{B} \qquad (4)$$

is the magnetic drift, and the finite Larmor radius effects are modelled by the 0^{th} Bessel function of the first kind $J_{0s} = J_0(b_s)$, where $b_s = k_\perp v_\perp/\Omega_s$, and $k_\perp = |\boldsymbol{k}_\perp|$. Note that $\Omega_{\mathrm{i}} = Z_{\mathrm{i}} eB/m_{\mathrm{i}} c > 0$, whereas $\Omega_{\mathrm{e}} = -eB/m_{\mathrm{e}} c < 0$. The frequency $\omega_{*,s}$ contains the equilibrium drives of instability:

$$\omega_{*,s} = \omega_{*,s}^n \left(1 + \eta_s \left(\frac{\varepsilon}{T_s} - \frac{3}{2}\right)\right), \qquad (5)$$

with

$$\omega_{*,s}^n = -\frac{c k_\alpha T_s}{Z_s e n_s} \frac{d n_s}{d\psi}, \qquad (6)$$

and n_s the equilibrium number density of species s, ψ the poloidal magnetic flux (defined implicitly in section 2.2), and

$$\eta_s = \frac{d \ln T_s}{d \ln n_s}. \tag{7}$$

Finally, the collision operator $C_s^{\rm GK}[\cdot]$ is shorthand for the linearised gyrokinetic collision operator of the species s.

For ions, the linearised gyrokinetic collision operator is defined by

$$C_{\rm i}^{\rm GK}\left[h_{\rm i}\right] = \langle \exp\left[{\rm i}\boldsymbol{k}_\perp \cdot \boldsymbol{\rho}_i\right] C_{\rm ii}\left[\exp\left[-{\rm i}\boldsymbol{k}_\perp \cdot \boldsymbol{\rho}_i\right] h_{\rm i}\right]\rangle_{\boldsymbol{R}}^{\gamma}, \tag{8}$$

with $C_{\rm ii}[\cdot]$ the linearised self-collision operator of the ion species, and $\langle\cdot\rangle_{\boldsymbol{R}}^{\gamma}$ the gyrophase average at fixed $\boldsymbol{R}$, ε, and λ. The self-collision operator of the species s, $C_{ss}[\cdot]$, is defined by

$$C_{ss}\left[f\right] = \frac{2\pi Z_s^4 e^4 \ln\Lambda}{m_s^2}\frac{\partial}{\partial \boldsymbol{v}} \cdot \int F_{0s}F_{0s}^{\prime}\boldsymbol{U}(\boldsymbol{v}-\boldsymbol{v}^{\prime}) \cdot \left(\frac{\partial}{\partial \boldsymbol{v}}\left(\frac{f}{F_{0s}}\right) - \frac{\partial}{\partial \boldsymbol{v}^{\prime}}\left(\frac{f^{\prime}}{F_{0s}^{\prime}}\right)\right) d^3\boldsymbol{v}^{\prime}, \tag{9}$$

where f is a distribution function, and we have used the shorthand notation $f = f(\boldsymbol{v})$, $f^{\prime} = f(\boldsymbol{v}^{\prime})$, $F_{0s} = F_{0s}(\boldsymbol{v})$, $F_{0s}^{\prime} = F_{0s}(\boldsymbol{v}^{\prime})$, and

$$\boldsymbol{U}(\boldsymbol{v}-\boldsymbol{v}^{\prime}) = \frac{\boldsymbol{I}|\boldsymbol{v}-\boldsymbol{v}^{\prime}|^2 - (\boldsymbol{v}-\boldsymbol{v}^{\prime})(\boldsymbol{v}-\boldsymbol{v}^{\prime})}{|\boldsymbol{v}-\boldsymbol{v}^{\prime}|^3}, \tag{10}$$

with $\boldsymbol{I}$ is the identity matrix. We note that the Coloumb logarithm $\ln\Lambda \approx 17$ [25]. After Braginskii [26], we define the ion self-collision frequency $\nu_{\rm ii}$ by

$$\nu_{\rm ii} = \frac{4\sqrt{\pi}}{3}\frac{Z_{\rm i}^4 n_{\rm i} e^4 \ln\Lambda}{m_{\rm i}^{1/2} T_{\rm i}^{3/2}}, \tag{11}$$

and we define the electron self-collision frequency $\nu_{\rm ee}$ by

$$\nu_{\rm ee} = \frac{4\sqrt{2\pi}}{3}\frac{n_{\rm e} e^4 \ln\Lambda}{m_{\rm e}^{1/2} T_{\rm e}^{3/2}}, \tag{12}$$

noting the factor of $\sqrt{2}$ difference in the definitions of $\nu_{\rm ee}$ and $\nu_{\rm ii}$.

For electrons, the linearised gyrokinetic collision operator is defined by

$$C_{\rm e}^{\rm GK}\left[h_{\rm e}\right] = \langle \exp\left[{\rm i}\boldsymbol{k}_\perp \cdot \boldsymbol{\rho}_e\right] C_{\rm ee}\left[\exp\left[-{\rm i}\boldsymbol{k}_\perp \cdot \boldsymbol{\rho}_e\right] h_{\rm e}\right]\rangle_{\boldsymbol{R}}^{\gamma}$$

$$+ \left\langle \exp\left[{\rm i}\boldsymbol{k}_\perp \cdot \boldsymbol{\rho}_e\right] \mathcal{L}\left[\exp\left[-{\rm i}\boldsymbol{k}_\perp \cdot \boldsymbol{\rho}_e\right] h_{\rm e} - \frac{m_{\rm e}\boldsymbol{v}\cdot\delta\boldsymbol{u}_{\rm i}}{T_{\rm e}} F_{0e}\right]\right\rangle_{\boldsymbol{R}}^{\gamma}, \tag{13}$$

where $C_{\rm ee}[\cdot]$ is the linearised self-collision operator of the electron species, defined by equation (9), and

$$\mathcal{L}\left[f\right] = \frac{3\sqrt{\pi}}{8}\nu_{\rm ei} v_{\rm th,e}^3 \frac{\partial}{\partial \boldsymbol{v}} \cdot \left(\frac{v^2\boldsymbol{I} - \boldsymbol{v}\boldsymbol{v}}{v^3} \cdot \frac{\partial f}{\partial \boldsymbol{v}}\right), \tag{14}$$

is the Lorentz collision operator resulting from electron-ion collisions, with the electron-ion collision frequency $\nu_{\rm ei}$ defined following Braginskii [26], i.e.,

$$\nu_{\rm ei} = \frac{4\sqrt{2\pi}}{3}\frac{Z_{\rm i}^2 n_{\rm i} e^4 \ln\Lambda}{m_{\rm e}^{1/2} T_{\rm e}^{3/2}}. \tag{15}$$

In equation (13),

$$\delta \boldsymbol{u}_{\rm i} = \frac{1}{n_{\rm i}} \int \left(J_{0{\rm i}} v_\parallel \boldsymbol{b} + {\rm i} J_{1{\rm i}} \frac{v_\perp}{k_\perp} \boldsymbol{k}_\perp \times \boldsymbol{b} \right) \, h_{\rm i} \, d^3\boldsymbol{v}, \tag{16}$$

where $J_{1s} = J_1(b_s)$, the $1^{\rm st}$ Bessel function of the first kind.

For a simple two-species plasma of ions and electrons, quasineutrality implies that the equilibrium densities satisfy $Z_{\rm i} n_{\rm i} = n_{\rm e}$. In the electrostatic limit, the system of gyrokinetic equations for the fluctuations is closed by the quasineutrality relation. The quasineutrality relation has the form

$$\left(\frac{Z_{\rm i} T_{\rm e}}{T_{\rm i}} + 1 \right) \frac{e\phi}{T_{\rm e}} = \frac{\delta n_{\rm i}}{n_{\rm i}} - \frac{\delta n_{\rm e}}{n_{\rm e}}, \tag{17}$$

where the fluctuating *nonadiabatic* densities δn_s are defined by

$$\delta n_s = \int J_{0s} h_s \, d^3\boldsymbol{v}. \tag{18}$$

2.2. Magnetic coordinates and boundary conditions

To describe the plane perpendicular to the magnetic field line, we use the dimensionless binormal field-line-label coordinate α, and the flux label ψ, defined such that the magnetic field may be written in the Clebsch form

$$\boldsymbol{B} = \nabla\alpha \times \nabla\psi. \tag{19}$$

We restrict our attention to axisymmetric magnetic fields of the form

$$\boldsymbol{B} = I\nabla\zeta + \nabla\zeta \times \nabla\psi, \tag{20}$$

where ζ is the toroidal angle, and $I(\psi)$ is the toroidal current function. An explicit formula for α, in terms of ψ, ζ, and the poloidal angle θ, may be obtained by equating expressions (19) and (20):

$$\alpha(\psi, \zeta, \theta) = \zeta - q(\psi)\theta - \nu(\psi, \theta), \tag{21}$$

with the safety factor

$$q(\psi) = \frac{1}{2\pi} \int_0^{2\pi} \frac{\boldsymbol{B} \cdot \nabla\zeta}{\boldsymbol{B} \cdot \nabla\theta} d\theta', \tag{22}$$

and

$$\nu(\psi, \theta) = \int_0^{\theta} \frac{\boldsymbol{B} \cdot \nabla\zeta}{\boldsymbol{B} \cdot \nabla\theta} d\theta' - q\theta. \tag{23}$$

Note that $\nu(\psi, 2\pi) = \nu(\psi, 0) = 0$. Using the (ψ, α) coordinates, we write the perpendicular wave vector as

$$\boldsymbol{k}_\perp = k_\psi \nabla\psi + k_\alpha \nabla\alpha, \tag{24}$$

with the field-aligned radial and binormal wave numbers k_ψ and k_α, respectively.

In the study of linear modes, it is convenient to consider the coordinate θ as an extended ballooning angle, and to replace k_ψ with $\theta_0 = k_\psi / q' k_\alpha$, where $q' = dq/d\psi$. In this formulation, $h_{\theta_0,k_\alpha} = h_{\theta_0,k_\alpha}(\theta)$, with $-\infty < \theta < \infty$ and the boundary conditions

$$h_{\theta_0,k_\alpha}(\theta) = 0 \text{ at } \theta \to -\infty, \text{ for } v_\parallel > 0, \text{ and}$$

$$h_{\theta_0,k_\alpha}(\theta) = 0 \text{ at } \theta \to \infty, \text{ for } v_\| < 0. \tag{25}$$

Much of the discussion in the following sections of this paper is focused on the behaviour of the solution at large θ. The large θ part of the mode corresponds to a narrow radial layer in the real-space representation. To see this, consider the (contravariant) radial wave number

$$k_r = \boldsymbol{k}_\perp \cdot \nabla r = (\theta_0 - \theta) k_\alpha \frac{dq}{dr} |\nabla r|^2 - k_\alpha (q \nabla\theta \cdot \nabla r + \nabla\nu \cdot \nabla r), \tag{26}$$

where $r = r(\psi)$ is a minor radial coordinate that is a function of ψ only, and has dimensions of length. For large $|\theta_0 - \theta|$, we find that $k_r \simeq (\theta_0 - \theta) k_\alpha (dq/dr) |\nabla r|^2$, i.e., we may obtain narrow radial structures in a ballooning mode by either imposing a large θ_0 $(= k_\psi / q' k_\alpha)$, or by following the field line, as a result of magnetic shear.

It will be interesting to consider the behaviour of the magnetic drift. The term due to the magnetic drift, $\mathrm{i}\boldsymbol{k}_\perp \cdot \boldsymbol{v}_{\mathrm{M},s}$, may be written in the following convenient form

$$\mathrm{i}\boldsymbol{k}_\perp \cdot \boldsymbol{v}_{\mathrm{M},s} = \mathrm{i} k_\alpha \boldsymbol{v}_{\mathrm{M},s} \cdot (\nabla\alpha + \theta \nabla q) + \mathrm{i} k_\alpha \frac{dq}{dr} (\theta_0 - \theta) \boldsymbol{v}_{\mathrm{M},s} \cdot \nabla r. \tag{27}$$

We note that the quantity $\nabla\alpha + \theta\nabla q = \nabla\zeta - q\nabla\theta - \nabla\nu$ contains no secular variation in θ. Hence, for large $|\theta_0 - \theta|$ the magnetic drift is dominated by the radial component: $\mathrm{i}\boldsymbol{k}_\perp \cdot \boldsymbol{v}_{\mathrm{M},s} \simeq \mathrm{i} k_r \boldsymbol{v}_{\mathrm{M},s} \cdot \nabla r / |\nabla r|^2$ for $|\theta_0 - \theta| \gg 1$. Thus, the leading behaviour of a ballooning mode at large θ should be expected to involve the radial magnetic drift. We will often make use of the identity for the radial magnetic drift in an axisymmetric magnetic field,

$$\boldsymbol{v}_{\mathrm{M},s} \cdot \nabla\psi = v_\| \boldsymbol{b} \cdot \nabla\theta \frac{\partial}{\partial\theta} \left(\frac{I v_\|}{\Omega_s} \right). \tag{28}$$

Finally, we complete this discussion of coordinates by defining a field-aligned radial wave number and binormal wave number with dimensions of length, k_x and k_y, respectively. First, we define local radial and binormal coordinates with units of length, $x = (\psi - \psi_0)(d\psi/dx)^{-1}$ and $y = (\alpha - \alpha_0)(d\alpha/dy)^{-1}$, respectively, where (ψ_0, α_0) are the coordinates of the field line of interest. Then, the field-aligned radial wavenumber $k_x = k_\psi (d\psi/dx)$ and the binormal wave number $k_y = k_\alpha (d\alpha/dy)$. We take the proportionality constants to be $d\psi/dx = rI/qR_0$ and $d\alpha/dy = (I/R_0) dr/d\psi$. The functions $I(\psi)$, $r(\psi)$, and $q(\psi)$ appearing in the proportionality constants should be evaluated on the local flux surface of interest, and R_0 is the major radius at the magnetic axis. Using these normalisations, we find that the true radial wave number $k_r \simeq (\theta_0 - \theta) k_y \hat{s} \hat{\kappa} |\nabla r|^2$ for $|\theta_0 - \theta| \gg 1$, with the magnetic shear defined by $\hat{s} = (r/q) dq/dr$ and the geometrical factor $\hat{\kappa} = (qR_0/Ir) d\psi/dr$.

3. A convenient form of the gyrokinetic equation

It is possible to use the identity for the radial magnetic drift in equation (28) to rewrite the gyrokinetic equation in a way that will simplify the asymptotic analysis of the electron response. Collecting terms due to parallel streaming, and radial drifts, we find that we can write

$$v_\parallel \boldsymbol{b}\cdot\nabla\theta \frac{\partial h_s}{\partial \theta} + \mathrm{i}k_\alpha q'(\theta_0-\theta)v_\parallel \boldsymbol{b}\cdot\nabla\theta\frac{\partial}{\partial\theta}\left(\frac{Iv_\parallel}{\Omega_s}\right)h_s$$

$$= \exp\left[-\mathrm{i}\lambda_s(\theta_0-\theta)\right]v_\parallel \boldsymbol{b}\cdot\nabla\theta\frac{\partial}{\partial\theta}\left(\exp\left[\mathrm{i}\lambda_s(\theta_0-\theta)\right]h_s\right) + \mathrm{i}\boldsymbol{b}\cdot\nabla\theta\frac{k_\alpha q' I v_\parallel^2}{\Omega_s}h_s, \quad (29)$$

with

$$\lambda_s = \frac{k_\alpha q' I v_\parallel}{\Omega_s}. \quad (30)$$

Note that λ_s should not be confused with the pitch angle coordinate λ. We define the new function H_s by

$$H_s = \exp\left[\mathrm{i}\lambda_s(\theta_0-\theta)\right]h_s, \quad (31)$$

and hence we can rewrite the gyrokinetic equation, equation, (3), as

$$v_\parallel \boldsymbol{b}\cdot\nabla\theta\frac{\partial H_s}{\partial\theta} + \mathrm{i}(\omega_{\mathrm{M},s}-\omega)H_s - \widehat{C}_s[H_s] = \mathrm{i}\left(\omega_{*,s}-\omega\right)\exp\left[\mathrm{i}\lambda_s(\theta_0-\theta)\right]J_{0s}F_{0s}\frac{Z_s e\phi}{T_s}, \quad (32)$$

where

$$\omega_{\mathrm{M},s} = k_\alpha\left(\boldsymbol{v}_{\mathrm{M},s}\cdot(\nabla\alpha+\theta\nabla q) + \boldsymbol{b}\cdot\nabla\theta\frac{q' I v_\parallel^2}{\Omega_s}\right), \quad (33)$$

and

$$\widehat{C}_s[H_s] = \exp\left[\mathrm{i}\lambda_s(\theta_0-\theta)\right]C_s^{\mathrm{GK}}\left[\exp\left[-\mathrm{i}\lambda_s(\theta_0-\theta)\right]H_s\right]. \quad (34)$$

It is also useful to consider the form of the nonadiabatic density appearing in the quasineutrality relation, equation (17). In terms of H_s, we can write the nonadiabatic, fluctuating density δn_s as

$$\delta n_s = \int \exp\left[-\mathrm{i}\lambda_s(\theta_0-\theta)\right]J_{0s}H_s\, d^3\boldsymbol{v}. \quad (35)$$

When the gyrokinetic equation is written in terms of H_s, the oscillation in the distribution function due to the radial magnetic drift appears explicitly as the phase $\exp\left[\mathrm{i}\lambda_s(\theta_0-\theta)\right]$ – this phase may be thought of in analogy to the phase $\exp\left[\mathrm{i}\boldsymbol{k}_\perp\cdot\boldsymbol{\rho}_s\right]$ arising from the finite Larmor radius in gyrokinetic theory. In fact, the appearance of $\exp\left[\mathrm{i}\lambda_s(\theta_0-\theta)\right]$ is due to the finite particle drift orbit width. This may be noted by writing $\lambda_s(\theta_0-\theta) = k_\alpha q'(\theta_0-\theta)\Delta\psi$, recalling that $\Delta\psi = Iv_\parallel/\Omega_s$ is the excursion in flux label ψ made by trapped particles in a banana orbit [27], and finally, noting that, in the limit of large $|\theta_0-\theta|$, $\lambda_s(\theta_0-\theta)\simeq k_r(dr/d\psi)\Delta\psi/|\nabla r|^2$.

4. Long-wavelength collisionless electrostatic modes in the $(m_\mathrm{e}/m_\mathrm{i})^{1/2}\to 0$ limit

In this section we derive reduced model equations for long-wavelength, collisionless, electrostatic modes in the $(m_\mathrm{e}/m_\mathrm{i})^{1/2}\to 0$ limit. We will focus on modes that exist at the long wavelengths of the ion gyroradius scale, i.e., $k_y\rho_{\rm th,i} \sim 1$ and $\theta_0 \sim 1$. For the modes described in this section, we take the "collisionless" ordering for the electron collision frequency. Electron-ion collisions occur at a rate $\nu_{\rm ei}$, and electron-electron self collisions occur at a rate $\nu_{\rm ee}$. The collisionless ordering is

$$\frac{qR_0\nu_{\rm ee}}{v_{\rm th,e}} \sim \frac{qR_0\nu_{\rm ei}}{v_{\rm th,e}} \sim \left(\frac{m_{\rm e}}{m_{\rm i}}\right)^{1/2} \ll 1. \tag{36}$$

In this ordering, the electron collision operator competes with the source term due to the electrostatic potential and with the precessional magnetic drift. For consistency with the electron species, we take the ion self-collision frequency $\nu_{\rm ii} \sim (m_{\rm e}/m_{\rm i})^{1/2}\, v_{\rm th,i}/qR_0 \ll v_{\rm th,i}/qR_0 \sim \omega$. We find that the extent of the ballooning mode is controlled by the collisionless terms in the electron gyrokinetic equation, with the result that the mode extends to a ballooning angle $\theta \sim (m_{\rm i}/m_{\rm e})^{1/2} \gg 1$. In the following section, we begin the derivation of the reduced model equations by examining the $\theta \sim 1$ region of the ballooning mode. This discussion reveals the existence of passing-electron-response-driven modes, in addition to the usual ion-response-driven and trapped-electron-response-driven modes, and motivates an examination of the $\theta \sim (m_{\rm i}/m_{\rm e})^{1/2}$ region of the collisionless ballooning mode in section 4.2. To aid comprehension, we summarise the results of this section for trapped-electron-response-driven and ion-response-driven modes in section 4.3, and for passing-electron-response-driven modes in section 4.4. Finally, in section 4.5, we comment on the relationship between the derivation of gyrokinetics and the derivation of the reduced model equations for the electron response: although these theories have fundamental differences, they have a similar structure, relying on the finite Lamor radius and the finite (magnetic drift) orbit width of particles, respectively.

4.1. Outer solution – $k_r\rho_{\rm th,i} \sim 1$

We define the outer region of the mode to be the region where $\theta \sim 1$, equivalently, the region where $k_r\rho_{\rm th,i} \sim 1$. In real space, the outer region is the large-scale region far from the rational flux surface.

In the collisionless ordering, it is natural to expand the electric potential and distribution functions in $(m_{\rm e}/m_{\rm i})^{1/2}$:

$$\phi = \phi^{(0)} + \phi^{(1)} + {\rm O}\left(\left(\frac{m_{\rm e}}{m_{\rm i}}\right)\phi\right), \tag{37}$$

with $\phi^{(n)} \sim (m_{\rm e}/m_{\rm i})^{n/2}\,\phi^{(0)}$; and

$$h_s = {h_s}^{(0)} + {h_s}^{(1)} + {\rm O}\left(\left(\frac{m_{\rm e}}{m_{\rm i}}\right)h_s\right), \tag{38}$$

where ${h_s}^{(n)} \sim (m_{\rm e}/m_{\rm i})^{n/2}\,(e\phi/T_{\rm e})F_{0s}$. Similarly, it will be natural to expand the frequency of the mode in powers of $(m_{\rm e}/m_{\rm i})^{1/2}$:

$$\omega = \omega^{(0)} + \omega^{(1)} + {\rm O}\left(\left(\frac{m_{\rm e}}{m_{\rm i}}\right)\omega\right). \tag{39}$$

We now derive the equations for the ion response, before moving on to derive the equations for the electron response.

4.1.1. Ion response in the outer region. For the ion species, we start with the usual form of the gyrokinetic equation, equation (3). In the collisionless limit, the leading order equation for the ion response is

$$v_{\parallel}\boldsymbol{b}\cdot\nabla\theta\frac{\partial {h_{\rm i}}^{(0)}}{\partial\theta}+{\rm i}\left(\boldsymbol{k}_{\perp}\cdot\boldsymbol{v}_{\rm M,i}-\omega^{(0)}\right){h_{\rm i}}^{(0)}={\rm i}\left(\omega_{*,{\rm i}}-\omega^{(0)}\right)J_{0{\rm i}}F_{0i}\frac{Z_{\rm i}e\phi^{(0)}}{T_{\rm i}}. \qquad (40)$$

Using equation (40), and the estimates $\omega\sim v_{\rm th,i}/a\sim\omega_{*,{\rm i}}$ and $b_{\rm i}\sim 1$, we find that $h_{\rm i}/F_{0i}\sim e\phi^{(0)}/T_{\rm e}$. Hence, the ion nonadiabatic response contributes at leading order to ϕ. The equation for the nonadiabatic ion density is

$$\frac{\delta n_{\rm i}^{(0)}}{n_{\rm i}}=\int J_{0{\rm i}}\frac{{h_{\rm i}}^{(0)}}{n_{\rm i}}\,d^3\boldsymbol{v}\sim\frac{e\phi^{(0)}}{T_{\rm e}}. \qquad (41)$$

4.1.2. Electron response in the outer region. For the electron species we will use the modified form of the gyrokinetic equation, equation (32). We do this to avoid integrating the radial magnetic drift $\boldsymbol{v}_{\rm M,e}\cdot\nabla\psi$ by parts in θ at every order when applying transit or bounce averages. The leading order equation for the electron response is

$$v_{\parallel}\boldsymbol{b}\cdot\nabla\theta\frac{\partial H_{\rm e}^{(0)}}{\partial\theta}=0, \qquad (42)$$

where we have used that the electron parallel streaming term is larger than every other term in equation (32) by the ordering $\omega a/v_{\rm th,i}\sim k_y\rho_{\rm th,i}\sim 1$ and $v_{\rm th,i}/v_{\rm th,e}\sim(m_{\rm e}/m_{\rm i})^{1/2}$. We note that for electrons $\lambda_{\rm e}\sim(m_{\rm e}/m_{\rm i})^{1/2}$, and hence, for $\theta_0\sim\theta\sim 1$ the phase $\exp\left[{\rm i}\lambda_{\rm e}(\theta_0-\theta)\right]$ may be expanded as

$$\exp\left[{\rm i}\lambda_{\rm e}(\theta_0-\theta)\right]=1+{\rm i}\lambda_{\rm e}(\theta_0-\theta)-\frac{\lambda_{\rm e}^2}{2}(\theta_0-\theta)^2+{\rm O}\left(\left(\frac{m_{\rm e}}{m_{\rm i}}\right)^{3/2}\right). \qquad (43)$$

As a consequence of equation (42), the leading-order nonadiabatic electron response is independent of θ for $\theta\sim 1$. The remainder of the expansion must be carried out separately for passing and trapped particles.

Trapped particles occupy the range of pitch angles $1/B_{\max}<\lambda\leq 1/B(\theta)$, with $B_{\max}$ the maximum value of $B(\theta)$. In each well, trapped particles bounce at the upper and lower bounce points, θ_b^+ and θ_b^-, respectively. Equation (42) for trapped particles states that $H_{\rm e}^{(0)}$ is constant in θ within each magnetic well. Imposing the trapped particle boundary conditions

$$h_{\rm e}(\theta_b^{\pm},\sigma=1)=h_{\rm e}(\theta_b^{\pm},\sigma=-1), \qquad (44)$$

where $\sigma=v_{\parallel}/|v_{\parallel}|$, and using equation (31), we find that $H_{\rm e}^{(0)}(\sigma=1)=H_{\rm e}^{(0)}(\sigma=-1)$, and so $H_{\rm e}^{(0)}$ is independent of (θ,σ). The trapped electron piece of the distribution function $H_{\rm e}^{(0)}$ is determined by the equation for the next order in the electron response

$$v_{\parallel}\boldsymbol{b}\cdot\nabla\theta\frac{\partial H_{\rm e}^{(1)}}{\partial\theta}+{\rm i}(\omega_{\rm M,e}-\omega^{(0)})H_{\rm e}^{(0)}-C_{\rm ee}[H_{\rm e}^{(0)}]-\mathcal{L}[H_{\rm e}^{(0)}]$$

$$= -\mathrm{i}\left(\omega_{*,\mathrm{e}} - \omega^{(0)}\right) F_{0e}\frac{e\phi^{(0)}}{T_\mathrm{e}}, \tag{45}$$

where we have used that for $b_\mathrm{e} = \mathrm{O}((m_\mathrm{e}/m_\mathrm{i})^{1/2})$, $J_{0\mathrm{e}} = 1 + \mathrm{O}(m_\mathrm{e}/m_\mathrm{i})$, and $\exp\left[\mathrm{i}\lambda_\mathrm{e}(\theta_0 - \theta)\right] = 1 + \mathrm{O}\left((m_\mathrm{e}/m_\mathrm{i})^{1/2}\right)$, and we have employed $\boldsymbol{k}_\perp \cdot \boldsymbol{\rho}_e \sim b_\mathrm{e} \sim (m_\mathrm{e}/m_\mathrm{i})^{1/2}$ to reduce the collision operator in equation (45) to the drift kinetic electron collision operator $C_\mathrm{ee}[\cdot] + \mathcal{L}[\cdot]$. To close equation (45), we introduce the bounce average for trapped particles

$$\langle \cdot \rangle^\mathrm{b} = \frac{\sum_\sigma \int_{\theta_b^-}^{\theta_b^+} d\theta\ (\cdot)/|v_\parallel| \boldsymbol{b}\cdot\nabla\theta}{2\int_{\theta_b^-}^{\theta_b^+} d\theta/|v_\parallel|\boldsymbol{b}\cdot\nabla\theta}. \tag{46}$$

Applying $\langle \cdot \rangle^\mathrm{b}$ to equation (45), we find the solvability condition

$$\mathrm{i}\left(\langle \omega_{\mathrm{M,e}}\rangle^\mathrm{b} - \omega^{(0)}\right) H_\mathrm{e}^{(0)} - C_\mathrm{ee}[H_\mathrm{e}^{(0)}] - \mathcal{L}[H_\mathrm{e}^{(0)}] = -\mathrm{i}\left(\omega_{*,\mathrm{e}} - \omega^{(0)}\right) F_{0e}\frac{e\left\langle \phi^{(0)}\right\rangle^\mathrm{b}}{T_\mathrm{e}}, \tag{47}$$

where we have used the property

$$\left\langle v_\parallel \boldsymbol{b}\cdot\nabla\theta \frac{\partial f}{\partial\theta}\right\rangle^\mathrm{b} = 0 \tag{48}$$

of the bounce average, valid for any $f = f_{\theta_0,k_\alpha}(\varepsilon, \lambda, \sigma, \theta)$ satisfying the bounce condition $f_{\theta_0,k_\alpha}(\varepsilon, \lambda, \sigma = 1, \theta_b^\pm) = f_{\theta_0,k_\alpha}(\varepsilon, \lambda, \sigma = -1, \theta_b^\pm)$.

Passing particles occupy the range of pitch angles $0 \leq \lambda \leq 1/B_\mathrm{max}$, and hence, passing particles are free to travel between magnetic wells. For passing electrons, equation (42) determines that, for a given (θ_0, k_α) mode, $H_\mathrm{e}^{(0)}$ is a constant in θ for each sign of the parallel velocity σ, i.e.,

$$H_\mathrm{e}^{(0)} = H_\mathrm{e}^{(0)}(\varepsilon, \lambda, \sigma). \tag{49}$$

To determine this constant $H_\mathrm{e}^{(0)}$, we need to supply an appropriate incoming boundary condition to the $\theta \sim 1$ region. This will require us to consider the $\theta \gg 1$ region.

In the conventional treatment of passing electrons, it is argued that the incoming boundary condition (25) implies that $H_\mathrm{e}^{(0)} = 0$ in the passing piece of velocity space, cf. [28, 29]. This assumption results in modes driven at scales of $k_y\rho_\mathrm{th,i} \sim 1$ by the ion response or the trapped electron response. Under this assumption, the leading-order nonadiabatic response of passing electrons $H_\mathrm{e}^{(1)}$ is determined by the first-order equation

$$v_\parallel \boldsymbol{b}\cdot\nabla\theta \frac{\partial H_\mathrm{e}^{(1)}}{\partial\theta} - C_\mathrm{ee}[H_\mathrm{e}^{(0)}] = -\mathrm{i}\left(\omega_{*,\mathrm{e}} - \omega^{(0)}\right) F_{0e}\frac{e\phi^{(0)}}{T_\mathrm{e}}, \tag{50}$$

where the magnetic drift, frequency, and electron-ion collision terms are neglected because $H_\mathrm{e}^{(0)} = 0$ in the passing part of velocity space. The collision operator term $C_\mathrm{ee}[H_\mathrm{e}^{(0)}]$ is retained because $C_\mathrm{ee}[H_\mathrm{e}^{(0)}]$ is a nonlocal operator representing the drag of trapped particles on passing particles. In this ordering, passing electrons coming from the $\theta \gg 1$ region receive a $(m_\mathrm{e}/m_\mathrm{i})^{1/2}$ small impulse from the $\theta \sim 1$ electrostatic potential:

$$H_\mathrm{e}^{(1)}(\theta, \sigma = 1) = H_\mathrm{e}^{(1)}(-\infty, \sigma = 1) \tag{51}$$

$$+\int_{-\infty}^{\theta}\frac{1}{v_{\|}\boldsymbol{b}\cdot\nabla\theta}\left(C_{\rm ee}[H_{\rm e}^{(0)}]-{\rm i}\left(\omega_{*,{\rm e}}-\omega^{(0)}\right)\frac{e\phi^{(0)}}{T_{\rm e}}F_{0e}\right)d\theta',$$

and

$$H_{\rm e}^{(1)}(\theta,\sigma=-1)=H_{\rm e}^{(1)}(\infty,\sigma=-1) \qquad (52)$$

$$+\int_{\infty}^{\theta}\frac{1}{v_{\|}\boldsymbol{b}\cdot\nabla\theta}\left(C_{\rm ee}[H_{\rm e}^{(0)}]-{\rm i}\left(\omega_{*,{\rm e}}-\omega^{(0)}\right)\frac{e\phi^{(0)}}{T_{\rm e}}F_{0e}\right)d\theta',$$

where $H_{\rm e}^{(1)}(\mp\infty,\sigma=\pm1)$ should be determined consistently in the $\theta\gg1$ region. Because $H_{\rm e}^{(1)}$ contributes only a small correction to quasineutrality, the nonadiabatic response of passing electrons is conventionally ignored.

One of the key contributions of this paper is to notice a flaw in the conventional argument: in fact, $H_{\rm e}^{(0)}$ need not vanish, but instead $H_{\rm e}^{(0)}$ can be determined self-consistently in the $\theta\gg1$ region. The resulting class of modes are driven by the nonadiabatic response of passing electrons, with no leading-order impact from the ion response or trapped electron response in the $\theta\sim1$ region. We now turn to the $\theta\gg1$ region for the collisionless ordering. The equations that we obtain there will provide the nonadiabatic passing electron response, $H_{\rm e}^{(0)}(\varepsilon,\lambda,\sigma=\pm1)$, in the case of passing-electron-response driven modes, and the boundary conditions $H_{\rm e}^{(1)}(\theta=\mp\infty,\varepsilon,\lambda,\sigma=\pm1)$ in the case of modes in the conventional ordering.

4.2. Inner solution – $k_r\rho_{\rm th,e}\sim1$

In real space, the inner region is the radial layer close to the rational flux surface. The inner region is characterised by fine radial scales associated with electron physics. In order to capture these scales analytically in the ballooning formalism, we introduce an additional ballooning angle coordinate χ that measures distance along the magnetic field line. The coordinate θ will capture periodic variation in ballooning angle on the scale of 2π associated with the equilibrium geometry, whereas the coordinate χ will measure secular variation on scales much larger than 2π. In the inner region, distribution functions and fields become functions of the independent variables θ and χ, i.e.,

$$f(\theta)\rightarrow f(\theta,\chi), \qquad (53)$$

and parallel-to-the-field-line derivatives become

$$\frac{\partial}{\partial\theta}\rightarrow\frac{\partial}{\partial\theta}+\frac{\partial}{\partial\chi}. \qquad (54)$$

We order $\partial/\partial\chi\sim(m_{\rm e}/m_{\rm i})^{1/2}\,\partial/\partial\theta$, and we order $k_r\rho_{\rm th,e}\sim1$, whilst keeping $k_y\rho_{\rm th,i}\sim1$.

The parallel-to-the-field variable θ appears in two forms in the gyrokinetic equation (32): as the argument of periodic functions associated with the magnetic geometry; and linearly in the combination $-k_\alpha q'(\theta-\theta_0)$. To treat the scale separation within the part of the mode where $\theta\sim(m_{\rm i}/m_{\rm e})^{1/2}\gg1$, we send $\theta\rightarrow\chi$ where θ appears in secular terms (e.g. $-k_\alpha q'(\theta-\theta_0)$), and we take $\chi\sim(m_{\rm i}/m_{\rm e})^{1/2}\gg1$. This assignment captures the effect of the secular growth of the radial wave number k_r in the $\theta \gg 1$ region. With this procedure, we note that, in the inner region, we can usefully write

$$\boldsymbol{k}_\perp = \boldsymbol{k}_\perp^{(0)} + \boldsymbol{k}_\perp^{(1)}, \tag{55}$$

with

$$\boldsymbol{k}_\perp^{(0)} = -k_\alpha \chi \nabla q \tag{56}$$

and

$$\boldsymbol{k}_\perp^{(1)} = k_\alpha \theta_0 \nabla q + k_\alpha (\nabla \alpha + \theta \nabla q) = \mathrm{O}\left(\chi^{-1}\boldsymbol{k}_\perp^{(0)}\right), \tag{57}$$

where we recall that $\nabla\alpha + \theta\nabla q = \nabla\zeta - q\nabla\theta - \nabla\nu$ has no secular dependence on θ. Hence, we find that in the inner region

$$\mathrm{i}\boldsymbol{k}_\perp \cdot \boldsymbol{v}_{\mathrm{M},s} = \mathrm{i}\boldsymbol{k}_\perp^{(0)} \cdot \boldsymbol{v}_{\mathrm{M},s} + \mathrm{O}\left(\chi^{-1}\boldsymbol{k}_\perp^{(0)} \cdot \boldsymbol{v}_{\mathrm{M},s}\right). \tag{58}$$

We also need to consider the argument of the Bessel function

$$b_s = \frac{k_\perp v_\perp m_s c}{Z_s e B} = \frac{k_\perp(\theta) c}{Z_s e}\sqrt{\frac{2 m_s \varepsilon \lambda}{B(\theta)}}. \tag{59}$$

In the region $\chi \sim (m_\mathrm{e}/m_\mathrm{i})^{1/2}$, we find that

$$b_s = k_\alpha |\nabla q|(\theta) \frac{c}{Z_s e}\sqrt{\frac{2 m_s \varepsilon \lambda}{B(\theta)}}|\chi| + \mathrm{O}\left(\chi^{-1} b_s\right). \tag{60}$$

Note that b_s has a linear dependence on χ, whereas θ appears only through the periodic functions $|\nabla q| = |q'||\nabla\psi|(\theta)$ and $B(\theta)$. The plasma is magnetised, and hence $B(\theta)$ will have a large component independent of θ. Likewise, $|\nabla\psi|$ will be nowhere zero on any given flux surface (except perhaps if there is an X-point on the last closed flux surface). Hence, changes in θ cause only small oscillations in b_s, whereas changes in χ can cause arbitrarily large variations in b_s.

Finally, to solve for the electron distribution function, we need to impose a 2π periodic boundary condition on θ, and a “ballooning” boundary condition on χ, i.e.,

$$h_\mathrm{e}(\theta = \pi, \chi) = h_\mathrm{e}(\theta = -\pi, \chi), \tag{61}$$

and

$$h_\mathrm{e}(\chi = -\infty) = 0, \text{ for } v_\parallel > 0, \text{ and}$$

$$h_\mathrm{e}(\chi = \infty) = 0, \text{ for } v_\parallel < 0. \tag{62}$$

The results for large χ above, equations (55)-(62), are not peculiar to the ordering $\chi \sim (m_\mathrm{i}/m_\mathrm{e})^{1/2}$. We will reuse results (55)-(62) for $\chi \sim (m_\mathrm{i}/m_\mathrm{e})^{1/4}$ when we come to discuss the collisional inner region in section 5.1.

To solve for the electron response, we will again use the modified electron distribution function H_e, defined by equation (31), and the modified electron gyrokinetic equation (equation (32) with $s = \mathrm{e}$). We note that, in the inner region of the collisionless ordering, $\theta \sim (m_{\rm i}/m_{\rm e})^{1/2} \gg 1 \sim \theta_0 \gg \lambda_{\rm e} \sim (m_{\rm e}/m_{\rm i})^{1/2}$, and hence the phase in (31) becomes

$$\exp\left[{\rm i}\lambda_{\rm e}(\theta_0-\theta)\right] = \exp\left[-{\rm i}\lambda_{\rm e}\chi\right]\left(1+{\rm i}\lambda_{\rm e}\theta_0 - \frac{\lambda_{\rm e}^2\theta_0^2}{2} + {\rm O}\left(\left(\frac{m_{\rm e}}{m_{\rm i}}\right)^{3/2}\right)\right). \qquad (63)$$

Consistent with the expansion in the outer region, in the inner region we expand the electrostatic potential ϕ, the distribution functions $h_{\rm i}$ and $H_{\rm e}$, and the frequency ω in powers of $(m_{\rm e}/m_{\rm i})^{1/2}$. However, we leave the relative size of the fluctuations in the outer and inner regions to be determined. We will return to this point in sections 4.3 and 4.4.

4.2.1. Ion response in the inner region. The leading-order equation for the ion response in the inner region is

$$\left(\frac{k_\alpha^2 q'^2|\nabla\psi|^2\chi^2 v^2}{4\Omega_{\rm i}^2}\left(\nu_{\|,{\rm i}}\lambda B + \frac{\nu_{\perp,{\rm i}}}{2}\left(2-\lambda B\right)\right) - {\rm i}k_\alpha q'\chi \boldsymbol{v}_{\rm M,i}\cdot\nabla\psi\right) {h_{\rm i}}^{(0)}$$

$$= {\rm i}\left(\omega_{*,{\rm i}} - \omega^{(0)}\right) J_{0{\rm i}} F_{0i}\frac{Z_{\rm i}e\phi^{(0)}}{T_{\rm i}}, \qquad (64)$$

where we have defined the collision frequencies

$$\nu_{\|,{\rm i}} = \sqrt{\frac{\pi}{2}}\nu_{\rm ii}\frac{\Psi(v/v_{\rm th,i})}{(v/v_{\rm th,i})^3}, \qquad (65)$$

and

$$\nu_{\perp,{\rm i}} = \sqrt{\frac{\pi}{2}}\nu_{\rm ii}\frac{{\rm erf}(v/v_{\rm th,i}) - \Psi(v/v_{\rm th,i})}{(v/v_{\rm th,i})^3}, \qquad (66)$$

with the functions

$$\mathrm{erf}(z) = \frac{2}{\sqrt{\pi}}\int_0^z \exp\left[-s^2\right]\, ds, \qquad (67)$$

and

$$\Psi(z) = \frac{1}{2z^2}\left({\rm erf}(z) - \frac{2z}{\sqrt{\pi}}\exp\left[-z^2\right]\right). \qquad (68)$$

The first term on the left of equation (64) is due to the finite-Larmor-radius terms in the ion gyrokinetic self-collision operator (8) (cf. [30–32]). The ion response given by equation (64) is local in ballooning angle – a more detailed analysis demonstrating how this response arises is given in Appendix E. We note that $J_{0{\rm i}} \sim \chi^{-1/2} \sim (m_{\rm e}/m_{\rm i})^{1/4}$ for $b_{\rm i} \sim k_r\rho_{\rm th,i} \sim \chi \sim (m_{\rm i}/m_{\rm e})^{1/2} \gg 1$. Hence, if $\nu_{\rm ii}/\omega \sim (m_{\rm e}/m_{\rm i})^{1/2}$, we take the ion nonadiabatic response ${h_{\rm i}}^{(0)}/F_{0i} \sim \chi^{-3/2}(e\phi^{(0)}/T_{\rm e})$ everywhere in the inner region.

The contribution of ${h_{\rm i}}^{(0)}$ to ϕ is small in the inner region. Estimating the size of the ion nonadiabatic density $\delta n_{\rm i}$ in the inner region, we find that

$$\frac{\delta n_{\rm i}^{(0)}}{n_{\rm i}} = \frac{1}{n_{\rm i}}\int J_{0{\rm i}}{h_{\rm i}}^{(0)}\, d^3\boldsymbol{v} \sim \frac{m_{\rm e}}{m_{\rm i}}\frac{e\phi^{(0)}}{T_{\rm e}} \ll \frac{e\phi^{(0)}}{T_{\rm e}}. \qquad (69)$$

We have used the conventional distribution function $h_{\rm i}$ and conventional form of the gyrokinetic equation to describe the ion species. We could obtain the estimate (69) by using the alternative form of the gyrokinetic equation, equation (32). However, if we use the distribution function $H_{\rm i}$ and equation (32) for ions, we need to be careful with estimates involving integrals of the phase $\exp\left[-{\rm i}\lambda_{\rm i}\chi\right]$, because $\lambda_{\rm i}\chi \gg 1$ in the inner region.

4.2.2. Electron response in the inner region. The leading order equation for the electron response in the inner region is

$$v_{\|}\boldsymbol{b}\cdot\nabla\theta\frac{\partial H_{\rm e}^{(0)}}{\partial\theta} = 0. \tag{70}$$

Equation (70) appears to be trivially simple because of the choice to use the modified electron gyrokinetic equation (32), and modified distribution function $H_{\rm e}$. In terms of $h_{\rm e}$, and using equation (31), equation (70) tells us that the leading-order electron distribution function has the form

$${h_{\rm e}}^{(0)}(\theta,\chi) = \exp\left[-{\rm i}\lambda_{\rm e}\chi\right]H_{\rm e}^{(0)}(\chi). \tag{71}$$

In other words, the θ dependence in ${h_{\rm e}}^{(0)}$ comes entirely from the radial-magnetic-drift phase $\exp\left[-{\rm i}\lambda_{\rm e}\chi\right]$, and $H_{\rm e}^{(0)}(\chi)$ is the slowly decaying envelope of ${h_{\rm e}}^{(0)}$. This observation motivates the choice to present the derivation in terms of $H_{\rm e}$ rather than $h_{\rm e}$.

The distribution function $H_{\rm e}^{(0)}$ is determined by the first-order equation for the electron response in the inner region

$$v_{\|}\boldsymbol{b}\cdot\nabla\theta\frac{\partial H_{\rm e}^{(1)}}{\partial\theta} + v_{\|}\boldsymbol{b}\cdot\nabla\theta\frac{\partial H_{\rm e}^{(0)}}{\partial\chi} + {\rm i}\left(\omega_{\rm M,e}-\omega^{(0)}\right)H_{\rm e}^{(0)} - \widehat{C}_{\rm e}^{(0)}[H_{\rm e}^{(0)}]$$
$$= -{\rm i}\left(\omega_{*,\rm e}-\omega^{(0)}\right)\exp\left[-{\rm i}\lambda_{\rm e}\chi\right]J_{0\rm e}^{(0)}F_{0e}\frac{e\phi^{(0)}}{T_{\rm e}}, \tag{72}$$

where

$$\widehat{C}_{\rm e}^{(0)}[H_{\rm e}^{(0)}] = \exp\left[-{\rm i}\lambda_{\rm e}\chi\right]\left\langle \exp\left[{\rm i}\boldsymbol{k}_{\perp}^{(0)}\cdot\boldsymbol{\rho}_e\right]C_{\rm ee}\left[\exp\left[-{\rm i}\boldsymbol{k}_{\perp}^{(0)}\cdot\boldsymbol{\rho}_e\right]\exp\left[{\rm i}\lambda_{\rm e}\chi\right]H_{\rm e}^{(0)}\right]\right\rangle_{\boldsymbol{R}}^{\gamma}$$
$$+\exp\left[-{\rm i}\lambda_{\rm e}\chi\right]\left\langle \exp\left[{\rm i}\boldsymbol{k}_{\perp}^{(0)}\cdot\boldsymbol{\rho}_e\right]\mathcal{L}\left[\exp\left[-{\rm i}\boldsymbol{k}_{\perp}^{(0)}\cdot\boldsymbol{\rho}_e\right]\exp\left[{\rm i}\lambda_{\rm e}\chi\right]H_{\rm e}^{(0)}\right]\right\rangle_{\boldsymbol{R}}^{\gamma}, \tag{73}$$

and $J_{0\rm e}^{(0)} = J_0(b_{\rm e}^{(0)})$. In order to solve equation (72) for passing particles, we must impose the solvability condition that $H_{\rm e}^{(1)}$ is periodic in θ. This condition can be imposed by using the transit average

$$\langle\cdot\rangle^{\rm t} = \frac{\int_{-\pi}^{\pi} d\theta\;(\cdot)/v_{\|}\boldsymbol{b}\cdot\nabla\theta}{\int_{-\pi}^{\pi} d\theta/v_{\|}\boldsymbol{b}\cdot\nabla\theta}. \tag{74}$$

Applying the transit average to equation (72) results in the equation for $H_{\rm e}^{(0)}$;

$$\left\langle v_{\|}\boldsymbol{b}\cdot\nabla\theta\right\rangle^{\rm t}\frac{\partial H_{\rm e}^{(0)}}{\partial\chi} + {\rm i}\left(\langle\omega_{\rm M,e}\rangle^{\rm t}-\omega^{(0)}\right)\;H_{\rm e}^{(0)} - \left\langle\widehat{C}_{\rm e}^{(0)}\left[H_{\rm e}^{(0)}\right]\right\rangle^{\rm t}$$
$$= -{\rm i}\left(\omega_{*,\rm e}-\omega^{(0)}\right)F_{0e}\left\langle\exp\left[-{\rm i}\lambda_{\rm e}\chi\right]J_{0\rm e}^{(0)}\frac{e\phi^{(0)}}{T_{\rm e}}\right\rangle^{\rm t}. \tag{75}$$

For trapped electrons, we need to be careful in our interpretation of the two scales in equation (72). Physically, trapped particles cannot pass between wells in the magnetic field strength. Trapped particles can observe only changes of order unity in poloidal angle as they follow trapped orbits. This prohibits large variation in the ballooning poloidal angle χ for individual particles. The trapped particle distribution function should satisfy the trapped particle boundary conditions, equation (44). Noting that $\lambda_{\rm e}(\theta_b^{\pm}) = 0$ as $v_\parallel(\theta_b^{\pm}) = 0$, we have that for trapped particles $H_{\rm e}^{(0)}(\theta_b^{\pm}, \sigma = 1) = H_{\rm e}^{(0)}(\theta_b^{\pm}, \sigma = -1)$ and hence $H_{\rm e}^{(0)}$ is constant in both θ and σ. To go to higher order, we must impose the solvability condition that $H_{\rm e}^{(1)}$ satisfies the bounce conditions $H_{\rm e}^{(1)}(\theta_b^{\pm}, \sigma = 1) = H_{\rm e}^{(1)}(\theta_b^{\pm}, \sigma = -1)$. Hence, to obtain the equation for $H_{\rm e}^{(0)}$ for trapped electrons, we apply the bounce average $\langle \cdot \rangle^{\rm b}$, defined in equation (46), to equation (72). The result is

$$\begin{aligned} &{\rm i}\left(\langle \omega_{\rm M,e}\rangle^{\rm b} - \omega^{(0)}\right) H_{\rm e}^{(0)} - \left\langle \widehat{C}_{\rm e}^{(0)}\left[H_{\rm e}^{(0)}\right]\right\rangle^{\rm b} \\ &\qquad = -{\rm i}\left(\omega_{*,\rm e} - \omega^{(0)}\right) F_{0e} \left\langle \exp\left[-{\rm i}\lambda_{\rm e}\chi\right] J_{0\rm e}^{(0)} \frac{e\phi^{(0)}}{T_{\rm e}} \right\rangle^{\rm b}, \end{aligned} \tag{76}$$

where we have used the property (48) of the bounce average, to eliminate the parallel derivative in θ on the left-hand side of equation (72), and we have used the property

$$\left\langle v_\parallel g \right\rangle^{\rm b} = 0, \tag{77}$$

for any σ-independent function $g = g_{\theta_0,k_\alpha}(\varepsilon, \lambda, \theta)$, to eliminate the term $\left\langle v_\parallel \boldsymbol{b}\cdot\nabla\theta\right\rangle^{\rm b} \partial H_{\rm e}^{(0)}/\partial\chi$. Note that no derivatives in χ appear explicitly in equation (76), and hence for trapped particles $H_{\rm e}^{(0)}$ is only a parametric function of χ. This is the manifestation of the physical intuition that trapped particles do not move between magnetic wells.

4.3. Modes with $(m_{\rm e}/m_{\rm i})^{1/2}$ *small electron tails*

In this section we describe the class of modes in the collisionless ordering that have small electron tails. This class of modes includes the conventional ITG mode and the trapped-electron mode (TEM), so much of the discussion will be familiar. We describe the role of the electron response in these modes in detail to provide predictions for numerical results in sections 6.2 and 6.2.1, and to compare and contrast with the novel modes described in the next section.

To obtain the "small-tail" modes, we assume a priori that $H_{\rm e,outer}^{(0)} = 0$ for passing electrons in the outer region of the mode where $\theta \sim 1$ and $k_r\rho_{\rm th,i} \sim 1$. Then the passing electron response has a leading-order nonzero component $H_{\rm e,outer}^{(1)}$, given by equations (51) and (52). We obtain the leading-order trapped electron response $H_{\rm e,outer}^{(0)}$ from equation (47), and the leading-order ion response $h_{\rm i,outer}^{(0)}$ from equation (40). No parallel boundary condition is required to solve the trapped-electron equation (47). For equation (40) for the ion response, we supply the zero-incoming boundary condition (25), without referring to the inner region where $k_r\rho_{\rm th,i} \sim \theta \gg 1$. This is justified by the fact that in the inner region $h_{\rm i,inner}^{(0)}$ is small. We can regard $H_{\rm e,outer}^{(0)}$ and $h_{\rm i,outer}^{(0)}$ as functionals of $\phi_{\rm outer}^{(0)}$ and functions of $\omega^{(0)}$, i.e., $H_{\rm e,outer}^{(0)} = H_{\rm e,outer}^{(0)}[\phi_{\rm outer}^{(0)}, \omega^{(0)}]$ and $h_{\rm i,outer}^{(0)} = h_{\rm i,outer}^{(0)}[\phi_{\rm outer}^{(0)}, \omega^{(0)}]$. The frequency $\omega^{(0)}$ and potential $\phi^{(0)}$ are determined through the leading-order quasineutrality relation in the outer region

$$\left(\frac{Z_{\rm i}T_{\rm e}}{T_{\rm i}} + 1\right)\frac{e\phi^{(0)}}{T_{\rm e}} = \int J_{0\rm i}\frac{h_{\rm i}^{(0)}}{n_{\rm i}}\, d^3\boldsymbol{v} - \int \frac{H_{\rm e}^{(0)}}{n_{\rm e}}\, d^3\boldsymbol{v}, \tag{78}$$

where we have used that $J_{0\rm e} = 1 + {\rm O}\left(m_{\rm e}/m_{\rm i}\right)$ for $k_y\rho_{\rm th,i} \sim k_r\rho_{\rm th,i} \sim 1$. The small correction $H_{\rm e,outer}^{(1)}$ from passing electrons does not enter in the leading-order eigenvalue problem, equation (78). As a result, in small-tail modes the nonadiabatic passing electron response is a "cosmetic" feature that does not contribute to determining the basic properties of the mode. Nonetheless, observable electron tails can develop in $k_r\rho_{\rm th,e} \sim 1$ regions ($\theta \sim (m_{\rm i}/m_{\rm e})^{1/2}$). We illustrate this in figure 1. The mode is decomposed into three regions: $\theta \sim 1$, and $|\theta| \sim (m_{\rm i}/m_{\rm e})^{1/2}$ for $\theta > 0$ and $\theta < 0$. Forward-going passing electrons travel along the mode, receiving an impulse

$$\Delta H_{\rm e} = \int_{-\infty}^{\infty} \frac{1}{v_\| \boldsymbol{b}\cdot\nabla\theta}\left(C_{\rm ee}\left[H_{\rm e,outer}^{(0)}\right] - {\rm i}\left(\omega_{*,\rm e} - \omega^{(0)}\right)\frac{e\phi_{\rm outer}^{(0)}}{T_{\rm e}}F_{0e}\right) d\theta' \tag{79}$$

from the electrostatic potential ϕ in the $\theta \sim 1$ region. The impulse (79) sets the natural size of the electron nonadiabatic response in the $\theta \sim (m_{\rm i}/m_{\rm e})^{1/2}$ region $H_{\rm e,inner}$ compared to the size of the potential in the outer region:

$$H_{\rm e,inner} \sim \Delta H_{\rm e} \sim \left(\frac{m_{\rm e}}{m_{\rm i}}\right)^{1/2}\frac{e\phi_{\rm outer}}{T_{\rm e}}F_{0e}. \tag{80}$$

We can use the leading-order quasineutrality relation in the inner region to obtain an estimate for the size of the potential in the inner region. The leading-order quasineutrality relation in the inner region is

$$\left(\frac{Z_{\rm i}T_{\rm e}}{T_{\rm i}} + 1\right)\frac{e\phi^{(0)}}{T_{\rm e}} = -\int \exp\left[{\rm i}\lambda_{\rm e}\chi\right] J_{0\rm e}^{(0)}\frac{H_{\rm e}^{(0)}}{n_{\rm e}}\, d^3\boldsymbol{v}, \tag{81}$$

where we have used that the ion contribution to quasineutrality is small, cf. equation (69). Using equation (81), we find that the electrostatic potential in the inner region $\phi_{\rm inner}$ is of size

$$\frac{e\phi_{\rm inner}}{T_{\rm e}} \sim \left(\frac{m_{\rm e}}{m_{\rm i}}\right)^{1/2}\frac{e\phi_{\rm outer}}{T_{\rm e}}. \tag{82}$$

The matching condition for $H_{\rm e,inner}$ is obtained by demanding that the passing electron distribution function is continuous across the boundary between the outer and inner regions, i.e.,

$$H_{\rm e,outer}^{(1)}(\theta = \pm\infty) = H_{\rm e,inner}^{(0)}(\chi = 0^{\pm}),\ \text{for } 0 \leq \lambda B_{\rm max} \leq 1. \tag{83}$$

Note that the trapped electron distribution function need not be continuous across this boundary. Combining equations (51), (52), (79) and (83), we find that the matching condition for solving for the passing electron response in the small-tails limit is

$$H_{\rm e,inner}^{(0)}(\chi = 0^{+}) = H_{\rm e,inner}^{(0)}(\chi = 0^{-}) + \Delta H_{\rm e}, \tag{84}$$

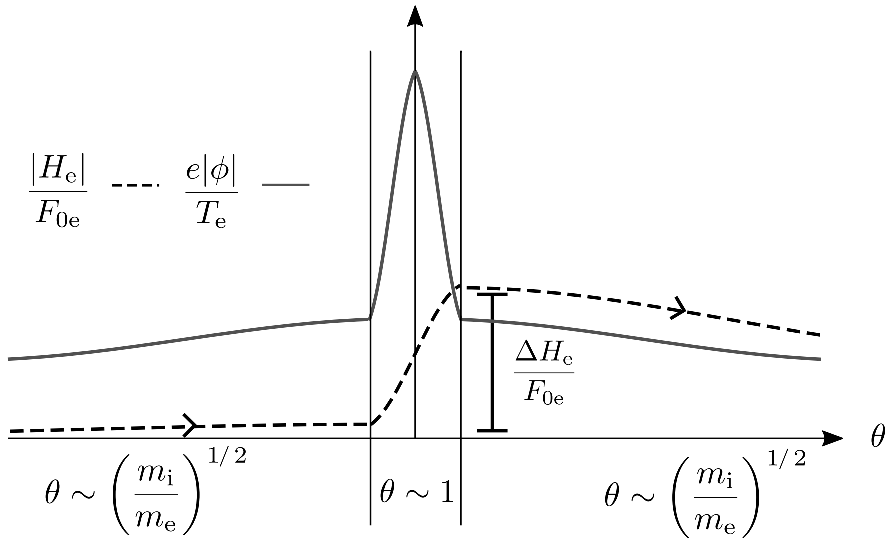

Figure 1. An illustration showing the nonadiabatic passing electron response for forward-going particles in the small-tail limit. At leading-order in the $(m_{\rm e}/m_{\rm i})^{1/2}$ expansion, the mode frequency is determined by the response of ions and trapped electrons in the outer region ($\theta \sim 1$), by solving equations (40) and (47), with quasineutrality (78). The passing part of the electron distribution function $H_{\rm e}$ is propagated from left to right, via equation (75), starting with zero amplitude at $\theta = -\infty$, receiving an impulse $\Delta H_{\rm e}$ from the potential ϕ in the outer region (see equation (79)), and finally, carrying that amplitude into the inner region ($\theta \sim (m_{\rm i}/m_{\rm e})^{1/2}$). In the inner region, the trapped electron response may be determined with equation (76), and the electron response determines ϕ, via quasineutrality (81).

valid for both $\sigma \pm 1$.

We can self-consistently obtain the electron tails associated with a small-tail mode in the following way. First, we solve the the eigenvalue problem (78), with $H^{(0)}_{\rm e,outer}$ and $h^{(0)}_{\rm i,outer}$ obtained from the equations (47) and (40), respectively. This determines $\omega^{(0)}$ and $\phi^{(0)}_{\rm outer}$. Second, we solve the inner region equations (75) and (76) for the nonadiabatic response of passing electrons and trapped electrons, respectively, subject to the jump condition (84) at $\chi = 0$. This obtains the functional $H^{(0)}_{\rm e,inner} = H^{(0)}_{\rm e,inner}[\phi^{(0)}_{\rm inner}, \phi^{(0)}_{\rm outer}, \omega^{(0)}]$. Finally, we impose quasineutrality, equation (81), to obtain a relation for $\phi^{(0)}_{\rm inner}$ in terms of the jump over $\phi^{(0)}_{\rm outer}$.

4.4. Modes with dominant electron tails

We now turn to the novel class of modes identified in this paper. To obtain a "large-tail" mode in the $(m_{\rm e}/m_{\rm i})^{1/2} \to 0$ limit, we assume that the leading-order nonadiabatic passing electron response is nonzero in the outer region, i.e.,

$$\frac{H_{\rm e,outer}}{F_{0e}} \sim \frac{e\phi_{\rm outer}}{T_{\rm e}}. \tag{85}$$

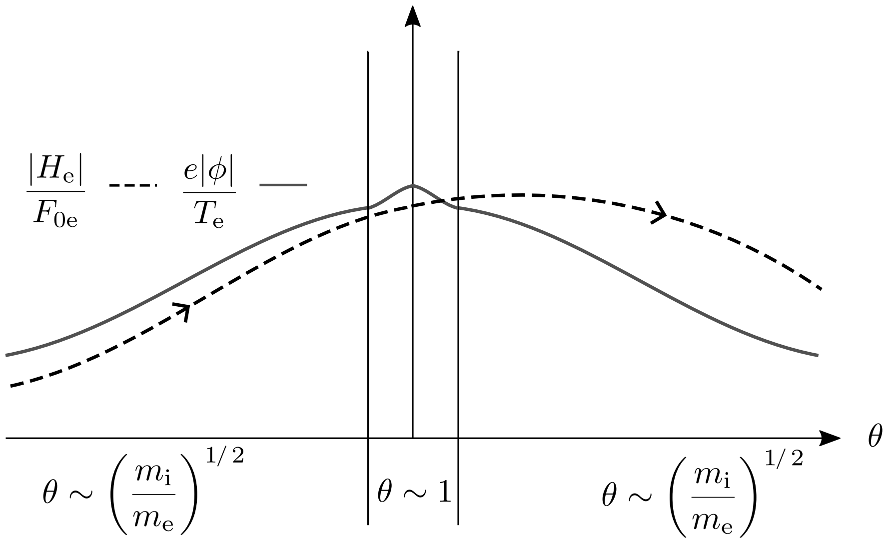

Figure 2. An illustration showing the nonadiabatic passing electron response for forward-going particles in the large-tail limit. In this limit, the electron response in the inner region ($\theta \sim (m_i/m_e)^{1/2}$) determines the mode frequency to leading order in the $(m_e/m_i)^{1/2}$ expansion: we solve equations (75) and (76) for the passing and trapped electron response, respectively, subject to quasineutrality (81). In the outer region, the electron response H_e is approximately constant, and ions respond passively, without modifying the frequency to leading order.

We recall from section 4.1.2 that $H^{(0)}_{e,\mathrm{outer}}$ is a constant in θ, and is independent of the ion response and the trapped electron response in the outer region. As a consequence, in the ordering (85) we may solve the leading-order equations (75) and (76) for $H^{(0)}_e$ in the inner region with the boundary condition that

$$H^{(0)}_{e,\mathrm{inner}}(\chi = 0^-) = H^{(0)}_{e,\mathrm{inner}}(\chi = 0^+). \tag{86}$$

Imposing quasineutrality via equation (81) results in an eigenvalue problem for $\phi^{(0)}_{\mathrm{inner}}$ and $\omega^{(0)}$. We illustrate the mode structure in the large-tail ordering in figure 2. Note in particular that the nonadiabatic passing electron response changes by only a small ($(m_e/m_i)^{1/2}$) amount over the $\theta \sim 1$ region. As a consequence of the ordering (85), and the boundary condition (86), we find that the electrostatic potential in the inner region has no mass ratio scaling with respect to the electrostatic potential in the outer region, i.e.,

$$\frac{e\phi_{\mathrm{inner}}}{T_e} \sim \frac{e\phi_{\mathrm{outer}}}{T_e}. \tag{87}$$

An interesting corollary of these arguments is that the leading order complex frequency $\omega^{(0)}$ of a large-tail mode should be independent of θ_0.

Finally, in a large-tail mode the role of the nonadiabatic ion response (and nonadiabatic trapped electron response for $\theta \sim 1$) is to modify the leading-order mode structure at $\theta \sim 1$ without modifying the frequency $\omega^{(0)}$. To see this, note that equations (75), (76), and (81) determine the frequency $\omega^{(0)}$. However, $\phi^{(0)}_{\rm outer}$ is not yet determined: in the $\theta \sim 1$ region only the nonadiabatic density due to passing electrons $\delta n^{(0)}_{\rm e,passing}$ is fixed by the passing electron tails. To obtain $\phi^{(0)}_{\rm outer}$, we solve equation (40) for the nonadiabatic ion response $h^{(0)}_{\rm i,outer} = h^{(0)}_{\rm i,outer}[\phi^{(0)}_{\rm outer}, \omega^{(0)}]$, and equation (47) for the nonadiabatic trapped electron response $H^{(0)}_{\rm e,outer-trapped} = H^{(0)}_{\rm e,outer-trapped}[\phi^{(0)}_{\rm outer}, \omega^{(0)}]$, where we have indicated that $h^{(0)}_{\rm i,outer}$ and $H^{(0)}_{\rm e,outer-trapped}$ are functionals of $\phi^{(0)}_{\rm outer}$ and functions of $\omega^{(0)}$. We then use $\theta \sim 1$ quasineutrality, equation (78), to obtain $\phi^{(0)}_{\rm outer}$ as a function of $\delta n^{(0)}_{\rm e,passing}$. The role of the nonadiabatic ion response (and the nonadiabatic trapped electron response) is to modify the response of the electrostatic potential $\phi^{(0)}_{\rm outer}$ to an input $\omega^{(0)}$ and $\delta n^{(0)}_{\rm e,passing}$.

4.5. Relating the derivation of gyrokinetics to the derivation of the transit and bounce averaged equations for the electron response

We conclude this section on collisionless physics by commenting on the relationship between the derivation of gyrokinetics and the derivation of the transit and bounce averaged equations for the electron response in the inner region. We note that in the derivation of the gyrokinetic equation the change of variables from $(\boldsymbol{r}, \varepsilon, \lambda, \gamma)$ to $(\boldsymbol{R}, \varepsilon, \lambda, \gamma)$ introduces the finite Larmor radius phase $\exp[{\rm i}\boldsymbol{k}_\perp \cdot \boldsymbol{\rho}_s]$ into the kinetic equation. The γ dependence in the kinetic equation can be removed by a gyroaverage $\langle \cdot \rangle^\gamma$ because the finite Larmor radius phases are converted into a Bessel function $J_0(b_s)$ by the gyroaverage $\langle \cdot \rangle^\gamma$, and the field $\phi(\boldsymbol{r})$ has no dependence on the gyrophase γ. In the derivation of the equations for the electron response in the inner region, equations (75) and (76), we find that the leading-order electron distribution function $H^{(0)}_{\rm e} = H^{(0)}_{\rm e}(\chi, \varepsilon, \lambda, \sigma)$ is independent of θ, and the phase $\exp[-{\rm i}\lambda_{\rm e}\chi]$ keeps track of the electron drift orbit motion. However, the potential $\phi^{(0)} = \phi^{(0)}(\theta, \chi)$ has a nontrivial dependence on θ. This can be observed by inspecting the inner region quasineutrality relation, equation (81), where we see that velocity-space structure in $H^{(0)}_{\rm e}$ influences the θ structure of $\phi^{(0)}$. As a consequence, we may not directly remove θ when solving the system of equations (75), (76), and (81).

5. Long-wavelength collisional electrostatic modes in the $(m_{\rm e}/m_{\rm i})^{1/2} \rightarrow 0$ limit

In this section, we derive reduced model equations for long-wavelength, collisional, electrostatic modes in the $(m_{\rm e}/m_{\rm i})^{1/2} \rightarrow 0$ limit. We define the collisional limit to be the limit where

$$\frac{qR_0\nu_{\rm ei}}{v_{\rm th,e}} \sim \frac{qR_0\nu_{\rm ee}}{v_{\rm th,e}} \sim 1. \tag{88}$$

We show that in the collisional limit, the scale of the mode in extended ballooning angle χ is set by the balance between parallel and perpendicular classical and neoclassical diffusion terms appearing in the equations for the mode. Heuristically, this means that we expect a balance

$$\frac{v_{\mathrm{th,e}}^2}{q^2 R_0^2 \nu_{\mathrm{ee}}} \frac{\partial^2}{\partial \chi^2} \sim \nu_{\mathrm{ee}} k_y^2 \rho_{\mathrm{th,e}}^2 \chi^2. \tag{89}$$

We can rearrange the balance (89) to give an estimate for the size of χ. We find that

$$\chi \sim \left(\frac{qR_0\nu_{\mathrm{ee}}}{v_{\mathrm{th,e}}}\right)^{-1/2} \left(\frac{m_{\mathrm{i}}}{m_{\mathrm{e}}}\right)^{1/4}. \tag{90}$$

For the collisional ordering of $qR_0\nu_{\mathrm{ee}}/v_{\mathrm{th,e}} \sim 1$, the scale of the electron tail is $\chi \sim (m_{\mathrm{i}}/m_{\mathrm{e}})^{1/4}$. As expected, the "collisionless" ordering of $qR_0\nu_{\mathrm{ee}}/v_{\mathrm{th,e}} \sim (m_{\mathrm{e}}/m_{\mathrm{i}})^{1/2}$ in the estimate (90) yields the scale $\chi \sim (m_{\mathrm{i}}/m_{\mathrm{e}})^{1/2}$. In consequence, we are able to demonstrate a smooth matching between the collisional and the collisionless limits. We discuss this matching in section 5.1.4.

In the following sections, we obtain the equations for the response of ions and electrons in a $k_y\rho_{\mathrm{th,i}} \sim 1$ mode with a $\theta \sim 1$ outer region, and a $\theta \sim (m_{\mathrm{i}}/m_{\mathrm{e}})^{1/4}$ inner region. Although the details of the equations obtained here are different to the collisionless case, the final result is qualitatively similar: two types of modes exist, large-tail modes driven by the nonadiabatic electron response at $\theta \sim (m_{\mathrm{i}}/m_{\mathrm{e}})^{1/4}$ scales, and conventional small-tail modes driven by the ion response at $\theta \sim 1$ scales. In order to motivate the $(m_{\mathrm{e}}/m_{\mathrm{i}})^{1/4}$ expansion, we first derive the equations in the $\theta \gg 1$ region. As in the collisionless case, the equations that we obtain in the $\theta \gg 1$ region are common to both classes of mode. In section 5.2, we then discuss the equations for the two different classes of modes in the $\theta \sim 1$ region. Section 5.2.2 provides a detailed description of the boundary matching between the outer and inner regions for the small-tail mode, in addition to a plenary summary for how to solve the small-tail mode equations. Finally, section 5.2.3 provides a description of the boundary matching between the outer and inner regions for the large-tail mode, and a plenary summary for how to solve the large-tail mode equations.

5.1. Collisional inner solution – $\theta \sim (m_{\mathrm{i}}/m_{\mathrm{e}})^{1/4}$ – $k_r\rho_{\mathrm{th,e}} \sim (m_{\mathrm{e}}/m_{\mathrm{i}})^{1/4}$

The collisional inner solution is characterised by fine radial scales associated with electron physics. To treat these scales, we again introduce an additional coordinate measuring distance along the magnetic field line, via the substitutions (53) and (54). We recall that the coordinate θ will measure 2π periodic variation, whereas $\chi \sim (m_{\mathrm{i}}/m_{\mathrm{e}})^{1/4}$ is an extended ballooning angle for the envelope of the mode. Refer to the discussion in section 4.2 for the details of the substitution in geometric quantities (equations (55)-(60)); and the modifications to the boundary conditions on the electron distribution function (equations (61) and (62)).

In the collisional inner region, we expand electrostatic potential ϕ, distribution functions h_s, and frequency ω in powers of $(m_{\mathrm{e}}/m_{\mathrm{i}})^{1/4}$, i.e.,

$$\phi = \phi^{(0)} + \phi^{(1/2)} + \phi^{(1)} + \mathrm{O}\left(\left(\frac{m_{\mathrm{e}}}{m_{\mathrm{i}}}\right)^{3/4}\phi\right), \tag{91}$$

with $\phi^{(n)} \sim (m_e/m_i)^{n/2}\,\phi$;

$$h_s = {h_s}^{(0)} + {h_s}^{(1/2)} + {h_s}^{(1)} + \mathrm{O}\left(\left(\frac{m_e}{m_i}\right)^{3/4} h_s\right), \tag{92}$$

where ${h_s}^{(n)} \sim (m_e/m_i)^{n/2}\,(e\phi/T_e)F_{0s}$, and

$$\omega = \omega^{(0)} + \omega^{(1/2)} + \omega^{(1)} + \mathrm{O}\left(\left(\frac{m_e}{m_i}\right)^{3/4} \omega\right). \tag{93}$$

As in the collisionless case, we leave the relative size of the fluctuations in the outer and inner regions to be determined. We will determine the relative sizes of the fluctuations in section 5.2.

To solve for the electron response we will again use the modified electron distribution function H_e, defined by equation (31). We note that in the ordering for the collisional inner region $\chi \sim (m_i/m_e)^{1/4} \gg 1 \sim \theta_0 \gg \lambda_e \sim (m_e/m_i)^{1/2}$, and hence the phase in (31) becomes

$$\exp\left[\mathrm{i}\lambda_e(\theta_0 - \theta)\right] = \left(1 - \mathrm{i}\lambda_e\chi - \frac{\lambda_e^2\chi^2}{2} + \mathrm{i}\lambda_e\theta_0 + \mathrm{O}\left(\left(\frac{m_e}{m_i}\right)^{3/4}\right)\right). \tag{94}$$

In addition, we will need to expand the phase due to the finite Larmor radius $\exp\left[\mathrm{i}\boldsymbol{k}_\perp\cdot\boldsymbol{\rho}_e\right]$ in the collision operator $C_e^{\mathrm{GK}}[\cdot]$. In the inner region, we find

$$\exp\left[\mathrm{i}\boldsymbol{k}_\perp\cdot\boldsymbol{\rho}_e\right] = 1 + \mathrm{i}\boldsymbol{k}_\perp^{(0)}\cdot\boldsymbol{\rho}_e - \frac{1}{2}(\boldsymbol{k}_\perp^{(0)}\cdot\boldsymbol{\rho}_e)^2 + \mathrm{i}\boldsymbol{k}_\perp^{(1)}\cdot\boldsymbol{\rho}_e + \mathrm{O}\left(\left(\frac{m_e}{m_i}\right)^{3/4}\right), \tag{95}$$

where we note that $\boldsymbol{k}_\perp^{(0)}\cdot\boldsymbol{\rho}_e \sim (m_e/m_i)^{1/4}$ and $\boldsymbol{k}_\perp^{(1)}\cdot\boldsymbol{\rho}_e \sim (m_e/m_i)^{1/2}$.

5.1.1. Ion response in the collisional inner region. Before considering the electron response, we first discuss the ion response in the inner region in the collisional limit. The analysis proceeds almost identically to the analysis presented in section 4.2.1 for the ion response in the collisionless limit. For $\nu_{ii}/\omega \sim 1$, we find that the leading-order equation for the ion response is

$$\frac{k_\alpha^2 q'^2|\nabla\psi|^2\chi^2 v^2}{4\Omega_i^2}\left(\nu_{\parallel,i}\lambda B + \frac{\nu_{\perp,i}}{2}\left(2-\lambda B\right)\right){h_i}^{(0)} = \mathrm{i}\left(\omega_{*,i} - \omega^{(0)}\right) J_{0i}F_{0i}\frac{Z_i e\phi^{(0)}}{T_i}. \tag{96}$$

Equation (96) has the same form as equation (64), apart from the fact that the radial magnetic drift is neglected because $\chi \sim (m_i/m_e)^{1/4}$. Equation (96) allows us to obtain an estimate for ${h_i}^{(0)}$:

$$\frac{{h_i}^{(0)}}{F_{0i}} \sim \chi^{-5/2}\frac{e\phi^{(0)}}{T_e} \sim \left(\frac{m_e}{m_i}\right)^{5/8}\frac{e\phi^{(0)}}{T_e}, \tag{97}$$

where we have employed that $J_{0i} \sim \mathrm{O}\left(\chi^{-1/2}\right)$ for $\chi \gg 1$. The estimate (97) yields estimates for the ion nonadiabatic density

$$\frac{\delta n_i^{(0)}}{n_i} \sim \left(\frac{m_e}{m_i}\right)^{3/4}\frac{e\phi^{(0)}}{T_e} \ll \frac{e\phi^{(0)}}{T_e}, \tag{98}$$

and the ion mean velocity

$$\frac{\delta \boldsymbol{u}_{\rm i}^{(0)}}{v_{\rm th,i}} \sim \left(\frac{m_{\rm e}}{m_{\rm i}}\right)^{3/4} \frac{e\phi^{(0)}}{T_{\rm e}} \ll \frac{e\phi^{(0)}}{T_{\rm e}}, \tag{99}$$

where we have used that $J_{0\rm i} \sim J_{1\rm i} \sim {\rm O}\left((m_{\rm e}/m_{\rm i})^{1/8}\right)$. We estimate the size of the ion flow velocity $\delta \boldsymbol{u}_{\rm i}$ in order to order the terms in the electron-ion piece of the electron collision operator, defined in equation (13).

5.1.2. Electron response in the collisional inner region. The calculation of the electron response in the collisional inner region has a structure that is reminiscent of neoclassical transport theory. The leading-order equation will constrain the leading-order electron distribution function to be a perturbed Maxwellian with no flows. The first-order equation takes the form of a Spitzer-Härm problem. Physically, the first-order terms control the self-consistent parallel flows that result from the leading-order perturbations. The second-order equation governs the time evolution of the leading-order fluctuations. Velocity moments of the second-order equation yield transport equations for the electron density and temperature fluctuations. In this section we calculate the forms of the transport equations in the $(m_{\rm e}/m_{\rm i})^{1/4} \to 0$ limit, with $qR_0\nu_{\rm ee}/v_{\rm th,e} \sim 1$. This calculation demonstrates that the transport equations contain background drives of instability, and parallel and perpendicular diffusion due to collisions. To obtain explicit analytical forms for the parallel flow and perpendicular diffusion terms appearing in the transport equations, in section 5.1.3, we consider the $qR_0\nu_{\rm ee}/v_{\rm th,e} \gg 1$ (Pfirsh-Schlüter) limit of collisionality. In section 5.1.4, we consider the $qR_0\nu_{\rm ee}/v_{\rm th,e} \ll 1$ (banana-plateau) limit of collisionality to demonstrate the matching between the collisionless and collisional limits.

The leading order equation for the electron response in the inner region is

$$v_\parallel \boldsymbol{b}\cdot\nabla\theta \frac{\partial H_{\rm e}^{(0)}}{\partial\theta} = C_{\rm ee}\left[H_{\rm e}^{(0)}\right] + \mathcal{L}\left[H_{\rm e}^{(0)}\right]. \tag{100}$$

To simplify the collision operators in equation (100), we have used the equations (94) and (95) for the finite-orbit-width and finite-Larmor-radius phases, respectively, and the estimate (99) for $\delta\boldsymbol{u}_{\rm i}$. We have also noted that $H_{\rm e}^{(0)}$ is gyrophase independent, and $C_{\rm ee}[\cdot]$ and $\mathcal{L}[\cdot]$ commute with $\langle\cdot\rangle^\gamma$.

To solve equation (100), we follow the standard H-theorem procedure [27, 33]: first, we multiply equation (100) by $H_{\rm e}^{(0)}/F_{0e}$, with the result

$$v_\parallel \boldsymbol{b}\cdot\nabla\theta \frac{\partial}{\partial\theta}\left(\left(H_{\rm e}^{(0)}\right)^2/2F_{0e}\right) = \frac{H_{\rm e}^{(0)}}{F_{0e}} C_{\rm ee}\left[H_{\rm e}^{(0)}\right] + \frac{H_{\rm e}^{(0)}}{F_{0e}}\mathcal{L}\left[H_{\rm e}^{(0)}\right]. \tag{101}$$

Second, we integrate over velocity space

$$\boldsymbol{B}\cdot\nabla\theta\frac{\partial}{\partial\theta}\left(\int \frac{v_\parallel}{B}\left(H_{\rm e}^{(0)}\right)^2/2F_{0e}\, d^3\boldsymbol{v}\right)$$

$$= \int \frac{H_{\rm e}^{(0)}}{F_{0e}} C_{\rm ee}\left[H_{\rm e}^{(0)}\right]\, d^3\boldsymbol{v} + \int \frac{H_{\rm e}^{(0)}}{F_{0e}}\mathcal{L}\left[H_{\rm e}^{(0)}\right]\, d^3\boldsymbol{v}, \tag{102}$$

where we have used the form of the velocity integral in (ε, λ) coordinates,

$$\int \cdot \, d^3\boldsymbol{v} = \sum_\sigma \int_0^\infty \int_0^{1/B} \frac{2\pi B \varepsilon}{m_s^2 |v_\parallel|} \cdot \, d\lambda \, d\varepsilon \tag{103}$$

and taken the $\partial/\partial\theta$ derivative through the integral. Finally, we apply the poloidal angle average

$$\langle \cdot \rangle^\theta = \int_{-\pi}^{\pi} \cdot \frac{d\theta}{\boldsymbol{B} \cdot \nabla\theta} \Big/ \int_{-\pi}^{\pi} \frac{d\theta}{\boldsymbol{B} \cdot \nabla\theta} \tag{104}$$

to equation (102), and impose periodicity of $H_{\rm e}^{(0)}$ in θ, to obtain

$$\left\langle \int \frac{H_{\rm e}^{(0)}}{F_{0e}} C_{\rm ee}\left[H_{\rm e}^{(0)}\right] \, d^3\boldsymbol{v} \right\rangle^\theta + \left\langle \int \frac{H_{\rm e}^{(0)}}{F_{0e}} \mathcal{L}\left[H_{\rm e}^{(0)}\right] \, d^3\boldsymbol{v} \right\rangle^\theta = 0. \tag{105}$$

The collision operators $C_{\rm ee}[\cdot]$ and $\mathcal{L}[\cdot]$ have the properties [27]

$$\int \frac{g}{F_{0e}} C_{\rm ee}[g] \, d^3\boldsymbol{v} \leq 0 \quad \text{and} \quad \int \frac{g}{F_{0e}} \mathcal{L}[g] \, d^3\boldsymbol{v} \leq 0, \tag{106}$$

respectively. Collisions always increase the entropy of the system. The equality $\int (g/F_{0e}) \, C_{\rm ee}[g] \, d^3\boldsymbol{v} = 0$ is only achieved when g is a perturbed Maxwellian so that $C_{\rm ee}[g] = 0$. The equality $\int (g/F_{0e}) \, \mathcal{L}[g] \, d^3\boldsymbol{v} = 0$ is only achieved when g is isotropic in $\boldsymbol{v}$ so that $\mathcal{L}[g] = 0$. As a consequence of equation (105), we find that $H_{\rm e}^{(0)}$ is a perturbed Maxwellian with no flow, i.e.,

$$H_{\rm e}^{(0)} = \left(\frac{\delta n_{\rm e}^{(0)}}{n_{\rm e}} + \frac{\delta T_{\rm e}^{(0)}}{T_{\rm e}} \left(\frac{\varepsilon}{T_{\rm e}} - \frac{3}{2} \right) \right) F_{0e}, \tag{107}$$

where $\delta n_{\rm e}^{(0)}$ and $\delta T_{\rm e}^{(0)}$ are functions of θ and χ to be determined. Returning to equation (100), we now find that $H_{\rm e}^{(0)}$ must satisfy

$$v_\parallel \boldsymbol{b} \cdot \nabla\theta \frac{\partial H_{\rm e}^{(0)}}{\partial\theta} = 0. \tag{108}$$

For equation (108) to hold for all ε, we must have that $\delta n_{\rm e}^{(0)}$ and $\delta T_{\rm e}^{(0)}$ are constant in θ, i.e.,

$$\delta n_{\rm e}^{(0)} = \delta n_{\rm e}^{(0)}(\chi), \quad \text{and} \quad \delta T_{\rm e}^{(0)} = \delta T_{\rm e}^{(0)}(\chi). \tag{109}$$

To obtain evolution equations for $\delta n_{\rm e}^{(0)}$ and $\delta T_{\rm e}^{(0)}$, we will need to go to $\mathrm{O}\left((m_{\rm e}/m_{\rm i})^{1/2}\right)$ in the expansion.

Before proceeding to higher order in the expansion, we consider the collisional inner-region quasineutrality relation. Using the expansion (94), the ordering (98), and the solution (107), with $J_{0\rm e} = 1 + \mathrm{O}\left((m_{\rm e}/m_{\rm i})^{1/2}\right)$ for $\chi \sim (m_{\rm i}/m_{\rm e})^{1/4}$, we find that the leading-order quasineutrality relation is

$$\left(\frac{Z_{\rm i} T_{\rm e}}{T_{\rm i}} + 1 \right) \frac{e\phi^{(0)}}{T_{\rm e}} = -\int \frac{H_{\rm e}^{(0)}}{n_{\rm e}} \, d^3\boldsymbol{v} = -\frac{\delta n_{\rm e}^{(0)}}{n_{\rm e}}. \tag{110}$$

Equation (110) allows us to note that the electrostatic potential in the inner region is not a function of geometric angle θ, i.e., $\phi^{(0)} = \phi^{(0)}(\chi)$. This is a significant simplification over the collisionless case (cf. equation (81)), where $\phi^{(0)} = \phi^{(0)}(\theta, \chi)$. This simplification arises in the collisional limit because, first, there is no distinction between trapped and passing particles, and second, the extent of the mode is shortened to $\chi \sim (m_\mathrm{i}/m_\mathrm{e})^{1/4}$ so that the phase $\exp[\mathrm{i}\lambda_\mathrm{e}\chi] = 1 + \mathrm{O}\left((m_\mathrm{e}/m_\mathrm{i})^{1/4}\right)$, and $J_{0\mathrm{e}} = 1 + \mathrm{O}\left((m_\mathrm{e}/m_\mathrm{i})^{1/2}\right)$.

The $\mathrm{O}\left((m_\mathrm{e}/m_\mathrm{i})^{1/4}\right)$ equation for the electron response in the inner region takes the form

$$v_\parallel \boldsymbol{b}\cdot\nabla\theta \frac{\partial H_\mathrm{e}^{(1/2)}}{\partial\theta} + v_\parallel \boldsymbol{b}\cdot\nabla\theta \frac{\partial H_\mathrm{e}^{(0)}}{\partial\chi} = \mathcal{C}\left[H_\mathrm{e}^{(1/2)} + \mathrm{i}\lambda_\mathrm{e}\chi H_\mathrm{e}^{(0)}\right], \tag{111}$$

where

$$\mathcal{C}[\cdot] = C_\mathrm{ee}[\cdot] + \mathcal{L}[\cdot]. \tag{112}$$

To expand the collision operator (34) for electrons, we have used the definition (13), equations (94) and (95), the estimate (99), and the identities

$$\left\langle \mathrm{i}\boldsymbol{k}_\perp^{(0)}\cdot\boldsymbol{\rho}_e\,\mathcal{C}\left[H_\mathrm{e}^{(0)}\right]\right\rangle^\gamma = 0, \tag{113}$$

$$\left\langle \mathcal{C}\left[\mathrm{i}\boldsymbol{k}_\perp^{(0)}\cdot\boldsymbol{\rho}_e\,H_\mathrm{e}^{(0)}\right]\right\rangle^\gamma = 0, \tag{114}$$

and

$$\mathcal{C}[H_\mathrm{e}^{(0)}] = 0. \tag{115}$$

Equation (111) bears a resemblance to the neoclassical drift-kinetic equation in the banana collisionality regime [27, 33]. We note that the term $v_\parallel \boldsymbol{b}\cdot\nabla\theta\partial H_\mathrm{e}^{(0)}/\partial\chi$ plays the role of the equilibrium inductive electric field in the corresponding neoclassical equation. The resemblance can be made explicit by absorbing the $v_\parallel \boldsymbol{b}\cdot\nabla\theta\partial H_\mathrm{e}^{(0)}/\partial\chi$ term into the collision operators by solving the Spitzer-Härm problem [26, 27, 34]

$$v_\parallel \boldsymbol{b}\cdot\nabla\theta\frac{\partial H_\mathrm{e}^{(0)}}{\partial\chi} = \mathcal{C}[H_\mathrm{SH}]. \tag{116}$$

It is useful to note that because the collision operator $\mathcal{C}[\cdot]$ is isotropic [27], H_SH must have the form

$$H_\mathrm{SH} = v_\parallel K_\mathrm{SH}(\varepsilon,\chi)F_{0e}, \tag{117}$$

where K_SH is a function of ε and χ. We determine K_SH in Appendix B.

Using the Spitzer-Härm solution provided by equation (116), we can rewrite the equation in the following form

$$v_\parallel \boldsymbol{b}\cdot\nabla\theta\frac{\partial H_\mathrm{e}^{(1/2)}}{\partial\theta} = \mathcal{C}\left[H_\mathrm{e}^{(1/2)} + \mathrm{i}\lambda_\mathrm{e}\chi H_\mathrm{e}^{(0)} - H_\mathrm{SH}\right]. \tag{118}$$

In general, equation (118) is not solvable analytically. To maximise the physical insight from the calculation we will subsequently solve equation (118) in the subsidiary limits of large and small collisionality, and comment on the result for the time evolution of $\delta n_\mathrm{e}^{(0)}$ and $\delta T_\mathrm{e}^{(0)}$.

To demonstrate the physics controlling the time evolution of $\delta n_{\rm e}^{(0)}$ and $\delta T_{\rm e}^{(0)}$, we continue to the $\mathrm{O}\left((m_{\rm e}/m_{\rm i})^{1/2}\right)$ equation, presuming that $H_{\rm e}^{(1/2)}$ in equation (118) can be satisfactorily solved for numerically. After collecting terms of $\mathrm{O}\left((m_{\rm e}/m_{\rm i})^{1/2}\right)$, we find that the equation that determines $H_{\rm e}^{(0)}$ is

$$\begin{aligned}
&v_\| \boldsymbol{b}\cdot\nabla\theta \frac{\partial H_{\rm e}^{(1)}}{\partial\theta} + v_\| \boldsymbol{b}\cdot\nabla\theta \frac{\partial H_{\rm e}^{(1/2)}}{\partial\chi} + {\rm i}(\omega_{\rm M,e} - \omega^{(0)}) H_{\rm e}^{(0)} \\
&-\mathcal{C}\left[H_{\rm e}^{(1)} + {\rm i}\lambda_{\rm e}\chi H_{\rm e}^{(1/2)} - \left(\frac{1}{2}\left(\lambda_{\rm e}^2\chi^2 + \left\langle (\boldsymbol{k}_\perp^{(0)}\cdot\boldsymbol{\rho}_e)^2\right\rangle^\gamma\right) + {\rm i}\lambda_{\rm e}\theta_0\right) H_{\rm e}^{(0)}\right] \qquad (119)\\
&+{\rm i}\lambda_{\rm e}\chi\,\mathcal{C}\left[H_{\rm e}^{(1/2)} + {\rm i}\lambda_{\rm e}\chi H_{\rm e}^{(0)}\right] - \left\langle \boldsymbol{k}_\perp^{(0)}\cdot\boldsymbol{\rho}_e\,\mathcal{C}\left[\boldsymbol{k}_\perp^{(0)}\cdot\boldsymbol{\rho}_e\,H_{\rm e}^{(0)}\right]\right\rangle^\gamma = -{\rm i}(\omega_{*,\rm e} - \omega^{(0)}) F_{0e}\frac{e\phi^{(0)}}{T_{\rm e}},
\end{aligned}$$

where, to obtain equation (119), we have used equations (94) and (95), estimate (99), identities (113)-(115), that $J_{0\rm e} = 1 + \mathrm{O}\left((m_{\rm e}/m_{\rm i})^{1/2}\right)$ for $\chi \sim (m_{\rm i}/m_{\rm e})^{1/4}$, and that $\mathcal{C}[\cdot]$ and $\langle\cdot\rangle^\gamma$ commute.

We can convert equation (119) into equations for $\delta n_{\rm e}^{(0)}(\chi)$ and $\delta T_{\rm e}^{(0)}(\chi)$ by multiplying equation (119) by the appropriate velocity space function (1 or $\varepsilon/T_{\rm e} - 3/2$), integrating over velocity space, integrating over θ, and finally imposing on $H_{\rm e}^{(1)}$ the condition of 2π-periodicity in θ. After performing these operations, and dividing by $n_{\rm e}$, the equation for the density moment is

$$\begin{aligned}
&\frac{\partial}{\partial\chi}\left(\left\langle \boldsymbol{b}\cdot\nabla\theta\;\delta U_{\|,\rm e}^{(1/2)}\right\rangle^\theta\right) + {\rm i}\left\langle\omega_{\rm M,e}^{\rm th}\right\rangle^\theta\left(\frac{\delta n_{\rm e}^{(0)}}{n_{\rm e}} + \frac{\delta T_{\rm e}^{(0)}}{T_{\rm e}}\right) - {\rm i}\omega^{(0)}\frac{\delta n_{\rm e}^{(0)}}{n_{\rm e}} \\
&+\left\langle \frac{1}{n_{\rm e}}\int {\rm i}\lambda_{\rm e}\chi\,\mathcal{C}\left[H_{\rm e}^{(1/2)} + {\rm i}\lambda_{\rm e}\chi H_{\rm e}^{(0)}\right]\,d^3\boldsymbol{v}\right\rangle^\theta - \left\langle\frac{1}{n_{\rm e}}\int\left\langle \boldsymbol{k}_\perp^{(0)}\cdot\boldsymbol{\rho}_e\,\mathcal{C}\left[\boldsymbol{k}_\perp^{(0)}\cdot\boldsymbol{\rho}_e\,H_{\rm e}^{(0)}\right]\right\rangle^\gamma\,d^3\boldsymbol{v}\right\rangle^\theta \\
&\qquad = -{\rm i}(\omega_{*,\rm e}^n - \omega^{(0)})\frac{e\phi^{(0)}}{T_{\rm e}}, \qquad (120)
\end{aligned}$$

where we have defined the thermal magnetic drift frequency

$$\omega_{\rm M,e}^{\rm th} = \frac{k_\alpha v_{\rm th,e}^2}{2\Omega_{\rm e}}\left(\boldsymbol{b}\times\left(\boldsymbol{b}\cdot\nabla\boldsymbol{b} + \frac{\nabla B}{B}\right)\cdot(\nabla\alpha + \theta\nabla q) + \boldsymbol{b}\cdot\nabla\theta q' I\right), \qquad (121)$$

the $n^{\rm th}$-order component of the $v_\|$ moment of $H_{\rm e}^{(0)}$

$$\delta U_{\|,\rm e}^{(n)} = \frac{1}{n_{\rm e}}\int v_\| H_{\rm e}^{(n)}\,d^3\boldsymbol{v}, \qquad (122)$$

and used that the collision operator $\mathcal{C}[\cdot]$ satisfies

$$\int \mathcal{C}[f]\;d^3\boldsymbol{v} = 0, \qquad (123)$$

for f an arbitrary function of $\boldsymbol{v}$. Similarly, the equation for the electron temperature is

$$\frac{\partial}{\partial\chi}\left(\left\langle \boldsymbol{b}\cdot\nabla\theta\left(\frac{\delta Q_{\|,\rm e}^{(1/2)}}{n_{\rm e}T_{\rm e}} + \delta U_{\|,\rm e}^{(1/2)}\right)\right\rangle^\theta\right) + {\rm i}\left\langle\omega_{\rm M,e}^{\rm th}\right\rangle^\theta\left(\frac{\delta n_{\rm e}^{(0)}}{n_{\rm e}} + \frac{7}{2}\frac{\delta T_{\rm e}^{(0)}}{T_{\rm e}}\right) - {\rm i}\frac{3}{2}\omega^{(0)}\frac{\delta T_{\rm e}^{(0)}}{T_{\rm e}}$$

$$+\left\langle \frac{1}{n_{\mathrm{e}}}\int \left(\frac{\varepsilon}{T_{\mathrm{e}}}-\frac{3}{2}\right) \mathrm{i}\lambda_{\mathrm{e}}\chi\, \mathcal{C}\left[H_{\mathrm{e}}^{(1/2)}+\mathrm{i}\lambda_{\mathrm{e}}\chi H_{\mathrm{e}}^{(0)}\right]\; d^3\boldsymbol{v}\right\rangle^{\theta} \tag{124}$$

$$-\left\langle \frac{1}{n_{\mathrm{e}}}\int \left(\frac{\varepsilon}{T_{\mathrm{e}}}-\frac{3}{2}\right) \left\langle \boldsymbol{k}_{\perp}^{(0)}\cdot\boldsymbol{\rho}_e\, \mathcal{C}\left[\boldsymbol{k}_{\perp}^{(0)}\cdot\boldsymbol{\rho}_e\; H_{\mathrm{e}}^{(0)}\right]\right\rangle^{\gamma}\; d^3\boldsymbol{v}\right\rangle^{\theta} = -\mathrm{i}\frac{3}{2}\omega_{*,\mathrm{e}}^{n}\eta_{\mathrm{e}}\frac{e\phi^{(0)}}{T_{\mathrm{e}}},$$

where we have defined the n^{th}-order component of the $v_{\parallel}(\varepsilon/T_{\mathrm{e}}-5/2)$ moment of $H_{\mathrm{e}}^{(0)}$

$$\delta Q_{\parallel,\mathrm{e}}^{(n)} = \int v_{\parallel}\left(\varepsilon-\frac{5T_{\mathrm{e}}}{2}\right) H_{\mathrm{e}}^{(n)}\; d^3\boldsymbol{v}, \tag{125}$$

and used that the collision operator $\mathcal{C}\left[\cdot\right]$ satisfies

$$\int \left(\frac{\varepsilon}{T_{\mathrm{e}}}-\frac{3}{2}\right)\mathcal{C}\left[f\right]\; d^3\boldsymbol{v} = 0. \tag{126}$$

With the solution of equation (118) for $H_{\mathrm{e}}^{(1/2)}$, equations (110), (120), and (124) represent a closed system of transport equations for $\phi^{(0)}$, $\delta n_{\mathrm{e}}^{(0)}$, and $\delta T_{\mathrm{e}}^{(0)}$.

Equations (120) and (124) may be written in a form where the terms admit simple physical interpretations. The simple forms of the density and temperature equations are

$$\langle \boldsymbol{b}\cdot\nabla\theta\rangle^{\theta}\frac{\partial\overline{\delta u_{\parallel}}}{\partial\chi} + \mathrm{i}\,\langle\omega_D\rangle^{\theta}\left(\frac{\delta n_{\mathrm{e}}^{(0)}}{n_{\mathrm{e}}}+\frac{\delta T_{\mathrm{e}}^{(0)}}{T_{\mathrm{e}}}\right) - \mathrm{i}\omega^{(0)}\frac{\delta n_{\mathrm{e}}^{(0)}}{n_{\mathrm{e}}} - \mathrm{i}k_y\hat{s}\hat{\kappa}\chi\left(\frac{\overline{\delta\Gamma}_{\mathrm{C}}}{n_{\mathrm{e}}}+\frac{\overline{\delta\Gamma}_{\mathrm{N}}}{n_{\mathrm{e}}}\right) \tag{127}$$

$$= -\mathrm{i}(\omega_{*,\mathrm{e}}^{n}-\omega^{(0)})\frac{e\phi^{(0)}}{T_{\mathrm{e}}},$$

and

$$\langle \boldsymbol{b}\cdot\nabla\theta\rangle^{\theta}\frac{\partial}{\partial\chi}\left(\frac{\overline{\delta q_{\parallel}}}{n_{\mathrm{e}}T_{\mathrm{e}}}+\overline{\delta u_{\parallel}}\right) + \mathrm{i}\,\langle\omega_D\rangle^{\theta}\left(\frac{\delta n_{\mathrm{e}}^{(0)}}{n_{\mathrm{e}}}+\frac{7}{2}\frac{\delta T_{\mathrm{e}}^{(0)}}{T_{\mathrm{e}}}\right) - \mathrm{i}\frac{3}{2}\omega^{(0)}\frac{\delta T_{\mathrm{e}}^{(0)}}{T_{\mathrm{e}}}$$

$$-\mathrm{i}k_y\hat{s}\hat{\kappa}\chi\left(\frac{\overline{\delta\Gamma}_{\mathrm{C}}}{n_{\mathrm{e}}}+\frac{\overline{\delta q}_{\mathrm{C}}}{n_{\mathrm{e}}T_{\mathrm{e}}}+\frac{\overline{\delta\Gamma}_{\mathrm{N}}}{n_{\mathrm{e}}}+\frac{\overline{\delta q}_{\mathrm{N}}}{n_{\mathrm{e}}T_{\mathrm{e}}}\right) = -\mathrm{i}\frac{3}{2}\omega_{*,\mathrm{e}}^{n}\eta_{\mathrm{e}}\frac{e\phi^{(0)}}{T_{\mathrm{e}}}, \tag{128}$$

respectively. To obtain equations (127) and (128), we use the definitions of the leading-order nonzero components of the electron parallel velocity,

$$\delta u_{\parallel,\mathrm{e}}^{(1/2)} = \frac{1}{n_{\mathrm{e}}}\int v_{\parallel}(H_{\mathrm{e}}^{(1/2)}+\mathrm{i}\lambda_{\mathrm{e}}\chi H_{\mathrm{e}}^{(0)})\; d^3\boldsymbol{v}, \tag{129}$$

and electron parallel heat flux

$$\delta q_{\parallel,\mathrm{e}}^{(1/2)} = \frac{1}{n_{\mathrm{e}}}\int v_{\parallel}\left(\varepsilon-\frac{5T_{\mathrm{e}}}{2}\right)(H_{\mathrm{e}}^{(1/2)}+\mathrm{i}\lambda_{\mathrm{e}}\chi H_{\mathrm{e}}^{(0)})\; d^3\boldsymbol{v}, \tag{130}$$

the definitions of the effective parallel velocity and effective parallel heat flux,

$$\overline{\delta u_{\parallel}} = \frac{1}{\langle \boldsymbol{b}\cdot\nabla\theta\rangle^{\theta}}\left\langle \boldsymbol{b}\cdot\nabla\theta\;\delta u_{\parallel,\mathrm{e}}^{(1/2)}\right\rangle^{\theta}, \tag{131}$$

and

$$\overline{\delta q_{\parallel}} = \frac{1}{\langle \boldsymbol{b}\cdot\nabla\theta\rangle^{\theta}}\left\langle \boldsymbol{b}\cdot\nabla\theta\;\delta q_{\parallel,\mathrm{e}}^{(1/2)}\right\rangle^{\theta}, \tag{132}$$

respectively, the definition of the thermal magnetic precession drift

$$\omega_D = \frac{k_\alpha v_{\rm th,e}^2}{2\Omega_{\rm e}} \boldsymbol{b} \times \left(\boldsymbol{b} \cdot \nabla \boldsymbol{b} + \frac{\nabla B}{B} \right) \cdot \left(\nabla \alpha + \theta \nabla q \right), \tag{133}$$

the definition of $H_{\rm SH}$ via equation (116), and the definition of the fluctuating perpendicular fluxes: the classical particle flux

$$\overline{\delta\Gamma}_{\rm C} = {\rm i} \left\langle \int \nabla r \cdot \boldsymbol{\rho}_e \, \mathcal{C} \left[\boldsymbol{k}_\perp^{(0)} \cdot \boldsymbol{\rho}_e \, H_{\rm e}^{(0)} \right] \, d^3\boldsymbol{v} \right\rangle^\theta, \tag{134}$$

the classical heat flux

$$\overline{\delta q}_{\rm C} = {\rm i} \left\langle \int \left(\varepsilon - \frac{5T_{\rm e}}{2} \right) \nabla r \cdot \boldsymbol{\rho}_e \, \mathcal{C} \left[\boldsymbol{k}_\perp^{(0)} \cdot \boldsymbol{\rho}_e \, H_{\rm e}^{(0)} \right] \, d^3\boldsymbol{v} \right\rangle^\theta, \tag{135}$$

the neoclassical particle flux

$$\overline{\delta\Gamma}_{\rm N} = -\left\langle \frac{I}{\Omega_{\rm e}} \frac{dr}{d\psi} \int v_\parallel \, \mathcal{C} \left[H_{\rm e}^{(1/2)} + {\rm i}\lambda_{\rm e} \chi H_{\rm e}^{(0)} - H_{\rm SH} \right] \, d^3\boldsymbol{v} \right\rangle^\theta, \tag{136}$$

and the neoclassical heat flux

$$\overline{\delta q}_{\rm N} = -\left\langle \frac{I}{\Omega_{\rm e}} \frac{dr}{d\psi} \int \left(\varepsilon - \frac{5T_{\rm e}}{2} \right) v_\parallel \, \mathcal{C} \left[H_{\rm e}^{(1/2)} + {\rm i}\lambda_{\rm e} \chi H_{\rm e}^{(0)} - H_{\rm SH} \right] \, d^3\boldsymbol{v} \right\rangle^\theta. \tag{137}$$

In writing the definitions (129) and (130), we have used that in the inner-region ${h_{\rm e}}^{(0)} = H_{\rm e}^{(0)}$, ${h_{\rm e}}^{(1/2)} = H_{\rm e}^{(1/2)} + {\rm i}\lambda_{\rm e}\chi H_{\rm e}^{(0)}$, and that $J_{0{\rm e}} = 1 + {\rm O}\left((m_{\rm e}/m_{\rm i})^{1/2} \right)$. The physical interpretations of the terms in equations (127) and (128) are the following, from left to right: parallel diffusion, magnetic (precession) drifts within the flux surface, time evolution, classical perpendicular diffusion, neoclassical perpendicular diffusion, and drives by equilibrium gradients.

The classical, finite-Larmor-radius perpendicular diffusion terms in equations (127) and (128) can be evaluated for arbitrary $qR_0\nu_{\rm ee}/v_{\rm th,e}$. We use the results of Appendix A to write down the classical particle flux $\overline{\delta\Gamma}_{\rm C}$ and classical heat flux $\overline{\delta q}_{\rm C}$. We use result (A.4) to find that

$$\frac{\overline{\delta\Gamma}_{\rm C}}{n_{\rm e}} = {\rm i}k_y \hat{s}\hat{\kappa}\chi \frac{\nu_{\rm ei}\overline{\rho}_{\rm th,e}^2}{2} \left\langle \overline{B}^2 \frac{|\nabla r|^2}{B^2} \right\rangle^\theta \left(\frac{\delta n_{\rm e}^{(0)}}{n_{\rm e}} - \frac{1}{2}\frac{\delta T_{\rm e}^{(0)}}{T_{\rm e}} \right), \tag{138}$$

where we have used that $\boldsymbol{k}_\perp^{(0)} = -k_\alpha (dq/dr)\chi \nabla r = -k_y \hat{s}\hat{\kappa}\chi\nabla r$, with $\overline{\rho}_{\rm th,e} = v_{\rm th,e}/\overline{\Omega}_{\rm e}$, $\overline{\Omega}_{\rm e} = -e\overline{B}/m_{\rm e}c$, and $\overline{B} = \langle B \rangle^\theta$. Similarly, we use the results (A.5) and (A.19) to find that

$$\frac{\overline{\delta q}_{\rm C}}{n_{\rm e}T_{\rm e}} = {\rm i}k_y \hat{s}\hat{\kappa}\chi \frac{\nu_{\rm ei}\overline{\rho}_{\rm th,e}^2}{2} \left\langle \overline{B}^2 \frac{|\nabla r|^2}{B^2} \right\rangle^\theta \left(\left(\frac{7}{4} + \frac{\sqrt{2}}{Z_{\rm i}} \right) \frac{\delta T_{\rm e}^{(0)}}{T_{\rm e}} - \frac{3}{2}\frac{\delta n_{\rm e}^{(0)}}{n_{\rm e}} \right), \tag{139}$$

where we have used that $\nu_{\rm ee}/\nu_{\rm ei} = 1/Z_{\rm i}$.

The mode evolution equations for the density and the temperature, equations (127) and (128), respectively, have the structure promised at the outset of this calculation. The envelope of the mode is controlled by the combination of the finite-orbit-width and finite-Larmor-radius perpendicular diffusion, and parallel diffusion. The perpendicular diffusion terms scale as $\nu_{\rm ei}(k_y\rho_{\rm th,e})^2\chi^2$, whereas equations (118), (131) and (132) show implicitly that the parallel diffusion terms scale as $(v_{\rm th,e}^2/\nu_{\rm ei}q^2R_0^2)\partial^2/\partial\chi^2$. This result justifies the initial ordering (90) and the discussion in section 5.1. To obtain explicit analytical forms for all terms in the transport equations (127) and (128), in the next section, we consider the $qR_0\nu_{\rm ee}/v_{\rm th,e} \gg 1$ (Pfirsh-Schlüter) regime. The resulting analytical forms for the transport equations illustrate the physics of the mode evolution. To demonstrate the matching between the collisionless and collisional regimes, in section 5.1.4, we consider the $qR_0\nu_{\rm ee}/v_{\rm th,e} \ll 1$ (banana-plateau) regime.

5.1.3. Parallel flows and perpendicular diffusion in the subsidiary limit of $qR_0\nu_{\rm ee}/v_{\rm th,e} \gg 1$ – the Pfirsh-Schlüter regime. In order to obtain the analytical form of the transport equations in the subsidiary limit $qR_0\nu_{\rm ee}/v_{\rm th,e} \gg 1$, we must solve equation (118) to obtain approximate solutions for $H_{\rm e}^{(1/2)}$. We expand

$$H_{\rm e}^{(1/2)} = H_{{\rm e},(-1)}^{(1/2)} + H_{{\rm e},(0)}^{(1/2)} + H_{{\rm e},(1)}^{(1/2)} + {\rm O}\left(\left(\frac{qR_0\nu_{\rm ee}}{v_{\rm th,e}}\right)^{-2} {\rm i}\lambda_{\rm e}\chi H_{\rm e}^{(0)}\right), \quad (140)$$

with

$$H_{{\rm e},(n)}^{(1/2)} \sim \left(\frac{qR_0\nu_{\rm ee}}{v_{\rm th,e}}\right)^{-n} H_{{\rm e},(0)}^{(1/2)} \quad (141)$$

and $H_{{\rm e},(0)}^{(1/2)} \sim {\rm i}\lambda_{\rm e}\chi H_{\rm e}^{(0)} \sim H_{\rm SH}$. The ordering ${\rm i}\lambda_{\rm e}\chi H_{\rm e}^{(0)} \sim H_{\rm SH}$ is a manifestation of the ordering (90) for χ.

With the expansion (140), the leading-order form of equation (118) is

$$\mathcal{C}\left[H_{{\rm e},(-1)}^{(1/2)}\right] = 0, \quad (142)$$

i.e.,

$$H_{{\rm e},(-1)}^{(1/2)} = \left(\frac{\delta n_{{\rm e},(-1)}^{(1/2)}}{n_{\rm e}} + \frac{\delta T_{{\rm e},(-1)}^{(1/2)}}{T_{\rm e}}\left(\frac{\varepsilon}{T_{\rm e}} - \frac{3}{2}\right)\right) F_{0e} \quad (143)$$

is a perturbed Maxwellian distribution function with no flow. Note that $\delta n_{{\rm e},(-1)}^{(1/2)} = \delta n_{{\rm e},(-1)}^{(1/2)}(\theta,\chi)$ and $\delta T_{{\rm e},(-1)}^{(1/2)} = \delta T_{{\rm e},(-1)}^{(1/2)}(\theta,\chi)$ are functions of both geometric poloidal angle θ and the ballooning angle χ.

To obtain equations for $\delta n_{{\rm e},(-1)}^{(1/2)}$ and $\delta T_{{\rm e},(-1)}^{(1/2)}$, we must go to the second-order equation in the subsidiary expansion. We proceed to the first-order equation in the subsidiary expansion, which is

$$v_\parallel \boldsymbol{b}\cdot\nabla\theta\frac{\partial}{\partial\theta}\left(H_{{\rm e},(-1)}^{(1/2)}\right) = \mathcal{C}\left[H_{{\rm e},(0)}^{(1/2)} + {\rm i}\lambda_{\rm e}\chi H_{\rm e}^{(0)} - H_{\rm SH}\right]. \quad (144)$$

Equation (144) can be solved by inverting an additional Spitzer-Härm problem

$$v_\parallel \boldsymbol{b}\cdot\nabla\theta\frac{\partial}{\partial\theta}\left(H_{{\rm e},(-1)}^{(1/2)}\right) = \mathcal{C}\left[H_{\rm SH}^{(1/2)}\right]. \quad (145)$$

With the Spitzer-Härm distribution $H_{\rm SH}^{(1/2)}$ defined by equation (145), we may write equation (144) in the form

$$\mathcal{C}\left[H_{{\rm e},(0)}^{(1/2)} + {\rm i}\lambda_{\rm e}\chi H_{\rm e}^{(0)} - H_{\rm SH} - H_{\rm SH}^{(1/2)}\right] = 0. \quad (146)$$

Hence, we find that

$$H^{(1/2)}_{\mathrm{e},(0)} = \left(\frac{\delta n^{(1/2)}_{\mathrm{e},(0)}}{n_\mathrm{e}} + \frac{\delta T^{(1/2)}_{\mathrm{e},(0)}}{T_\mathrm{e}} \left(\frac{\varepsilon}{T_\mathrm{e}} - \frac{3}{2} \right) \right) F_{0e} - \mathrm{i}\lambda_\mathrm{e}\chi H^{(0)}_\mathrm{e} + H_\mathrm{SH} + H^{(1/2)}_\mathrm{SH}, \tag{147}$$

where $\delta n^{(1/2)}_{\mathrm{e},(0)} = \delta n^{(1/2)}_{\mathrm{e},(0)}(\theta,\chi)$ and $\delta T^{(1/2)}_{\mathrm{e},(0)} = \delta T^{(1/2)}_{\mathrm{e},(0)}(\theta,\chi)$. The second-order equation in the subsidiary expansion of equation (118) is

$$v_\parallel \boldsymbol{b}\cdot\nabla\theta \frac{\partial}{\partial\theta}\left(H^{(1/2)}_{\mathrm{e},(0)}\right) = \mathcal{C}\left[H^{(1/2)}_{\mathrm{e},(1)}\right]. \tag{148}$$

The equations for $\delta n^{(1/2)}_{\mathrm{e},(-1)}$ and $\delta T^{(1/2)}_{\mathrm{e},(-1)}$ are obtained from the solvability conditions of equation (148). These are

$$\boldsymbol{B}\cdot\nabla\theta\frac{\partial}{\partial\theta}\left(\int \frac{v_\parallel}{B} H^{(1/2)}_{\mathrm{e},(0)}\, d^3\boldsymbol{v}\right) = 0 \tag{149}$$

and

$$\boldsymbol{B}\cdot\nabla\theta\frac{\partial}{\partial\theta}\left(\int \frac{v_\parallel}{B}\left(\frac{\varepsilon}{T_\mathrm{e}} - \frac{5}{2}\right) H^{(1/2)}_{\mathrm{e},(0)}\, d^3\boldsymbol{v}\right) = 0. \tag{150}$$

The conditions (149) and (150) are obtained by multiplying equation (148) by 1 and $\varepsilon/T_\mathrm{e} - 5/2$, respectively, and integrating over velocity space. Equations (149) and (150) indicate that

$$\int \frac{v_\parallel}{B} H^{(1/2)}_{\mathrm{e},(0)}\, d^3\boldsymbol{v} = \mathcal{K}_n(\chi) \tag{151}$$

and

$$\int \frac{v_\parallel}{B}\left(\frac{\varepsilon}{T_\mathrm{e}} - \frac{5}{2}\right) H^{(1/2)}_{\mathrm{e},(0)}\, d^3\boldsymbol{v} = \mathcal{K}_T(\chi), \tag{152}$$

respectively, where $\mathcal{K}_n(\chi)$ and $\mathcal{K}_T(\chi)$ are functions of the ballooning angle χ only. In Appendix C, we use these solvability conditions to obtain equations for $\delta n^{(1/2)}_{\mathrm{e},(-1)}$ and $\delta T^{(1/2)}_{\mathrm{e},(-1)}$, and to obtain the parallel flows and neoclassical perpendicular diffusion terms appearing in the transport equations (127) and (128).

Using the results of Appendix C, we can write down the effective parallel velocity, parallel heat flux, and perpendicular diffusion terms that appear in the transport equations (127) and (128) in the $qR_0\nu_\mathrm{ee}/v_\mathrm{th,e} \gg 1$ limit. We find that

$$\frac{\overline{\delta u}_\parallel}{v_\mathrm{th,e}} = -\frac{v_\mathrm{th,e}}{2\nu_\mathrm{ei}}\frac{(\langle\boldsymbol{B}\cdot\nabla\theta\rangle^\theta)^2}{\langle\boldsymbol{b}\cdot\nabla\theta\rangle^\theta\langle B^2\rangle^\theta}\left[1.97\frac{\partial}{\partial\chi}\left(\frac{\delta n^{(0)}_\mathrm{e}}{n_\mathrm{e}}\right) + 3.37\frac{\partial}{\partial\chi}\left(\frac{\delta T^{(0)}_\mathrm{e}}{T_\mathrm{e}}\right)\right] \tag{153}$$
$$+\frac{\mathrm{i}}{2}\frac{k_y\overline{\rho}_\mathrm{th,e}\hat{\kappa}\hat{s}\chi}{\langle\boldsymbol{b}\cdot\nabla\theta\rangle^\theta}\overline{B}I\frac{dr}{d\psi}\left(\left\langle\frac{\boldsymbol{B}\cdot\nabla\theta}{B^2}\right\rangle^\theta - \frac{\langle\boldsymbol{B}\cdot\nabla\theta\rangle^\theta}{\langle B^2\rangle^\theta}\right)\left(\frac{\delta n^{(0)}_\mathrm{e}}{n_\mathrm{e}} + \frac{\delta T^{(0)}_\mathrm{e}}{T_\mathrm{e}}\right),$$

where we have used equation (C.11), with the numerical results (B.16) and (B.17) for the transport coefficients, assuming $Z_\mathrm{i} = 1$. Similarly, using (C.12), we obtain the effective electron parallel heat flux

$$\frac{\overline{\delta q}_\parallel}{n_\mathrm{e}T_\mathrm{e}v_\mathrm{th,e}} = -\frac{5v_\mathrm{th,e}}{4\nu_\mathrm{ei}}\frac{(\langle\boldsymbol{B}\cdot\nabla\theta\rangle^\theta)^2}{\langle\boldsymbol{b}\cdot\nabla\theta\rangle^\theta\langle B^2\rangle^\theta}\left[0.56\frac{\partial}{\partial\chi}\left(\frac{\delta n^{(0)}_\mathrm{e}}{n_\mathrm{e}}\right) + 2.23\frac{\partial}{\partial\chi}\left(\frac{\delta T^{(0)}_\mathrm{e}}{T_\mathrm{e}}\right)\right] \tag{154}$$

$$+\frac{5\mathrm{i}}{4}\frac{k_y\overline{\rho}_{\mathrm{th,e}}\hat{\kappa}\hat{s}\chi}{\langle \boldsymbol{b}\cdot\nabla\theta\rangle^{\theta}}\overline{B}I\frac{dr}{d\psi}\left(\left\langle\frac{\boldsymbol{B}\cdot\nabla\theta}{B^2}\right\rangle^{\theta}-\frac{\langle\boldsymbol{B}\cdot\nabla\theta\rangle^{\theta}}{\langle B^2\rangle^{\theta}}\right)\frac{\delta T_{\mathrm{e}}^{(0)}}{T_{\mathrm{e}}}.$$

We note that the terms linear in χ in equations (153) and (154) arise from the radial magnetic drift, whereas the terms in $\partial/\partial\chi$ arise from the effective electric field generated by the leading-order electron response (cf. equation (111)).

The neoclassical particle flux $\overline{\delta\Gamma}_{\mathrm{N}}$ appearing in the nonadiabatic density transport equation, equation (127), can be evaluated using the result (C.15). We find that

$$\frac{\overline{\delta\Gamma}_{\mathrm{N}}}{n_{\mathrm{e}}}=-\frac{v_{\mathrm{th,e}}\overline{\rho}_{\mathrm{th,e}}}{2}I\frac{dr}{d\psi}\overline{B}\left(\frac{\langle\boldsymbol{B}\cdot\nabla\theta\rangle^{\theta}}{\langle B^2\rangle^{\theta}}-\left\langle\frac{\boldsymbol{B}\cdot\nabla\theta}{B^2}\right\rangle^{\theta}\right)\left(\frac{\partial}{\partial\chi}\left(\frac{\delta n_{\mathrm{e}}^{(0)}}{n_{\mathrm{e}}}\right)+\frac{\partial}{\partial\chi}\left(\frac{\delta T_{\mathrm{e}}^{(0)}}{T_{\mathrm{e}}}\right)\right)$$

$$+\mathrm{i}k_y\hat{s}\hat{\kappa}\chi\frac{\nu_{\mathrm{ei}}\overline{\rho}^2_{\mathrm{th,e}}}{2}\left(I\frac{dr}{d\psi}\right)^2\left(\left\langle\frac{\overline{B}^2}{B^2}\right\rangle^{\theta}-\frac{\overline{B}^2}{\langle B^2\rangle^{\theta}}\right)\left[0.67\frac{\delta n_{\mathrm{e}}^{(0)}}{n_{\mathrm{e}}}+0.11\frac{\delta T_{\mathrm{e}}^{(0)}}{T_{\mathrm{e}}}\right]. \tag{155}$$

Similarly, the neoclassical heat flux $\overline{\delta q}_{\mathrm{N}}$ appearing in the temperature transport equation, equation (128), can be evaluated using the result (C.16). We find that

$$\frac{\overline{\delta q}_{\mathrm{N}}}{n_{\mathrm{e}}T_{\mathrm{e}}}=-\frac{5v_{\mathrm{th,e}}\overline{\rho}_{\mathrm{th,e}}}{4}I\frac{dr}{d\psi}\overline{B}\left(\frac{\langle\boldsymbol{B}\cdot\nabla\theta\rangle^{\theta}}{\langle B^2\rangle^{\theta}}-\left\langle\frac{\boldsymbol{B}\cdot\nabla\theta}{B^2}\right\rangle^{\theta}\right)\frac{\partial}{\partial\chi}\left(\frac{\delta T_{\mathrm{e}}^{(0)}}{T_{\mathrm{e}}}\right) \tag{156}$$

$$+\mathrm{i}k_y\hat{s}\hat{\kappa}\chi\frac{\nu_{\mathrm{ei}}\overline{\rho}^2_{\mathrm{th,e}}}{2}\left(I\frac{dr}{d\psi}\right)^2\left(\left\langle\frac{\overline{B}^2}{B^2}\right\rangle^{\theta}-\frac{\overline{B}^2}{\langle B^2\rangle^{\theta}}\right)\left[1.41\frac{\delta T_{\mathrm{e}}^{(0)}}{T_{\mathrm{e}}}-0.56\frac{\delta n_{\mathrm{e}}^{(0)}}{n_{\mathrm{e}}}\right].$$

Physically, equations (155) and (156) indicate that diffusive transport arises from the radial magnetic drift (note the terms linear in χ).

We conclude this section on the $qR_0\nu_{\mathrm{ee}}/v_{\mathrm{th,e}} \gg 1$ limit by noting that the scale of the extended tail, χ, decreases with increasing $qR_0\nu_{\mathrm{ee}}/v_{\mathrm{th,e}}$. This is explicit in the estimate (90). Using (90), we can see that for extreme collision frequencies where $qR_0\nu_{\mathrm{ee}}/v_{\mathrm{th,e}} \sim (m_{\mathrm{i}}/m_{\mathrm{e}})^{1/2}$ there is no separation between the scale of the electron tail and the scale of the geometric quantities: for such an extreme collisionality, $\chi \sim 1$. The fluid equations for this extreme regime are not examined in this paper.

5.1.4. The subsidiary limit of $qR_0\nu_{\mathrm{ee}}/v_{\mathrm{th,e}} \ll 1$ – the banana-plateau regime. We now examine equation (118) in the subsidiary limit $qR_0\nu_{\mathrm{ee}}/v_{\mathrm{th,e}} \ll 1$. This discussion will enable us to demonstrate the matching between the collisionless and collisional regimes. We will need to go to first-order in the subsidiary expansion of $qR_0\nu_{\mathrm{ee}}/v_{\mathrm{th,e}} \ll 1$, and so we expand

$$H_{\mathrm{e}}^{(1/2)}=H_{\mathrm{e},(0)}^{(1/2)}+H_{\mathrm{e},(1)}^{(1/2)}+\mathrm{O}\left(\left(\frac{qR_0\nu_{\mathrm{ee}}}{v_{\mathrm{th,e}}}\right)^2H_{\mathrm{e},(0)}^{(1/2)}\right) \tag{157}$$

where $H_{\mathrm{e},(0)}^{(1/2)} \sim \mathrm{i}\lambda_{\mathrm{e}}\chi H_{\mathrm{e}}^{(0)} \sim H_{\mathrm{SH}}$ and $H_{\mathrm{e},(n)}^{(1/2)} \sim (qR_0\nu_{\mathrm{ee}}/v_{\mathrm{th,e}})^n H_{\mathrm{e},(0)}^{(1/2)}$. The leading-order form of equation (118) is

$$v_{\|}\boldsymbol{b}\cdot\nabla\theta\frac{\partial}{\partial\theta}\left(H_{\mathrm{e},(0)}^{(1/2)}\right)=0, \tag{158}$$

i.e., we learn that $H^{(1/2)}_{\mathrm{e},(0)} = H^{(1/2)}_{\mathrm{e},(0)}(\chi,\varepsilon,\lambda,\sigma)$. Going to first-order terms in the expansion of the drift-kinetic equation (118), we find that

$$v_\parallel \boldsymbol{b}\cdot\nabla\theta \frac{\partial}{\partial\theta}\left(H^{(1/2)}_{\mathrm{e},(1)}\right) = \mathcal{C}\left[H^{(1/2)}_{\mathrm{e},(0)} + \mathrm{i}\lambda_{\mathrm{e}}\chi H^{(0)}_{\mathrm{e}} - H_{\mathrm{SH}}\right]. \tag{159}$$

We now impose the solvability condition that $H^{(1/2)}_{\mathrm{e},(1)}(\theta,\chi,\varepsilon,\lambda,\sigma)$ should be 2π-periodic in θ. We must treat the passing and trapped part of the velocity space independently. For passing particles we apply the transit average $\langle\cdot\rangle^{\mathrm{t}}$, defined in equation (74), to obtain

$$\left\langle\mathcal{C}\left[H^{(1/2)}_{\mathrm{e},(0)} + \mathrm{i}\lambda_{\mathrm{e}}\chi H^{(0)}_{\mathrm{e}} - H_{\mathrm{SH}}\right]\right\rangle^{\mathrm{t}} = 0. \tag{160}$$

We note that equation (160) is a partial differential equation in (ε,λ) at fixed χ. For trapped particles we apply the bounce average $\langle\cdot\rangle^{\mathrm{b}}$, defined in equation (46), to obtain

$$\left\langle\mathcal{C}\left[H^{(1/2)}_{\mathrm{e},(0)}\right]\right\rangle^{\mathrm{b}} = 0, \tag{161}$$

where we have used that $\mathrm{i}\lambda_{\mathrm{e}}\chi H^{(0)}_{\mathrm{e}}$ and H_{SH} are odd in $\sigma = v_\parallel/|v_\parallel|$, and therefore vanish under $\langle\cdot\rangle^{\mathrm{b}}$. The trapped particle bounce condition requires that

$$H^{(1/2)}_{\mathrm{e}}(\theta^{\pm}_{b},\sigma=1) = H^{(1/2)}_{\mathrm{e}}(\theta^{\pm}_{b},\sigma=-1),$$

and hence $H^{(1/2)}_{\mathrm{e},(0)}$ is even in σ, by virtue of being constant in θ. In contrast, we can see from equation (160) that the passing particle response must be odd in σ. A Maxwellian solution to equation (161) is not valid, because of the change in the σ symmetry of $H^{(1/2)}_{\mathrm{e},(0)}$ at the trapped-passing boundary, and hence we must have that $H^{(1/2)}_{\mathrm{e},(0)} = 0$ for trapped particles. To obtain $H^{(1/2)}_{\mathrm{e},(0)}$ for passing particles, we must solve equation (160) subject to continuity in $H^{(1/2)}_{\mathrm{e},(0)}$ at the trapped-passing boundary.

In order to make progress analytically, it is necessary to expand in inverse aspect ratio $\epsilon = r/R_0 \ll 1$, where r is the minor radial coordinate of the flux surface of interest. We assume that the normalised collisionality

$$\nu_* = \frac{qR_0\nu_{\mathrm{ee}}}{\epsilon^{3/2}v_{\mathrm{th,e}}} \ll 1, \tag{162}$$

and assume that the equilibrium can be approximated by the solution with circular flux surfaces [25, 35]. Then, we can use the techniques of neoclassical theory [27, 33] to obtain $H^{(1/2)}_{\mathrm{e},(0)}$ to leading-order in ϵ, and the velocity $\overline{\delta u}_\parallel$ and flux $\overline{\delta q}_\parallel$, and the neoclassical perpendicular diffusion terms to order $\epsilon^{1/2}$. These calculations are performed in Appendix D. We conclude that for $\nu_* \ll 1$ the electron parallel velocity and electron parallel heat flux has a diffusive character.

Finally, we comment on the matching between the equations for the electron response in the collisionless and the collisional regimes, discussed in sections 4.2.2 and 5.1.2, respectively. We have demonstrated that for $(m_{\mathrm{e}}/m_{\mathrm{i}})^{1/2} \ll qR_0\nu_{\mathrm{ee}}/v_{\mathrm{th,e}} \ll 1$, the leading-order electron response is a perturbed Maxwellian, given by equation (107). Small, diffusive parallel flows are obtained by simultaneously solving equations (160) and (161). The evolution of the leading-order density and temperature is controlled by perpendicular diffusion, diffusive parallel flows, and drives of instability via the mode transport equations (127) and (128), respectively. To obtain the same physics from the equations in the collisionless limit for the passing electron response, equation (75), and the trapped electron response, equation (76), we take the following steps: First, in equations (75) and (76), we take the electron collision frequency to be large compared to the ion transit frequency, i.e., $qR_0\nu_{\rm ee}/v_{\rm th,i} \gg 1$, and we take the extent of the ballooning mode to be small, with

$$1 \ll \chi \sim \left(\frac{qR_0\nu_{\rm ee}}{v_{\rm th,i}}\right)^{-1/2} \left(\frac{m_{\rm i}}{m_{\rm e}}\right)^{1/2} \ll \left(\frac{m_{\rm i}}{m_{\rm e}}\right)^{1/2}. \qquad (163)$$

Then, the leading-order equation for the electron response is

$$\mathcal{C}\left[H_{\rm e}^{(0)}\right] = 0, \qquad (164)$$

i.e., $H_{\rm e}^{(0)}$ is a perturbed Maxwellian with no flow, and with no dependence on θ. Second, we collect terms of $\mathrm{O}\left((qR_0\nu_{\rm ee}/v_{\rm th,i})^{-1/2}\right)$ in the subsidiary expansion, and obtain equations for the passing and trapped electron response of the form (160) and (161), respectively. Finally, we collect terms of $\mathrm{O}\left((qR_0\nu_{\rm ee}/v_{\rm th,i})^{-1}\right)$ in the subsidiary expansion and obtain the transport equations for the nonadiabatic density and temperature, equations (127) and (128), respectively. Hence, we have demonstrated that the equations for the electron response in the $\chi \gg 1$ region match at the boundary of the collisionless and collisional limits. The fact that the extent of the mode shortens when going from the collisionless to the collisional limits, according to the ordering (163), along with the Maxwellianisation of the distribution function by increasing interparticle collisions, cf. equation (164), ensures that the collisionless inner-region quasineutrality relation (81) takes the form of the collisional inner-region quasineutrality relation (110).

5.2. Collisional outer solution – $\theta \sim 1$ – $k_r\rho_{\rm th,e} \sim (m_{\rm e}/m_{\rm i})^{1/2}$

As we saw in the previous section, the collisional $\theta \gg 1$ region requires the asymptotic expansion to be carried out in powers of $(m_{\rm e}/m_{\rm i})^{1/4}$. For consistency, we must also expand in powers of $(m_{\rm e}/m_{\rm i})^{1/4}$ in the $\theta \sim 1$ region. The potential, distribution functions, and frequency are expanded as in equations (91), (92), and (93), respectively.

In the following sections we consider the response of electrons in the outer region for both the small-tail and large-tail orderings, and we describe the small-tail and large-tail modes in the asymptotic limit. First, we describe the ion response in the outer region.

5.2.1. Ion response in the outer region. In the collisional ordering, we take $\nu_{\rm ii} \sim v_{\rm th,i}/qR$. As the electron mass does not appear in the ion gyrokinetic equation, no approximations are possible in this ordering and the gyrokinetic equation for the ions is simply equation (3) with $s = {\rm i}$. The main observation that we make in this section is that the nonadiabatic response of ions $h_{\rm i}$ contributes at leading-order to the potential ϕ in the outer region. As in the collisionless case (see equation (41)), the estimate for the size of the ion nonadiabatic density is $\delta n_{\rm i}/n_{\rm i} \sim e\phi/T_{\rm e}$.

5.2.2. Electron response in the outer region for small-tail modes. In a collisional small-tail mode, the fluctuations must satisfy the ordering

$$\frac{H_{\mathrm{e,inner}}}{F_{0e}} \sim \frac{e\phi_{\mathrm{inner}}}{T_{\mathrm{e}}} \sim \frac{H_{\mathrm{e,outer}}}{F_{0e}} \ll \frac{e\phi_{\mathrm{outer}}}{T_{\mathrm{e}}}, \tag{165}$$

so that the nonadiabatic electron response is subdominant to the nonadiabatic ion response in the outer region. This ordering will recover the ITG mode. We now determine the relative size of $H_{\mathrm{e,outer}}/F_{0e}$ to $e\phi_{\mathrm{outer}}/T_{\mathrm{e}}$. In the inner region, the electron flows are $(m_{\mathrm{e}}/m_{\mathrm{i}})^{1/4}$ smaller than the density and temperature components of the electron response. This must be true in the outer solution for the solutions to be matched.

To satisfy the ordering (165), in the outer region we take $H_{\mathrm{e}}^{(0)} = 0$. Expanding in $(m_{\mathrm{e}}/m_{\mathrm{i}})^{1/4}$, the next order equation is

$$v_{\|}\boldsymbol{b}\cdot\nabla\theta \frac{\partial H_{\mathrm{e}}^{(1/2)}}{\partial\theta} = C_{\mathrm{ee}}\left[H_{\mathrm{e}}^{(1/2)}\right] + \mathcal{L}\left[H_{\mathrm{e}}^{(1/2)}\right]. \tag{166}$$

Superficially, equation (166) has an identical form to equation (100). However, in the outer region, $H_{\mathrm{e}}^{(1/2)}$ cannot be assumed to be periodic in θ. To solve for $H_{\mathrm{e}}^{(1/2)}$, we multiply equation (166) by $H_{\mathrm{e}}^{(1/2)}/F_{0e}$, and integrate over velocity and θ. We obtain

$$\left[\int \frac{v_{\|}}{B}\frac{\left(H_{\mathrm{e}}^{(1/2)}\right)^2}{2F_{0e}}\, d^3\boldsymbol{v}\right]_{\theta=-\infty}^{\theta=\infty} =$$

$$\int_{-\infty}^{\infty}\left[\int \frac{H_{\mathrm{e}}^{(1/2)}}{F_{0e}}\, C_{\mathrm{ee}}\left[H_{\mathrm{e}}^{(1/2)}\right]\, d^3\boldsymbol{v} + \int \frac{H_{\mathrm{e}}^{(1/2)}}{F_{0e}}\,\mathcal{L}\left[H_{\mathrm{e}}^{(1/2)}\right]\, d^3\boldsymbol{v}\right]\frac{d\theta}{\boldsymbol{B}\cdot\nabla\theta}. \tag{167}$$

In the inner region the leading-order distribution function is Maxwellian, with no flow. Assuming continuity of the leading-order piece of H_{e} in the matching region, we have that the term on the left-hand side of equation (167) is identically zero, i.e.,

$$\int_{-\infty}^{\infty}\left[\int \frac{H_{\mathrm{e}}^{(1/2)}}{F_{0e}}\, C_{\mathrm{ee}}\left[H_{\mathrm{e}}^{(1/2)}\right]\, d^3\boldsymbol{v} + \int \frac{H_{\mathrm{e}}^{(1/2)}}{F_{0e}}\,\mathcal{L}\left[H_{\mathrm{e}}^{(1/2)}\right]\, d^3\boldsymbol{v}\right]\frac{d\theta}{\boldsymbol{B}\cdot\nabla\theta} = 0. \tag{168}$$

With the entropy production properties (106), equation (168) shows that

$$H_{\mathrm{e}}^{(1/2)} = \left(\frac{\delta n_{\mathrm{e}}^{(1/2)}}{n_{\mathrm{e}}} + \frac{\delta T_{\mathrm{e}}^{(1/2)}}{T_{\mathrm{e}}}\left(\frac{\varepsilon}{T_{\mathrm{e}}} - \frac{3}{2}\right)\right)F_{0e}, \tag{169}$$

where $\delta n_{\mathrm{e}}^{(1/2)}$ and $\delta T_{\mathrm{e}}^{(1/2)}$ are a constant density and temperature, respectively, determined by matching to the inner region. To calculate the electron flows needed to match to the inner region, we proceed to the next order equation

$$v_{\|}\boldsymbol{b}\cdot\nabla\theta \frac{\partial H_{\mathrm{e}}^{(1)}}{\partial\theta} - C_{\mathrm{ee}}\left[H_{\mathrm{e}}^{(1)}\right] - \mathcal{L}\left[H_{\mathrm{e}}^{(1)} - \frac{m_{\mathrm{e}} v_{\|}\delta u_{\|,\mathrm{i}}^{(0)}}{T_{\mathrm{e}}}F_{0e}\right] = -\mathrm{i}\left(\omega_{*,\mathrm{e}} - \omega^{(0)}\right)F_{0e}\frac{e\phi^{(0)}}{T_{\mathrm{e}}}, \tag{170}$$

where

$$\delta u_{\|,\mathrm{i}}^{(0)} = \frac{1}{n_{\mathrm{i}}}\int v_{\|} J_{0\mathrm{i}} h_{\mathrm{i}}^{(0)}\, d^3\boldsymbol{v}. \tag{171}$$

We cannot solve equation (170) for $H_{\rm e}^{(1)}$, but it transpires that we do not need to. Instead, we extract equations for the leading-order (nonzero) electron mean velocity $\delta u_{\|,{\rm e}}^{(1)}$, and electron heat flux $\delta q_{\|,{\rm e}}^{(1)}$. Noting that $h_{\rm e}{}^{(1)} = H_{\rm e}^{(1)}$ for $H_{\rm e}^{(0)} = 0$, $\lambda_{\rm e} \sim (m_{\rm e}/m_{\rm i})^{1/2}$ and $\theta \sim 1$, by virtue of expanding the definition (31), we obtain that $\delta u_{\|,{\rm e}}^{(1)} = \delta U_{\|,{\rm e}}^{(1)}$ and $\delta q_{\|,{\rm e}}^{(1)} = \delta Q_{\|,{\rm e}}^{(1)}$, where $\delta U_{\|,{\rm e}}^{(1)}$ and $\delta Q_{\|,{\rm e}}^{(1)}$ are the moments of $H_{\rm e}^{(1)}$ defined by equations (122) and (125), respectively. Taking density and temperature velocity moments, we find that

$$\boldsymbol{B} \cdot \nabla \theta \frac{\partial}{\partial \theta} \left(\frac{\delta u_{\|,{\rm e}}^{(1)}}{B} \right) = -{\rm i}(\omega_{*,{\rm e}}^{n} - \omega^{(0)}) \frac{e\phi^{(0)}}{T_{\rm e}}, \tag{172}$$

and

$$\boldsymbol{B} \cdot \nabla \theta \frac{\partial}{\partial \theta} \left(\frac{\delta q_{\|,{\rm e}}^{(1)}}{B n_{\rm e} T_{\rm e}} + \frac{\delta u_{\|,{\rm e}}^{(1)}}{B} \right) = -{\rm i}\frac{3}{2}\omega_{*,{\rm e}}^{n}\eta_{\rm e} \frac{e\phi^{(0)}}{T_{\rm e}}. \tag{173}$$

Equations (172) and (173) can be integrated to obtain the leading-order jump in $\delta u_{\|,{\rm e}}$ and $\delta q_{\|,{\rm e}}$ across the outer region. We find that

$$\left[\frac{\delta u_{\|,{\rm e}}^{(1)}}{B} \right]_{\theta=-\infty}^{\theta=\infty} = -{\rm i}(\omega_{*,{\rm e}}^{n} - \omega^{(0)}) \int_{-\infty}^{\infty} \frac{e\phi^{(0)}(\theta)}{T_{\rm e}} \frac{d\theta}{\boldsymbol{B} \cdot \nabla \theta}, \tag{174}$$

and

$$\left[\frac{\delta q_{\|,{\rm e}}^{(1)}}{n_{\rm e} T_{\rm e} B} \right]_{\theta=-\infty}^{\theta=\infty} = -{\rm i}\left(\frac{3}{2}\omega_{*,{\rm e}}^{n}\eta_{\rm e} - \omega_{*,{\rm e}}^{n} + \omega^{(0)} \right) \int_{-\infty}^{\infty} \frac{e\phi^{(0)}(\theta)}{T_{\rm e}} \frac{d\theta}{\boldsymbol{B} \cdot \nabla \theta}. \tag{175}$$

Equations (174) and (175) give the estimates for the jump in the electron flows across the outer region. These are

$$\left[\frac{\delta u_{\|,{\rm e}}}{v_{\rm th,e}} \right]_{\theta=-\infty}^{\theta=\infty} \sim \left[\frac{\delta q_{\|,{\rm e}}}{v_{\rm th,e} n_{\rm e} T_{\rm e}} \right]_{\theta=-\infty}^{\theta=\infty} \sim \left(\frac{m_{\rm e}}{m_{\rm i}} \right)^{1/2} \frac{e\phi_{\rm outer}}{T_{\rm e}}. \tag{176}$$

Note that the size of the jump is set entirely by size of the potential fluctuation in the outer region. There is an implicit assumption that the potential due to the nonadiabatic ion response decays for large θ in the outer region, such that the integrals in equations (174) and (175) exist. In fact, it is possible to show that there is a logarithmic matching region between the outer and inner regions where the nonadiabatic ion response decays exponentially with θ, and both the nonadiabatic ion and electron responses contribute to a $(m_{\rm e}/m_{\rm i})^{1/4}$ small potential. Formally, we can neglect this matching region in our analysis because the electron density, temperature, and flows remain constant over the matching region, and because no information about the ions in this region is propagated into either the outer or inner regions. See Appendix E for further details regarding the local (in ballooning space) response of ions at large θ.

The matching of the leading-order electrons flows at the boundary between the outer and inner regions requires that

$$\delta u_{\|,{\rm e,outer}}^{(1)} \sim \delta u_{\|,{\rm e,inner}}^{(1/2)}, \quad \text{and} \quad \delta q_{\|,{\rm e,outer}}^{(1)} \sim \delta q_{\|,{\rm e,inner}}^{(1/2)}. \tag{177}$$

In the collisional inner region, there is always a fixed relationship between the size of the electron flows and the density and temperature fluctuations. We can see this in equations (153) and (154). In terms of estimates, we find that

$$\frac{\delta u^{(1/2)}_{\parallel,\mathrm{e,inner}}}{v_{\mathrm{th,e}}} \sim \frac{\delta q^{(1/2)}_{\parallel,\mathrm{e,inner}}}{v_{\mathrm{th,e}} n_{\mathrm{e}} T_{\mathrm{e}}} \sim \left(\frac{m_{\mathrm{e}}}{m_{\mathrm{i}}}\right)^{1/4} \frac{\delta n^{(0)}_{\mathrm{e,inner}}}{n_{\mathrm{e}}} \sim \left(\frac{m_{\mathrm{e}}}{m_{\mathrm{i}}}\right)^{1/4} \frac{\delta T^{(0)}_{\mathrm{e,inner}}}{T_{\mathrm{e}}}. \tag{178}$$

Combining estimates (176), (177), and (178), we find an estimate for the size of the fluctuations in the inner region:

$$\frac{e\phi^{(0)}_{\mathrm{inner}}}{T_{\mathrm{e}}} \sim \frac{\delta n^{(0)}_{\mathrm{e,inner}}}{n_{\mathrm{e}}} \sim \frac{\delta T^{(0)}_{\mathrm{e,inner}}}{T_{\mathrm{e}}} \sim \left(\frac{m_{\mathrm{e}}}{m_{\mathrm{i}}}\right)^{1/4} \frac{e\phi^{(0)}_{\mathrm{outer}}}{T_{\mathrm{e}}}. \tag{179}$$

Finally, we can describe the procedure for solving for the small-tail mode in the $(m_{\mathrm{e}}/m_{\mathrm{i}})^{1/2} \to 0$ limit. To determine the frequency $\omega^{(0)}$ and the potential $\phi^{(0)}_{\mathrm{outer}}$, we solve the ion gyrokinetic equation (3) with $s = \mathrm{i}$, closed by the quasineutrality relation (neglecting the electron nonadiabatic response)

$$\left(\frac{Z_{\mathrm{i}} T_{\mathrm{e}}}{T_{\mathrm{i}}} + 1\right) \frac{e\phi^{(0)}_{\mathrm{outer}}}{T_{\mathrm{e}}} = \int J_{0\mathrm{i}} \frac{h^{(0)}_{\mathrm{i,outer}}}{n_{\mathrm{i}}}\, d^3\boldsymbol{v}. \tag{180}$$

With $\omega^{(0)}$ and $\phi^{(0)}_{\mathrm{outer}}$ determined, we can solve for the electron response using equations (127) and (128), with the inner-region quasineutrality equation (110). The causal link between the solution in the outer region and the inner region is provided by boundary matching. The matching conditions are continuity of the electron density and temperature

$$\delta n^{(1/2)}_{\mathrm{e,outer}} = \delta n^{(0)}_{\mathrm{e,inner}}(\chi = 0), \tag{181}$$

and

$$\delta T^{(1/2)}_{\mathrm{e,outer}} = \delta T^{(0)}_{\mathrm{e,inner}}(\chi = 0), \tag{182}$$

respectively, with jump conditions on the electron mean velocity and heat flux.

The jump conditions can be obtained by taking the following steps. First, we note that taking the $|\theta| \to \infty$ limit in equations (172) and (173) leads to the results

$$\boldsymbol{B} \cdot \nabla\theta \frac{\partial}{\partial\theta} \left(\frac{\delta u^{(1)}_{\parallel,\mathrm{e,outer}}}{B}\right) = 0, \tag{183}$$

and

$$\boldsymbol{B} \cdot \nabla\theta \frac{\partial}{\partial\theta} \left(\frac{\delta q^{(1)}_{\parallel,\mathrm{e}}}{B n_{\mathrm{e}} T_{\mathrm{e}}} + \frac{\delta u^{(1)}_{\parallel,\mathrm{e,outer}}}{B}\right) = 0, \tag{184}$$

where we have used that $e\phi^{(0)}_{\mathrm{outer}}/T_{\mathrm{e}}$ becomes exponentially small for large $|\theta|$, due to the decaying nonadiabatic ion response. Equations (183) and (184) state that $\delta u^{(1)}_{\parallel,\mathrm{e,outer}}/B$ and $\delta q^{(1)}_{\parallel,\mathrm{e,outer}}/B$ are independent of θ at large $|\theta|$. Second, we note that, in the inner region, we can show that $\delta u^{(1/2)}_{\parallel,\mathrm{e,inner}}/B$ and $\delta q^{(1/2)}_{\parallel,\mathrm{e,inner}}/B$ are independent of θ by taking the density and temperature moments of equation (118). Third, we demand that $\delta u_{\parallel,\mathrm{e}}/B$

and $\delta q_{\parallel,\mathrm{e}}/B$ should be continuous over the boundaries between the outer and inner regions, i.e., $\delta u_{\parallel,\mathrm{e}}$ and $\delta q_{\parallel,\mathrm{e}}$ should satisfy

$$\left.\frac{\delta u^{(1)}_{\parallel,\mathrm{e,outer}}}{B}\right|_{\theta\to\pm\infty} = \left.\frac{\delta u^{(1/2)}_{\parallel,\mathrm{e,inner}}}{B}\right|_{\chi\to 0^{\pm}}, \tag{185}$$

and

$$\left.\frac{\delta q^{(1)}_{\parallel,\mathrm{e,outer}}}{B}\right|_{\theta\to\pm\infty} = \left.\frac{\delta q^{(1/2)}_{\parallel,\mathrm{e,inner}}}{B}\right|_{\chi\to 0^{\pm}}, \tag{186}$$

Finally, we combine equations (174), (175), (185), and (186) to find the appropriate boundary conditions on $\overline{\delta u}_{\parallel}$ and $\overline{\delta q}_{\parallel}$. These are

$$\left[\overline{\delta u}_{\parallel}\right]^{\chi=0^+}_{\chi=0^-} = -\mathrm{i}(\omega^n_{*,\mathrm{e}} - \omega^{(0)})\frac{\langle \boldsymbol{B}\cdot\nabla\theta\rangle^{\theta}}{\langle \boldsymbol{b}\cdot\nabla\theta\rangle^{\theta}}\int_{-\infty}^{\infty}\frac{e\phi^{(0)}_{\mathrm{outer}}(\theta)}{T_{\mathrm{e}}}\frac{d\theta}{\boldsymbol{B}\cdot\nabla\theta}, \tag{187}$$

and

$$\left[\frac{\overline{\delta q}_{\parallel}}{n_{\mathrm{e}}T_{\mathrm{e}}}\right]^{\chi=0^+}_{\chi=0^-} = -\mathrm{i}\left(\frac{3}{2}\omega^n_{*,\mathrm{e}}\eta_{\mathrm{e}} - \omega^n_{*,\mathrm{e}} + \omega^{(0)}\right)\frac{\langle \boldsymbol{B}\cdot\nabla\theta\rangle^{\theta}}{\langle \boldsymbol{b}\cdot\nabla\theta\rangle^{\theta}}\int_{-\infty}^{\infty}\frac{e\phi^{(0)}_{\mathrm{outer}}(\theta)}{T_{\mathrm{e}}}\frac{d\theta}{\boldsymbol{B}\cdot\nabla\theta}. \tag{188}$$

The fact that there are changes in $\delta u^{(1)}_{\parallel,\mathrm{e,outer}}$ and $\delta q^{(1)}_{\parallel,\mathrm{e,outer}}$ across the outer region leads the appearance of apparent discontinuities in $\delta u^{(1/2)}_{\parallel,\mathrm{e,inner}}$ and $\delta q^{(1/2)}_{\parallel,\mathrm{e,inner}}$. An illustration demonstrating the matching in the collisional small-tail mode is given in figure 3.

5.2.3. Electron response in the outer region for large-tail modes. In the large-tail ordering, we have that

$$\frac{H_{\mathrm{e,inner}}}{F_{0e}} \sim \frac{e\phi_{\mathrm{inner}}}{T_{\mathrm{e}}} \sim \frac{H_{\mathrm{e,outer}}}{F_{0e}} \sim \frac{e\phi_{\mathrm{outer}}}{T_{\mathrm{e}}}. \tag{189}$$

In consequence, the equation for the leading-order electron response $H^{(0)}_{\mathrm{e}}$ in the outer region takes the form of equation (100), where we note that $H^{(0)}_{\mathrm{e}}$ is not periodic in θ in the outer region. Following the same arguments as used to solve equation (166) in section 5.2.2, we can demonstrate that the solution to equation (100) is that the electron distribution is a perturbed Maxwellian with no flow, and no dependence on θ at fixed (ε, λ). Thus, we learn that, in the outer region, $H^{(0)}_{\mathrm{e}}$ is given by equation (107) where the fluctuating nonadiabatic density $\delta n^{(0)}_{\mathrm{e}}$ and the fluctuating temperature $\delta T^{(0)}_{\mathrm{e}}$ are constants. This solution for $H^{(0)}_{\mathrm{e,outer}}$ trivially matches to the solution for $H^{(0)}_{\mathrm{e,inner}}$. We simply require that the constant nonadiabatic density and temperature that define the electron distribution function take the values

$$\delta n^{(0)}_{\mathrm{e,outer}} = \delta n^{(0)}_{\mathrm{e,inner}}(\chi = 0), \tag{190}$$

and

$$\delta T^{(0)}_{\mathrm{e,outer}} = \delta T^{(0)}_{\mathrm{e,inner}}(\chi = 0). \tag{191}$$

For this class of modes, the frequency is determined by the eigenmode equations (127) and (128), with the inner-region quasineutrality equation (110) and the matching

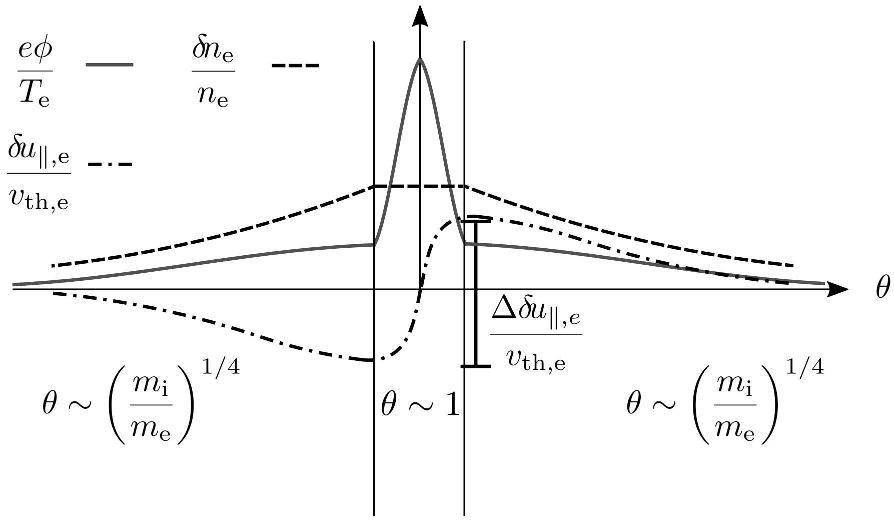

Figure 3. An illustration showing the nonadiabatic electron density δn_e and electron mean velocity $\delta u_{\|,e}$ in the collisional, small-tail limit. The leading-order mode frequency is determined by ions in the $\theta \sim 1$ (outer) region, by solving equation (3) (with $s = i$) subject to quasineutrality, equation (180). The electron tails at $\theta \sim (m_i/m_e)^{1/4}$ are obtained by solving the transport equations (127) and (128), with inner-region quasineutrality (110) and the boundary conditions (181), (182), (187), and (188). From the perspective of the $\theta \sim (m_i/m_e)^{1/4}$ region, the electron density is a cusp, set up by the discontinuity in $\delta u_{\|,e}$, $\Delta\delta u_{\|,e}$.

conditions (190) and (191). Because the eigenmode equations are second order differential equations in χ, two further matching conditions are required. These conditions are that the electron flows $\overline{\delta u}_{\|}$ and $\overline{\delta q}_{\|}$ are continuous across $\chi = 0$, i.e.,

$$\overline{\delta u}_{\|}(\chi = 0^+) = \overline{\delta u}_{\|}(\chi = 0^-), \tag{192}$$

and

$$\overline{\delta q}_{\|}(\chi = 0^+) = \overline{\delta q}_{\|}(\chi = 0^-). \tag{193}$$

Equations (192) and (193) can be derived by noting that the jump in the electron parallel flows across the outer region have a fixed size, given by the estimate (176). In a large tail mode, we have that

$$\frac{\delta u_{\|,e}}{v_{th,e}} \sim \frac{\delta q_{\|,e}}{v_{th,e} n_e T_e} \sim \left(\frac{m_e}{m_i}\right)^{1/4} \frac{e\phi_{inner}}{T_e} \sim \left(\frac{m_e}{m_i}\right)^{1/4} \frac{e\phi_{outer}}{T_e} \gg \left(\frac{m_e}{m_i}\right)^{1/2} \frac{e\phi_{outer}}{T_e}. \tag{194}$$

and hence the flows are continuous across the outer region to leading order. This result can be obtained explicitly by inspecting equations (187) and (188), with the ordering (194). An illustration of the structure of the collisional, large-tail mode is presented in figure 4.

Finally, we note that the nonadiabatic ion response has no role in determining the leading-order frequency $\omega^{(0)}$. Instead, the ions effectively respond passively,

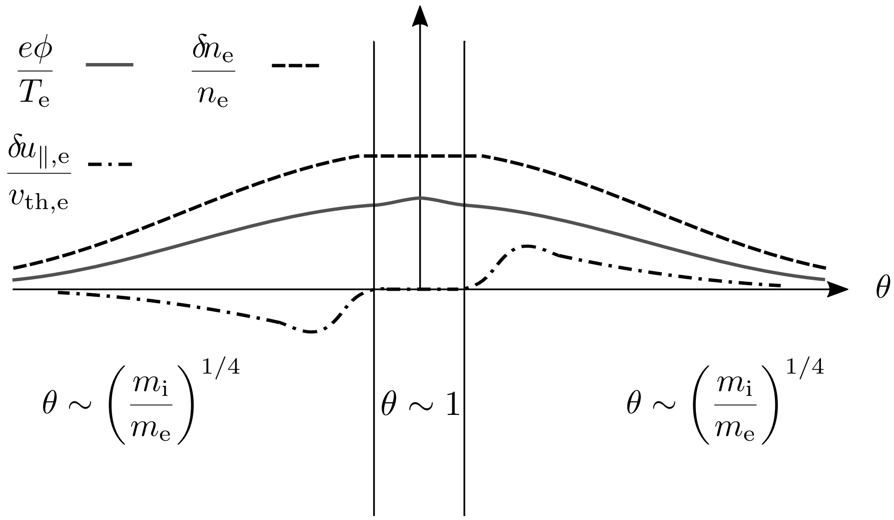

Figure 4. An illustration showing the nonadiabatic electron density δn_e and electron mean velocity $\delta u_{\|,e}$ in the collisional, large-tail limit. At leading-order, the mode frequency is determined by the nonadiabatic electron response in the $\theta \sim (m_i/m_e)^{1/4}$ (inner) region, by solving the transport equations (127) and (128), with inner-region quasineutrality (110), and the boundary conditions (190)-(193). The ion response to the leading-order frequency can be obtained by solving equation (3) (with $s = i$) subject to quasineutrality, equation (78). In contrast to the small-tail mode, in the large-tail mode the leading-order flows are developed in the $\theta \sim (m_i/m_e)^{1/4}$ region, and there is no leading-order electron density cusp near the boundary of the $\theta \sim 1$ region.

serving only to self-consistently determine the electrostatic potential $\phi^{(0)}_{\mathrm{outer}}$ through the quasineutrality equation (78) (noting that here the velocity space dependence of $H^{(0)}_e$ is given by equation (107)). Note that $\phi^{(0)}_{\mathrm{outer}}$ has not entered into the equations that determine the electron response in the large-tail mode.

6. Numerical results

In this section we present numerical results that support the analytical theory presented in the previous sections. We use the gyrokinetic code `GS2` [23] to calculate the fastest-growing linear modes for parameters where we observe extended electron-driven tails in the ballooning eigenfunction. As discussed in the introduction, extended tails have been observed in both electrostatic modes [12, 13, 15] and (electromagnetic) micro-tearing modes [16–18] for a variety of magnetic geometries. In the analytical theory that we have developed, the geometrical factors enter into the equations for the inner region only through the poloidal angle average $\langle \cdot \rangle^{\theta}$. Hence, modes that are driven by the electron response in the inner region are unlikely to be sensitive to the details of any given magnetic geometry. We therefore choose the simple Cyclone Base Case (CBC) [36] magnetic geometry to illustrate our theory: we study modes on a circular flux surface centred on the magnetic axis.

To specify the magnetic geometry, we use the Miller equilibrium parameterisation [37]. We take the major radius at the magnetic axis $R_0 = 3.0a$, with the normalising length a the half-diameter of the last-closed flux surface. We examine micro-stability on the flux surface with minor radius $r = 0.54a$. We take the safety factor to be $q = 1.4$, the magnetic shear to be $\hat{s} = (q/r)dq/dr = 0.8$, the plasma beta $\beta = 0$, the Shafranov shift derivative $d\Delta/dr = 0$, the elongation $\kappa = 1.0$, the elongation derivative $d\kappa/dr = 0.0$, the triangularity $\delta = 0.0$, and the triangularity derivative $d\delta/dr = 0.0$. The reference magnetic field is given by $B_{\rm ref} = I(\psi)/R_{\rm geo}$, i.e., toroidal magnetic field at the reference major radial position $R_{\rm geo}$. We take $R_{\rm geo} = R_0$. In section 2.2, we define local radial and binormal coordinates with units of length x and y, respectively, and associated radial and binormal wavenumbers k_x and k_y, respectively. We parameterise the radial wave number k_x with $\theta_0 = k_x/\hat{s}k_y$.

For the simulations presented here, we use the following numerical resolutions: $n_\theta = 33$ points per 2π element in the ballooning angle grid; $n_\lambda = 27$ points in the pitch angle grid; and $n_\varepsilon = 24$ points in the energy grid. The energy grid is constructed from a spectral speed grid [38], and the pitch angle grid is constructed from a Radau-Gauss grid for passing particles and an unevenly spaced grid for trapped particles. The number of 2π elements in the ballooning grid was chosen to be $n_{2\pi} = 65$ for the approximate deuterium mass ratio $(m_{\rm D}/m_{\rm e})^{1/2} = 61$. For different ion masses $m_{\rm i}$, the number of 2π elements was taken to be $n_{2\pi} = 65\sqrt{m_{\rm i}/m_{\rm D}}$. Unless otherwise stated, the timestep size was taken to be $\Delta t = 0.025a/v_{\rm th,i}$. The convergence of these resolutions was tested by doubling each parameter.

We consider a two-species plasma of ions and electrons, with $Z_{\rm i} = 1$, equal temperatures $T_{\rm i} = T_{\rm e}$, and an equilibrium density gradient $a/L_n = 0.733$, where the length scale $L_n = -dr/d\ln n_{\rm e}$. In order to examine different instabilities, we vary θ_0, the equilibrium temperature gradient length scales $L_{T_s} = -dr/d\ln T_s$, and the normalised electron collisionality $\nu_* = qR_0\nu_{\rm ee}/v_{\rm th,e}\epsilon^{3/2}$, where $\epsilon = r/R_0 = 0.18$. We vary the ion collision frequency $\nu_{\rm ii}$ consistently with ν_*, i.e., $\nu_{\rm ii} = \epsilon^{3/2}\nu_* v_{\rm th,i}/\sqrt{2}qR_0$. In section 6.1, we take $\theta_0 = 1.57$ and $a/L_{T_{\rm e}} = 3a/L_{T_{\rm i}} = 6.9$, and consider example modes that conform to the large-tail mode ordering. In section 6.2, we take $\theta_0 = 0.1$ and $a/L_{T_{\rm e}} = a/L_{T_{\rm i}} = 2.3$, and consider example modes that conform to the small-tail mode ordering. Finally, in section 6.3, we briefly discuss the transition between large-tail and small-tail modes as a function of θ_0.

6.1. Large tail modes

In this section we present numerical results that are consistent with the asymptotic theory of linear modes with large electron tails, summarised in sections 4.4 (the collisionless case) and 5.2.3 (the collisional case). In order to make the passing-electron-response-driven modes the fastest growing instability in the system, it is necessary to increase the electron drive with respect to the ion drive. We present results where the

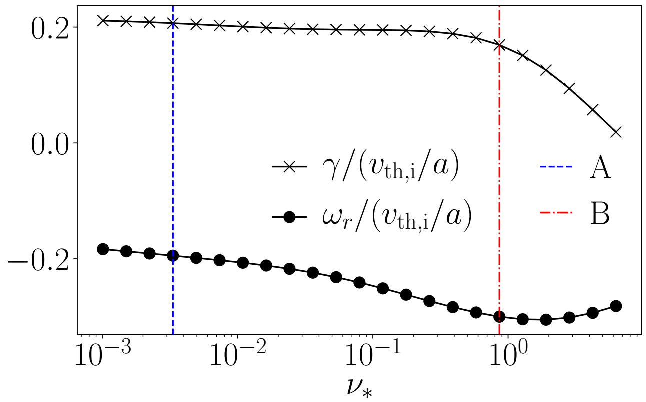

Figure 5. The growth rate γ and frequency ω_{r} for the large-tail mode with $(m_{\mathrm{i}}/m_{\mathrm{e}})^{1/2} = 61$ $k_y\rho_{\mathrm{th,i}} = 0.5$ and $\theta_0 = 1.57$, as a function of ν_*. For $\nu_* < 10^{-3}$ the large-tail mode is no longer the fastest-growing mode at this (k_y, θ_0). The vertical dashed lines A and B indicate the ν_* of the collisionless and collisional examples of large-tail modes that are discussed in sections 4.4 and 5.2.3, respectively.

normalised electron temperature gradient scale $a/L_{T_{\mathrm{e}}} = 3a/L_{T_{\mathrm{i}}} = 6.9$, and we focus on modes at $k_y\rho_{\mathrm{th,i}} = 0.5$ with $\theta_0 = \pi/2$. We vary ν_* in order to see the effect of electron collisionality on the mode – although we present results where ν_{ii} is varied consistently with ν_*, qualitatively and quantitatively similar results may be obtained by artificially setting $\nu_{\mathrm{ii}} = 0$. The geometry and physical parameters of the simulations are otherwise as described at the start this section. We use the full `GS2` model collision operator [31, 32], including pitch angle scattering, energy diffusion, and momentum and energy conserving terms. We find that the inclusion of pitch-angle scattering collisions is crucial for making the large-tail mode the fastest-growing instability.

We now briefly describe the method by which we identify large-tail modes numerically, before going on to discuss the identification of a collisionless large-tail mode and a collisional large-tail mode in detail. We recall the cartoon given in figure 2. In a collisionless large-tail mode, the relative amplitude of the electron distribution function H_{e} in the outer and inner regions remains fixed as $(m_{\mathrm{e}}/m_{\mathrm{i}})^{1/2} \rightarrow 0$. To test this numerically, we scan in $(m_{\mathrm{e}}/m_{\mathrm{i}})^{1/2}$ and determine whether or not we can rescale $H_{\mathrm{e}}(\theta) \rightarrow H_{\mathrm{e}}(\theta\,(m_{\mathrm{e}}/m_{\mathrm{i}})^{1/2})$ and so overlay a measure of H_{e} for the modes with different values of $(m_{\mathrm{e}}/m_{\mathrm{i}})^{1/2}$. We also must find that ϕ has the same size in the outer and inner regions as $(m_{\mathrm{e}}/m_{\mathrm{i}})^{1/2} \rightarrow 0$, although we expect to see $\mathrm{O}(1)$ oscillatory features in ϕ. For a collisional large-tail mode the procedure is the same, with $(m_{\mathrm{e}}/m_{\mathrm{i}})^{1/2}$ replaced by $(m_{\mathrm{e}}/m_{\mathrm{i}})^{1/4}$.

In figure 5 we show the result of calculating the linear growth rate γ and frequency ω_{r} for the deuterium mass ratio $(m_{\mathrm{e}}/m_{\mathrm{i}})^{1/2} \approx 1/61$. For the range of ν_* shown in figure 5, we identify that the modes are large-tail modes. For $\nu_* \ll 1$ we are able to identify the modes with the collisionless ordering described in section 4.4, and for $\nu_* \gtrsim 1$ we are able to identify the modes with the collisional ordering described in section 5.2.3. For intermediate ν_* neither ordering for the scaling of χ perfectly describes the structure of the eigenmode, but the basic orderings $H_{\rm e,outer} \sim H_{\rm e,inner}$ and $\phi_{\rm outer} \sim \phi_{\rm inner}$ continue to hold. We now focus on the clean example of a collisionless large-tail mode, indicated by "A" on figure 5, before moving on to the example of a collisional large-tail mode, indicated by "B" on figure 5.

6.1.1. Case A – a collisionless large-tail mode. To identify a mode as a collisionless large-tail mode, we must demonstrate first that $H_{\rm e,outer} \sim H_{\rm e,inner}$ and $\phi_{\rm outer} \sim \phi_{\rm inner}$ as $(m_{\rm e}/m_{\rm i})^{1/2} \to 0$, and second, that the scale of the ballooning envelope $\chi \sim (m_{\rm i}/m_{\rm e})^{1/2}$. We will also study the dependence of growth rate γ and real frequency $\omega_{\rm r}$ on $(m_{\rm e}/m_{\rm i})^{1/2}$. We use the geometric parameters described at the start of section 6, with the density and temperature gradient scale lengths $a/L_n = 0.733$, $a/L_{T_{\rm i}} = 2.3$, and $a/L_{T_{\rm e}} = 6.9$. We scan in the electron mass ratio from $m_{\rm e}/m_{\rm i} = 5.4 \times 10^{-4}$ to 1.08×10^{-3}, whilst holding fixed $\nu_* = 3.32 \times 10^{-3}$.

We define a useful measure of the electron distribution function

$$j_\parallel = j_\parallel^+ - j_\parallel^- \tag{195}$$

with

$$j_\parallel^\pm = -en_{\rm e} \int_0^\infty \int_0^{1/B_{\rm max}} \frac{|v_\parallel|}{B} H_{\rm e}(\sigma = \pm 1)\, \frac{2\pi B \varepsilon}{m_{\rm e}^2 |v_\parallel|}\, d\lambda\, d\varepsilon. \tag{196}$$

The field $j_\parallel$ has dimensions of current over magnetic field strength, and the quantities $j_\parallel^+$ and $j_\parallel^-$are the contributions from the forward going ($\sigma = 1$) and backward going ($\sigma = -1$) particles, respectively. The prime usefulness of $j_\parallel^\pm$ stems from the fact that $H_{\rm e}^{(0)}$ is independent of the 2π-periodic poloidal angle θ in the asymptotic theory, and hence, we expect that $j_\parallel^\pm$ are smoothly varying functions of ballooning angle, with minimal geometric 2π-periodic oscillation. We can use $j_\parallel^+$ as a proxy to visualise the distribution of forward-going particles. In figure 6, we plot $|j_\parallel^+|$, normalised to its maximum value, for three values of $(m_{\rm i}/m_{\rm e})^{1/2}$: the maximum, and minimum values in the scan, and the approximate value of the deuterium-ion-to-electron-mass ratio. Figure 6 shows that $j_\parallel^+$ is self-similar for modes with different $(m_{\rm e}/m_{\rm i})^{1/2}$, provided that the ballooning angle θ is rescaled to $\theta/\left(m_{\rm i}/m_{\rm e}\right)^{1/2}$. This confirms that $H_{\rm e,outer} \sim H_{\rm e,inner}$, and that $\chi \sim (m_{\rm i}/m_{\rm e})^{1/2}$.

Having inspected a measure of $H_{\rm e}$, we comment on the use of the modified distribution function $H_{\rm e}$ in place of the usual nonadiabatic response $h_{\rm e}$. In figure 7, we plot the distribution functions $h_{\rm e}$ and $H_{\rm e}$, as a function of θ, for the velocity space element $\varepsilon/T_{\rm e} = 0.79$, $\lambda B_{\rm ref} = 0.22$ and $\sigma = 1$. We show the distribution functions for the $(m_{\rm i}/m_{\rm e})^{1/2} = 61$ mode featured in figure 6. We observe that the distribution function $h_{\rm e}$ shows large 2π-scale oscillations in phase, whereas $H_{\rm e}$ is a smoothly varying function. In general, $H_{\rm e}$ appears to be a smoother variable than $h_{\rm e}$ for the parts of the electron distribution function where $v_\parallel \sim v_{\rm th,e} \gg v_{\rm th,i}$. These observations justify the choice to use the modified distribution function $H_{\rm e}$ in the asymptotic theory.

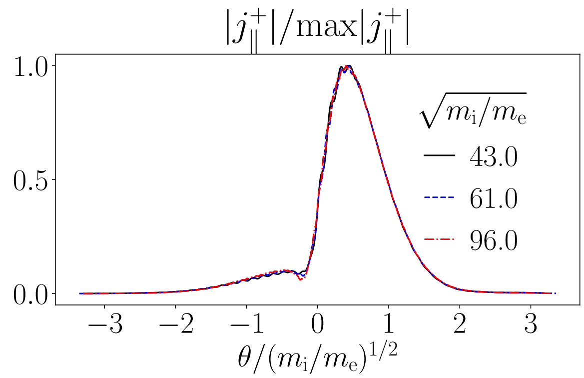

Figure 6. The field $j_\parallel^+$, calculated for $\nu_* = 3.32 \times 10^{-3}$ (case A of figure 5) for three different mass ratios. The fact that the curves overlay on the $\theta/\left(m_i/m_e\right)^{1/2}$ axis confirms that the mode is a collisionless large-tail mode.

We visualise the electrostatic potential in figure 8. We normalise the potential to the maximum value of $|j_\parallel^+|$, and give the result $|\phi|/|j_\parallel^+|$ in the units of $\phi^{\rm ref}/j_\parallel^{\rm ref}$, where $\phi^{\rm ref} = T_e/e$ and $j_\parallel^{\rm ref} = en_e v_{\rm th,e}/B_{\rm ref}$. We note that in contrast to the leading order component of $j_\parallel^\pm$, ϕ has oscillatory structures in geometric poloidal angle θ. These oscillations appear because of geometric poloidal angle dependence in the Jacobian $B\varepsilon/|v_\parallel|$ of the velocity integral, equation (103); because of the inclusion of trapped particles in the velocity integral; and because of the appearance of the Bessel function $J_{0e}^{(0)}$ and phase $\exp[i\lambda_e\chi]$ in the quasineutrality relation in the large-θ region, equation (81). Inspecting figure 8 (left), we can see that the ϕ curves for different $(m_e/m_i)^{1/2}$ modes do not exactly overlay. This is a result of the irreducible 2π geometric scale in θ. From figure 8 (right), we can see that the general envelope of the mode amplitude

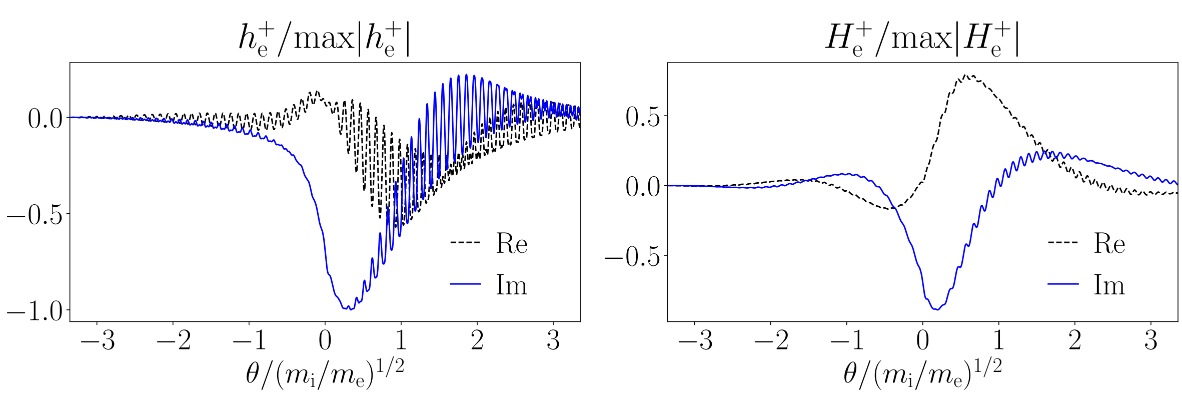

Figure 7. The distribution function for forward going particles, for the mode with $(m_i/m_e)^{1/2} = 61$ in figure 6, for $\varepsilon/T_e = 0.79$ and $\lambda B_{\rm ref} = 0.22$. Left, we plot h_e for forward going particles. Note the rapid oscillation in θ for $\theta \gg 1$. Right, we plot H_e for forward going particles. Note the smoothness of H_e compared to h_e for $\theta \gg 1$.

is independent of $(m_e/m_i)^{1/2}$, consistent with $\phi_{outer} \sim \phi_{inner}$. We note that the central peak in ϕ does change with $(m_e/m_i)^{1/2}$ – this might be a result of the change in the ion (and $\theta \sim 1$ trapped electron) nonadiabatic density with $(m_e/m_i)^{1/2}$.

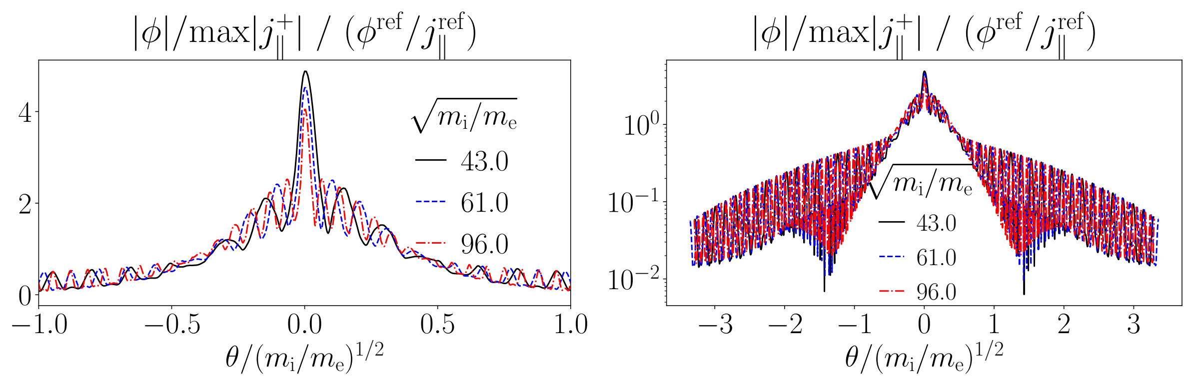

Figure 8. Two views of the electrostatic potential ϕ, calculated for $\nu_* = 3.32 \times 10^{-3}$ (case A of figure 5) for three different mass ratios. The potential is plotted against the scaled ballooning angle $\theta/(m_i/m_e)^{1/2}$, and normalised to the maximum value of $j_\parallel^+$ (see equation (196) and figure 6). Note the geometric 2π-periodic oscillation in ϕ due to geometric factors in the velocity integral over the electron distribution function (cf. equation (81)). The dimensions are $\phi^{ref} = T_e/e$ and $j_\parallel^{ref} = en_e v_{th,e}/B_{ref}$.

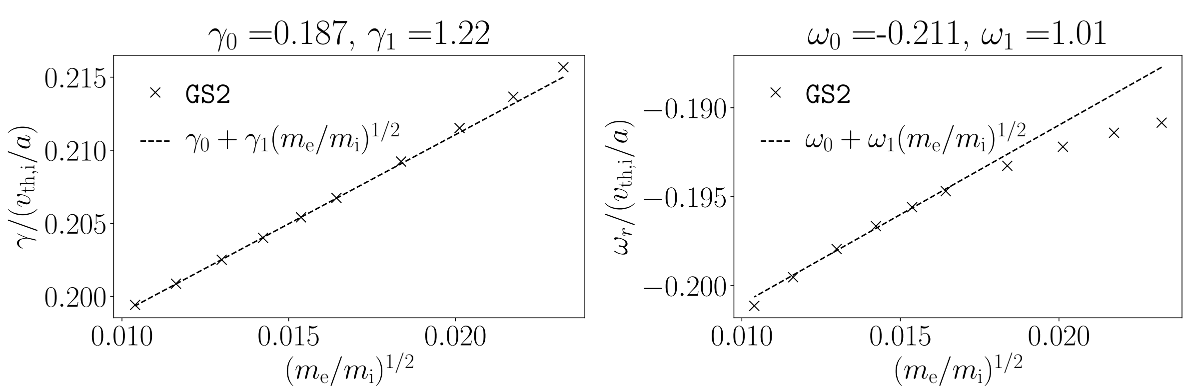

Figure 9. Plots of the growth rate γ (left) and real frequency ω_r (right) as a function of $(m_e/m_i)^{1/2}$, for $\nu_* = 3.32 \times 10^{-3}$ (case A of figure 5). We give a linear fit to demonstrate that the dependence of γ and ω_r on $(m_e/m_i)^{1/2}$ is consistent with a $(m_e/m_i)^{1/2}$ expansion.

Finally, we discuss the change in γ and ω_r with $(m_e/m_i)^{1/2}$. In figure 9 we plot γ and ω_r as functions of $(m_e/m_i)^{1/2}$, with a linear fit. From the asymptotic theory in section 4, we would expect to see that the growth rate had a leading order piece $\gamma^{(0)}$, and an $O\left((m_e/m_i)^{1/2}\right)$ small correction $\gamma^{(1)}$. This is borne out by figure 9 (left), which shows a linear trend in $(m_e/m_i)^{1/2}$. We would have a similar expectation for the real frequency $\omega_{\rm r}$. In fact, figure 9 (right) does not show a linear trend for all $(m_{\rm e}/m_{\rm i})^{1/2}$. In general, we observed linear trends in both γ and $\omega_{\rm r}$ for the relatively small range of $(m_{\rm e}/m_{\rm i})^{1/2}$ shown in figure 9. The breakdown of the asymptotic behaviour for very small $(m_{\rm e}/m_{\rm i})^{1/2}$ may be a numerical artefact, although we cannot rule out the possibility of a more complicated asymptotic theory. Non-asymptotic behaviour is to be expected for $(m_{\rm e}/m_{\rm i})^{1/2}$ too large.

6.1.2. Case B – a collisional large-tail mode. We now move on to examine an example of a collisional large-tail mode. We must demonstrate that $H_{\rm e,outer} \sim H_{\rm e,inner}$ and $\phi_{\rm outer} \sim \phi_{\rm inner}$ as $(m_{\rm e}/m_{\rm i})^{1/4} \rightarrow 0$, and show that the envelope of the eigenmode scales like $\chi \sim (m_{\rm i}/m_{\rm e})^{1/4}$. The physics parameters are identical to those described for the collisionless large-tail mode in section 6.1.1, except that the electron collisionality is increased to $\nu_* = 0.86$. We scan in the electron mass ratio from $m_{\rm e}/m_{\rm i} = 5.4 \times 10^{-4}$ to 1.08×10^{-3} while holding ν_* fixed.

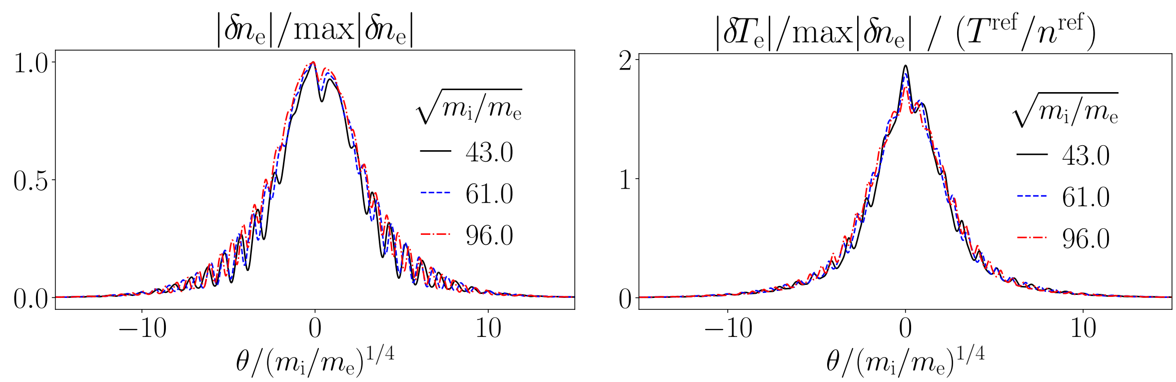

Figure 10. (left) The electron nonadiabatic density $\delta n_{\rm e}$, calculated for $\nu_* = 0.86$ (case B of figure 5) for three different mass ratios. The density is normalised to its maximum value, and plotted against the scaled ballooning angle $\theta/\left(m_{\rm i}/m_{\rm e}\right)^{1/4}$. (right) The electron temperature, normalised to the maximum value of the electron nonadiabatic density. Here $n^{\rm ref} = n_{\rm e}$, $T^{\rm ref} = T_{\rm e}$.

We first consider the eigenmodes. In the collisional ordering, the asymptotic theory of large-tail modes in sections 5 and 5.1.2 indicate that there are three leading-order quantities that are free from geometric 2π poloidal angle oscillations, the electron nonadiabatic density $\delta n_{\rm e}$, the electron temperature $\delta T_{\rm e}$, and the electrostatic potential ϕ. The electron nonadiabatic density and temperature are plotted in figure 10, with the ballooning angle θ rescaled by $(m_{\rm i}/m_{\rm e})^{1/4}$. We observe good agreement for different $(m_{\rm i}/m_{\rm e})^{1/2}$ in the mass ratio scan. The rescaled electrostatic potential ϕ is plotted in figure 11, again, with good agreement for different $(m_{\rm i}/m_{\rm e})^{1/2}$. In the asymptotic theory of the collisional large-tail mode, the parallel-to-the-field flows play an important diffusive role, despite being small by $(m_{\rm e}/m_{\rm i})^{1/4}$. In figure 12, we plot the current-like field $j_{\|}$, defined in equation (195), with the ballooning angle θ rescaled by $(m_{\rm i}/m_{\rm e})^{1/4}$,

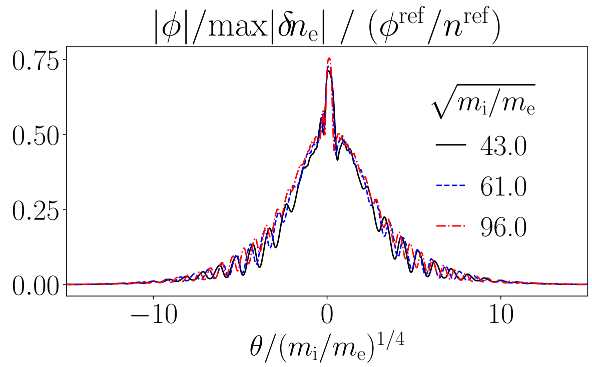

Figure 11. The electrostatic ϕ, calculated for $\nu_* = 0.86$ (case B of figure 5) for three different mass ratios. The potential is normalised to the maximum value of δn_e, $\max|\delta n_e|$. The good agreement for the rescaled potential normalised to $\max|\delta n_e|$ suggests that this mode can be regarded as a collisional large-tail mode. Here $\phi^{\rm ref} = T_e/e$ and $n^{\rm ref} = n_e$.

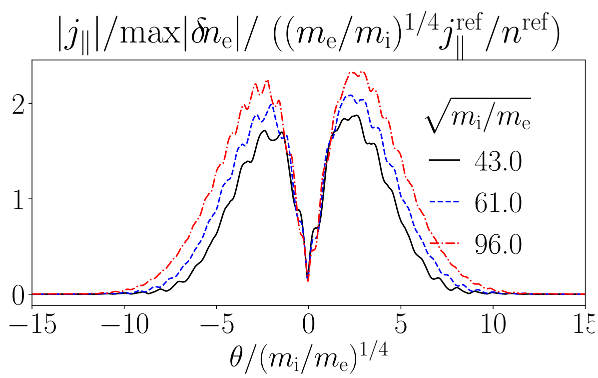

Figure 12. The current-like field $j_\parallel$, defined in equation (195), normalised to the maximum value of δn_e. Note that $j_\parallel$ is a $(m_e/m_i)^{1/4}$ small quantity. If the numerics perfectly reproduced the asymptotic theory of section 5 the plotted curves would overlay. The $(m_i/m_e)^{1/4}$ rescaling at produces better agreement than a $(m_i/m_e)^{1/2}$ rescaling. Here, $j_\parallel^{\rm ref} = e n_e v_{\rm th,e}/B_{\rm ref}$ and $n^{\rm ref} = n_e$.

and the amplitude rescaled by $(m_e/m_i)^{1/4}$. Although the curves do not overlay perfectly in the $(m_i/m_e)^{1/4}$ ballooning angle rescaling, we note that the $(m_i/m_e)^{1/4}$ ballooning angle rescaling shown in figure 12 gives better agreement than a $(m_i/m_e)^{1/2}$ ballooning angle rescaling.

Finally, we discuss the dependence of the growth rate γ and the real frequency ω_r on $(m_e/m_i)^{1/4}$ for the collisional large-tail mode. The asymptotic expansion for the collisional large-tail mode is carried out in powers of $(m_e/m_i)^{1/4}$. In consequence, we would expect that γ and ω_r would have leading order component $\gamma^{(0)}$ and $\omega_r^{(0)}$,

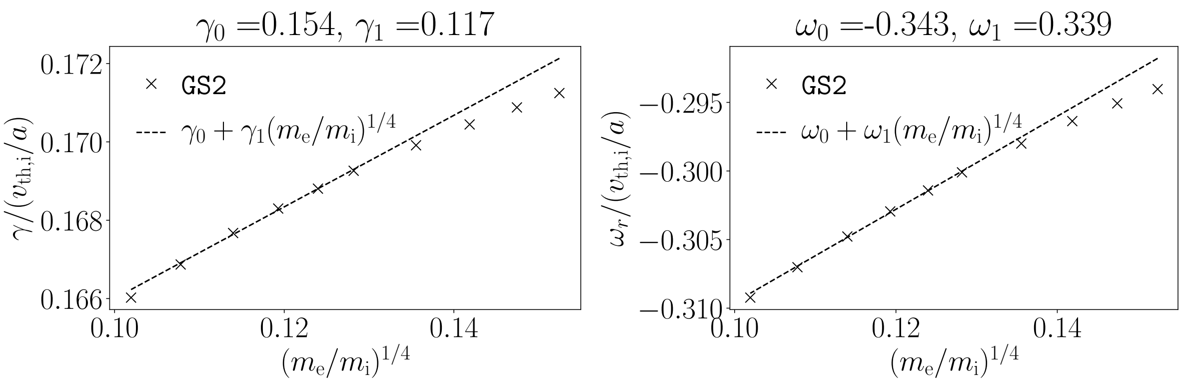

Figure 13. Plots of the growth rate γ (left) and real frequency $\omega_{\rm r}$ (right) as a function of $(m_{\rm e}/m_{\rm i})^{1/4}$, for $\nu_* = 0.86$ (case B of figure 5). We give a linear fit to illustrate the dependence of γ and $\omega_{\rm r}$ on $(m_{\rm e}/m_{\rm i})^{1/4}$.

respectively, that are independent of mass ratio, and sub-leading components $\gamma^{(1/2)}$ and $\omega_{\rm r}^{(1/2)}$, respectively, that scale linearly with $(m_{\rm e}/m_{\rm i})^{1/4}$. In figure 13 we plot γ and $\omega_{\rm r}$ with $(m_{\rm e}/m_{\rm i})^{1/4}$: the linear fit in figure 13 is good for a range of $(m_{\rm e}/m_{\rm i})^{1/2}$, although we again note the non-asymptotic behaviour for the smallest $(m_{\rm e}/m_{\rm i})^{1/2}$. Although we cannot rule out a more complicated asymptotic theory, the scaling with $(m_{\rm e}/m_{\rm i})^{1/4}$ of the leading-order eigenmodes of ϕ, $\delta n_{\rm e}$, and $\delta T_{\rm e}$ strongly suggests that the mode considered here is a collisional large-tail mode.

6.2. Small tail modes

In this section we verify the mass ratio scalings for collisionless small-tail modes, described in section 4.3, and collisional small-tail modes, described in section 5.2.2. We focus on the example of the ITG mode. We perform simulations using the magnetic geometry described at the start of section 6, we take the temperature and density scale lengths to be $a/L_{T_{\rm i}} = a/L_{T_{\rm e}} = 2.3$ and $a/L_n = 0.733$, respectively. We examine the mode with $k_y \rho_{\rm th,i} = 0.5$ and $\theta_0 = 0.1$. We calculate the fastest-growing mode for a range of normalised electron collision frequencies ν_*. For each ν_*, we scan in $(m_{\rm e}/m_{\rm i})^{1/2}$ to test the $(m_{\rm e}/m_{\rm i})^{1/2}$ dependence of the solution. We vary $\nu_{\rm ii}$ consistently with ν_*. As in the large-tail mode case, we note that qualitatively and quantitatively similar results are obtained by artificially setting $\nu_{\rm ii} = 0$ in the scan. In figure 14, we plot the growth rate γ and real frequency $\omega_{\rm r}$ as a function of ν_*, for $(m_{\rm i}/m_{\rm e})^{1/2} = 61$. We identify that the modes in figure 14 are small-tail modes by verifying that the $\theta \gg 1$ part of the eigenmode $e\phi_{\rm inner}/T_{\rm e}$ is bounded by the estimates $(m_{\rm e}/m_{\rm i})^{1/2}\, e\phi_{\rm outer}/T_{\rm e}$ (the collisionless case) and $(m_{\rm e}/m_{\rm i})^{1/4}\, e\phi_{\rm outer}/T_{\rm e}$ (the collisional case). The vertical dashed lines indicate the ν_* of the clean examples of the collisionless and collisional small-tail modes that we describe in detail in the following sections. Figure 14 shows that γ and $\omega_{\rm r}$ depend on ν_* for $\nu_* \gtrsim 10^{-2}$, in contrast to the theoretical expectations for small-tail modes. Since similar behaviour is observed for $\nu_{\rm ii} = 0$, this dependence on ν_* in figure 14 results from

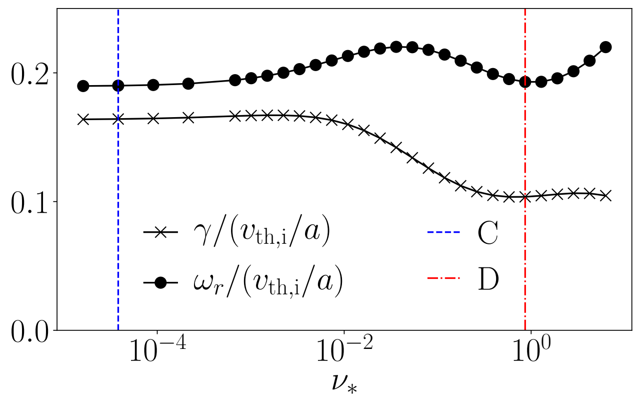

Figure 14. The growth rate γ and real frequency ω_{r} of the (small-tail), ITG mode with $k_y\rho_{\mathrm{th,i}} = 0.5$, $\theta_0 = 0.1$, and $(m_{\mathrm{i}}/m_{\mathrm{e}})^{1/2} = 61$, as a function of normalised electron collisionality ν_*. We vary the ion collision frequency ν_{ii} consistently with ν_*, but quantitatively similar results may be obtained for $\nu_{\mathrm{ii}} = 0$. Note that γ and ω_{r} experience $\mathrm{O}(1)$ changes for $\nu_* \gtrsim 10^{-2}$. This indicates that the $(m_{\mathrm{e}}/m_{\mathrm{i}})^{1/4}$ small nonadiabatic response of electrons in collisional modes can, in practice, matter numerically for the physical value of $(m_{\mathrm{i}}/m_{\mathrm{e}})^{1/4} \approx 8$. The vertical dashed lines C and D indicate the ν_* of the collisionless and collisional examples of the small-tail mode that are discussed in sections 4.3 and 5.2.2 respectively.

the nonadiabatic electron response. For collisionless small-tail modes, the nonadiabatic electron response is small by $(m_{\mathrm{e}}/m_{\mathrm{i}})^{1/2} \approx 1/60$, but for collisional small-tail modes, the nonadiabatic electron response is only small by $(m_{\mathrm{e}}/m_{\mathrm{i}})^{1/4} \approx 1/8$. Hence, we take figure 14 to indicate that, in collisional modes, in practice, for realistic $(m_{\mathrm{e}}/m_{\mathrm{i}})^{1/2}$, the $(m_{\mathrm{e}}/m_{\mathrm{i}})^{1/4}$ small nonadiabatic electron response matters numerically.

6.2.1. Case C – a collisionless small-tail mode. We consider the ITG mode from figure 14 with $\nu_* = 3.82 \times 10^{-5}$. To identify a mode as a collisionless small-tail mode, we must demonstrate several properties. First, that there is a $\theta \sim 1$ region where $e\phi/T_{\mathrm{e}}$ is independent of $(m_{\mathrm{e}}/m_{\mathrm{i}})^{1/2}$ at leading order. Second, that the potential in the $\theta \gg 1$ region has an amplitude given by estimate (82), and an envelope $\theta \sim (m_{\mathrm{i}}/m_{\mathrm{e}})^{1/2}$. Third, that the electron distribution function has a size given by estimate (80), and an envelope with scale $\theta \sim (m_{\mathrm{i}}/m_{\mathrm{e}})^{1/2}$. In figure 15, we demonstrate that the first and second properties are satisfied. In figure 16, we use $j_{\|}^{+}$ as a measure of H_{e} to demonstrate that the third property is satisfied.

Finally, we discuss the $(m_{\mathrm{e}}/m_{\mathrm{i}})^{1/2}$ dependence of the growth rate γ and real frequency ω_{r} in the $\nu_* = 3.82 \times 10^{-5}$ example of a small-tail mode. The growth rate and frequency are plotted in figure 17. As the asymptotic expansion is carried out in $(m_{\mathrm{e}}/m_{\mathrm{i}})^{1/2}$, we expect to see a linear dependence in $(m_{\mathrm{e}}/m_{\mathrm{i}})^{1/2}$. This is observed for a wide range of $(m_{\mathrm{e}}/m_{\mathrm{i}})^{1/2}$ in γ, but for a smaller range of $(m_{\mathrm{e}}/m_{\mathrm{i}})^{1/2}$ for ω_{r}. We note

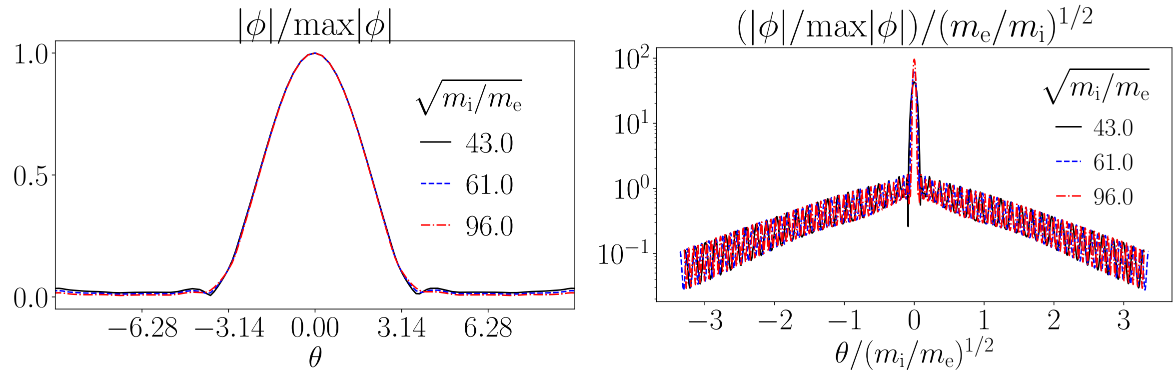

Figure 15. Two views of the electrostatic potential ϕ, calculated for $\nu_* = 3.82 \times 10^{-5}$ (case C of figure 14) for three different mass ratios. (left) The potential ϕ is plotted against the unscaled ballooning angle θ, and normalised to its maximum value. The fact that the curves overlay for $\theta \sim 1$ indicates that the potential eigenmode is independent of $(m_e/m_i)^{1/2}$ to leading order. (right) The potential is plotted against the scaled ballooning angle $\theta/(m_i/m_e)^{1/2}$, and normalised by a factor of $(m_e/m_i)^{1/2} \max|\phi|$. The fact that the curves overlap in the region $\theta \sim (m_i/m_e)^{1/2}$ indicates that the mode is a small-tail mode, satisfying the ordering (82).

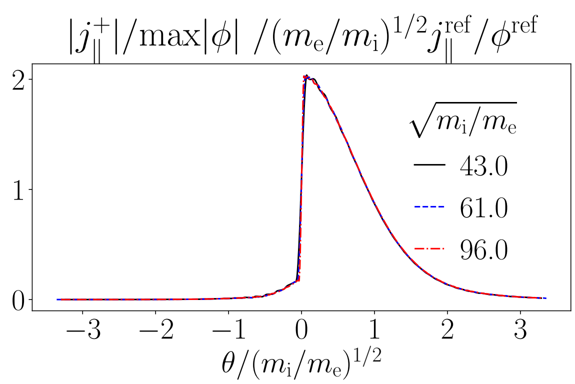

Figure 16. The field $j_\parallel^+$, calculated for $\nu_* = 3.82 \times 10^{-5}$ (case C of figure 14) for three different mass ratios. The fact that the curves overlay on the $\theta/(m_i/m_e)^{1/2}$ axis confirms that the mode is a collisionless small-tail mode, satisfying the ordering (80).

that an ITG mode with $\nu_* = 0$ shows notably better linear fits for both γ and ω_r.

6.2.2. Case D – a collisional small-tail mode. In the collisional limit, the electron response of a small-tail mode is characterised by a jump in the electron flows across the $\theta \sim 1$ region. This results in the scalings (179) for the electrostatic potential, electron density, and electron temperature in the $\theta \gg 1$ region. As in the large-tail collisional mode, the size of the envelope of the mode is expected to be of scale $\theta \sim (m_i/m_e)^{1/4}$. To test these scalings, we examine an ITG mode with normalised electron collision

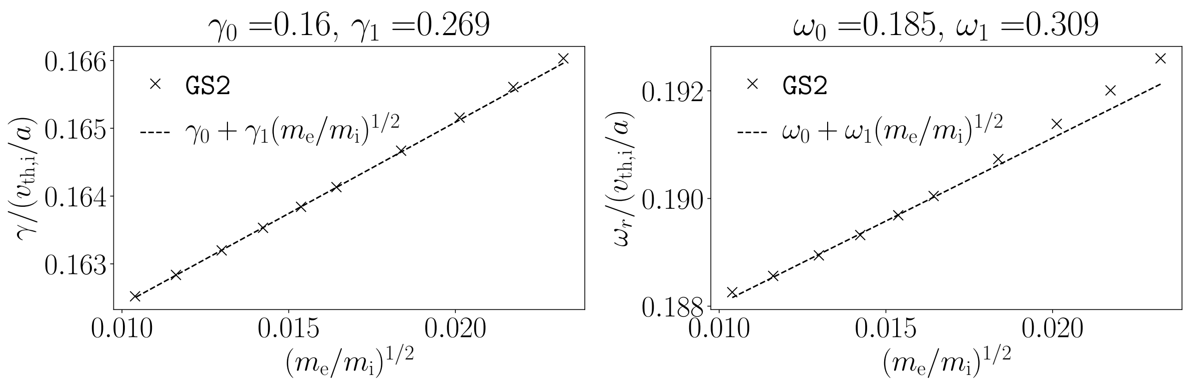

Figure 17. Plots of the growth rate γ (left) and real frequency ω_r (right) as a function of $(m_e/m_i)^{1/2}$, for $\nu_* = 3.82 \times 10^{-5}$ (case A of figure 14). We give a linear fit to demonstrate that the dependence of γ and ω_r on $(m_e/m_i)^{1/1}$ is consistent with a $(m_e/m_i)^{1/2}$ expansion.

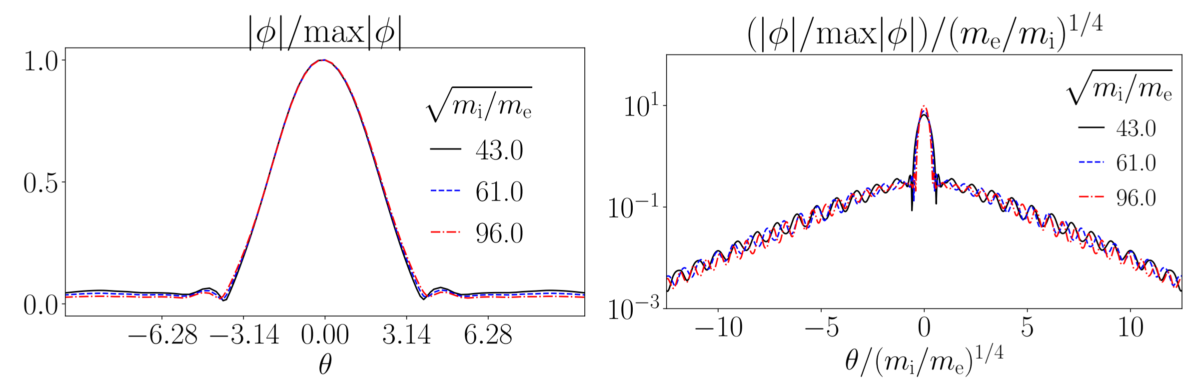

Figure 18. Two views of the electrostatic potential ϕ, calculated for $\nu_* = 0.86$ (case D of figure 14) for three different mass ratios. (left) The potential ϕ is plotted against the unscaled ballooning angle, and normalised to its maximum value. That the curves overlay in the $\theta \sim 1$ region indicates that the mode is a small-tail mode. (right) The potential ϕ is plotted against the scaled ballooning angle $\theta/(m_i/m_e)^{1/4}$, and normalised to its maximum value, divided by $(m_e/m_i)^{1/4}$. That the curves overlay for $\theta \sim (m_i/m_e)^{1/4}$ indicates that we have correctly identified the scaling (179) for the size of the electron response, and the size of the mode envelope.

frequency $\nu_* = 0.86$ (case D of figure 14). We plot the electrostatic potential ϕ in figure 18. We note that ϕ has no mass dependence for $\theta \sim 1$, and that ϕ has the mass scaling given by the estimate (179) for $\theta \sim (m_i/m_e)^{1/4}$. This confirms that the mode is a collisional, small-tail mode.

To illustrate the electron response further, we plot the nonadiabatic electron density δn_e and electron temperature δT_e in figure 19. The scaling (179) is confirmed by the fact that the curves overlay with the mass scaling $(m_e/m_i)^{1/4}$ in the amplitude, and the mass scaling $(m_i/m_e)^{1/4}$ in the ballooning angle. In figure 20, we plot the field $j_\parallel$, normalised to the maximum value of $|\phi|$. Consistent with the identification of the mode

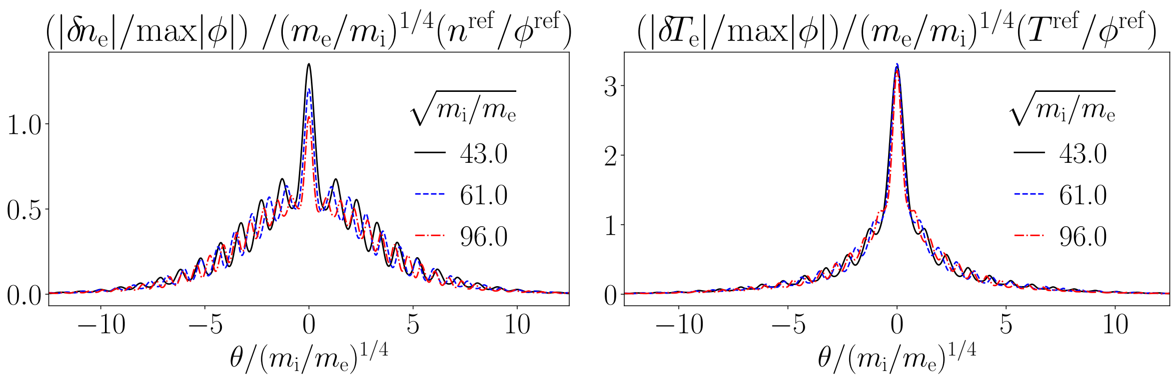

Figure 19. (left) The electron nonadiabatic density δn_{e}, and (right) the electron temperature δT_{e}, calculated for $\nu_* = 0.86$ (case D of figure 14) for three different mass ratios.

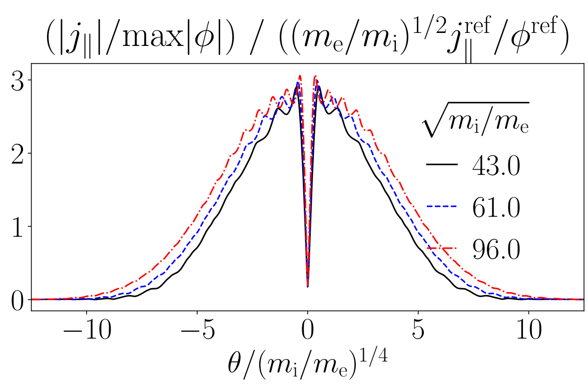

Figure 20. The field $j_\|$, calculated for $\nu_* = 0.86$ (case D of figure 14) for three different mass ratios.

as a collisional small-tail mode, the envelope of $j_\|$ appears to scale like $\theta \sim (m_{\mathrm{i}}/m_{\mathrm{e}})^{1/4}$, and the amplitude is small by $(m_{\mathrm{e}}/m_{\mathrm{i}})^{1/2}$. Although the envelope rescaling is not perfect in figure 20, the $(m_{\mathrm{i}}/m_{\mathrm{e}})^{1/4}$ rescaling is better than a $(m_{\mathrm{i}}/m_{\mathrm{e}})^{1/2}$ rescaling. This figure completes the demonstration of the physical picture for the collisional small-tail mode: the ions generate an electrostatic potential at $\theta \sim 1$, the electrons respond with a $(m_{\mathrm{e}}/m_{\mathrm{i}})^{1/2}$ small flow, and a small electron flow self-consistently sets up a $(m_{\mathrm{e}}/m_{\mathrm{i}})^{1/4}$ nonadiabatic electron density and temperature response.

Finally, in figure 21 we plot the growth rate γ and the real frequency ω_{r} as a function of $(m_{\mathrm{e}}/m_{\mathrm{i}})^{1/4}$. The asymptotic expansion for the collisional small-tail mode is carried out in powers of $(m_{\mathrm{e}}/m_{\mathrm{i}})^{1/4}$. Hence, we would expect small corrections to the frequency to scale as $\omega^{(1/2)}/\omega^{(0)} \sim (m_{\mathrm{e}}/m_{\mathrm{i}})^{1/4}$. Consistent with this, in figure 21 we see that the linear fit is plausible for a range of $(m_{\mathrm{e}}/m_{\mathrm{i}})^{1/4}$.

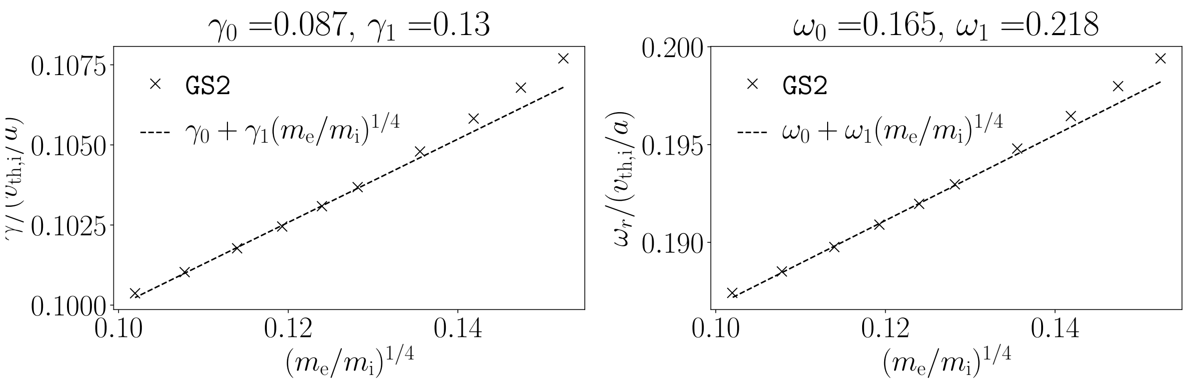

Figure 21. Plots of the growth rate γ (left) and real frequency ω_r (right) as a function of $(m_e/m_i)^{1/4}$, for $\nu_* = 0.86$ (case D of figure 14). We give a linear fit to demonstrate that the dependence of γ and ω_r on $(m_e/m_i)^{1/4}$ is consistent with a $(m_e/m_i)^{1/4}$ expansion.

6.3. The transition between the large-tail and small-tail modes

In the results that we have presented in the previous sections, we have focused on examples where either a large-tail or the small-tail mode is clearly dominant. However, in practice it is possible to find cases where these different asymptotic branches have similar growth rates, and so a transition can be observed with the variation of some parameter. To illustrate this, we consider modes in a range of θ_0, for $k_y\rho_{th,i} = 0.5$, $a/L_{T_e} = 3a/L_{T_i} = 6.9$ (the temperature gradients used in section 6.1), and a normalised electron collisionality of $\nu_* = 3.82 \times 10^{-5}$. Figure 22 shows the real frequency ω_r and growth rate γ of these modes as a function of θ_0, for different values of $(m_i/m_e)^{1/2}$. For the smallest value of $(m_i/m_e)^{1/2}$, $(m_i/m_e)^{1/2} = 43$, ω_r and γ are continuous functions of θ_0. However, for increasing $(m_i/m_e)^{1/2}$ a discontinuity in ω_r appears. This indicates a transition between different mode branches. By examining the eigenmodes using the techniques of sections 6.1 and 6.2, we verify that the modes to the right of the dashed line are collisionless large-tail modes. In accordance with the predictions of section 4.4, the growth rate and frequency of the large tail mode are approximately independent of θ_0. In contrast, we identify that the modes to the left of the dashed line are collisionless small-tail modes. The small-tail mode observed here is likely to be a TEM, since it is stabilised by sufficiently large ν_*.

We note that initial-value simulations of eigenmodes are challenging to converge when distinct instabilities exist at the same (k_y, θ_0) with the same γ. The data plotted in figure 22 are for modes where the ω_r and γ are converged to 1% (compared to values averaged over a $5a/v_{th,i}$ window) after $500a/v_{th,i}$. A time step size of $\Delta t = 0.1a/v_{th,i}$ was found to be adequate to resolve the collisionless modes featured in this section.

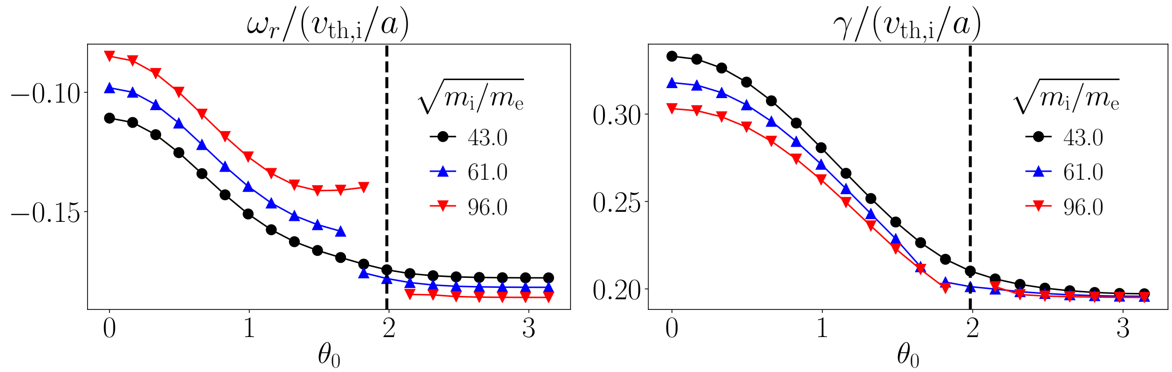

Figure 22. The real frequency ω_r (left) and growth rate γ (right) as a function of θ_0 and $(m_\mathrm{i}/m_\mathrm{e})^{1/2}$, for $\nu_* = 3.82 \times 10^{-5}$ and $a/L_{T_\mathrm{e}} = 3a/L_{T_\mathrm{i}} = 6.9$. A discontinuity in the frequency opens up for increasing $(m_\mathrm{i}/m_\mathrm{e})^{1/2}$ – indicating a transition between different instability branches. Modes to the left of the dashed line are small-tail modes (driven by trapped electrons and ions), whereas modes to the right of the dashed line are large-tail modes (driven by passing electrons). Note that ω_r and γ are approximately independent of θ_0 for the large-tail modes.

7. Discussion

In the traditional treatment of the nonadiabatic electron response in modes with binormal wavenumbers on the scale of the ion thermal gyroradius, i.e., in modes with $k_y\rho_{\mathrm{th,i}} \sim 1$, rapid electron parallel streaming is assumed to imply that the nonadiabatic response of passing electrons should be small. This assumption leads to the usual ITG-driven modes and TEMs where the nonadiabatic passing electron response is subdominant. However, several numerical investigations have revealed the existence of long-wavelength modes with extended ballooning tails where the nonadiabatic passing electron response appears to play a significant role, see, e.g., [12, 13, 15–18, 39, 40]. In terms of a wavenumber-space description, these electron-driven modes are fluctuations with large radial wave numbers, i.e., $k_r\rho_{\mathrm{th,i}} \gg 1$. In the real-space description, these modes are fine-scale fluctuations with significant amplitudes near mode-rational flux surfaces. Examples of these modes may be found in the core of tokamaks [12, 13], and in the pedestal [15]. Qualitatively, micro-tearing modes in tokamaks share the same features as the extended electrostatic modes in [12, 13, 15], with both extended ballooning tails and an ETG drive [16–18].

In this paper, we show that it is possible to obtain an asymptotic theory for novel electron-response-driven $k_y\rho_{\mathrm{th,i}} \sim 1$ modes by assuming that the nonadiabatic response of passing electrons cannot be neglected, and by carefully considering the regions in the mode with large k_r. The physics of these novel modes turn out to be dominated by the physics at $k_r\rho_{\mathrm{th,i}} \gg 1$, and surprisingly, the nonadiabatic ion response is unimportant (but not small). When the nonadiabatic-electron-response-driven modes are unstable, their growth rate is expected to be insensitive to the exact details of the magnetic geometry, because the leading-order equations for the mode contain only poloidal-angle-averaged geometric quantities. As a corollary, the growth rate of the mode is expected to be independent of θ_0. Hence, this type of mode may be insensitive to equilibrium flow shear.

We identify two limits where there are simple orderings. First, we examine the collisionless limit, where $qR_0\nu_{\rm ee}/v_{\rm th,e} \sim (m_{\rm e}/m_{\rm i})^{1/2} \ll 1$, the radial wave number satisfies $k_r\rho_{\rm th,e} \sim 1$, and the fundamental expansion parameter is $(m_{\rm e}/m_{\rm i})^{1/2} \ll 1$. In the collisionless ordering, the extent of the mode is set by the physics of electron free streaming, and electron finite Larmor radius and electron finite orbit width effects. Second, we examine the collisional limit where $qR_0\nu_{\rm ee}/v_{\rm th,e} \sim 1$, the radial wave number satisfies $k_r\rho_{\rm th,e} \sim (m_{\rm e}/m_{\rm i})^{1/4}$, and the fundamental expansion parameter is $(m_{\rm e}/m_{\rm i})^{1/4} \ll 1$. In the collisional ordering, the extent of the mode is set by parallel and perpendicular classical and neoclassical diffusion.

We derive scaling laws for the relative sizes of the electron and ion responses in the $k_r\rho_{\rm th,i} \sim 1$ and $k_r\rho_{\rm th,i} \gg 1$ regions of the ballooning mode. To confirm our analytically derived scalings, we use the gyrokinetic stability code `GS2` to perform a series of linear simulations for a range of normalised electron collisionality $\nu_* = qR_0\nu_{\rm ee}/\epsilon^{3/2}v_{\rm th,e}$, and a range of $m_{\rm e}/m_{\rm i}$. We identify parameters where a novel passing-electron-driven mode is the fastest unstable mode. We present two relatively clean examples of the passing-electron-driven mode: a collisionless case and a collisional case. We perform the same analysis for an ITG mode, and verify the scalings for the subdominant nonadiabatic electron response.

Although the theory presented here neglects electromagnetic fluctuations, many features of these novel electrostatic modes are common to micro-tearing modes. We speculate that some classes of micro-tearing modes may be well described by an collisionless $(m_{\rm e}/m_{\rm i})^{1/2} \to 0$ theory or collisional $(m_{\rm e}/m_{\rm i})^{1/4} \to 0$ theory similar to the theories presented in this paper. Development of these asymptotic theories provides not just physical insight, but also the possibility of performing reduced linear simulations of nonadiabatic-electron-response-driven modes. Simulations of extended ballooning modes can be expensive in comparison to simulations of familiar ITG-driven modes: a reduction of the size of the problem by removing the geometric 2π poloidal-angle scale from the gyrokinetic equations may be an advantage. We anticipate that the need for computational efficiency in simulating extended ballooning modes will become more urgent in light of recent work [41] that suggests high-β spherical tokamak reactor equilibria may be unstable to extended micro-tearing modes for a wide range of k_y.

The nonadiabatic response of passing electrons has recently been shown to be a significant factor in determining the isotope effect [42, 43]. In fact, [43] argues that changes in a $(m_{\rm e}/m_{\rm i})^{1/2}$-small passing electron nonadiabatic response can lead to $\mathrm{O}(1)$ changes in the heat fluxes as a result of the divergent asymptotic expansion in $(m_{\rm e}/m_{\rm i})^{1/2}$. In this paper we have seen that, in linear modes, the nonadiabatic response of passing electrons does not need to be small in $(m_{\rm e}/m_{\rm i})^{1/2}$. Indeed, it is not even obvious that an expansion should be carried out in $(m_{\rm e}/m_{\rm i})^{1/2}$. Instead,

$(m_e/m_i)^{1/4}$ could be the relevant expansion parameter for sufficiently large collisionality. This is an important observation, because, in practice, $(m_e/m_i)^{1/4} \approx 1/8$ is likely to a be worse expansion parameter than $(m_e/m_i)^{1/2} \approx 1/60$. For sufficiently large collisionality, nonasymptotic behaviour may perhaps be observed because the physical value of $(m_e/m_i)^{1/4}$ is not small enough. Whilst we do not develop a nonlinear theory in this paper, we speculate that the isotope effect may well be the result of the nonadiabatic response of passing electrons in $k_r\rho_{\mathrm{th,i}} \gg 1$ narrow layers regulating turbulent transport.

The impact of electron-driven narrow radial layers in nonlinearly saturated turbulence is the subject of active research. Studies of turbulence using DNS have demonstrated that the nonadiabatic response of passing electrons in narrow layers near the mode-rational flux surfaces can have a significant impact on turbulence saturation levels and fluxes, see, e.g., [13, 39, 40, 44, 45]. The regulation of turbulent fluxes by narrow radial layers formed by toroidal ETG modes near the top and bottom of the tokamak has recently been observed in nonlinear DNS of ETG-driven pedestal turbulence [46]. Further evidence for the importance of the nonadiabatic response of passing electrons in narrow layers may be found in DNS that bridge $k_y\rho_{\mathrm{th,i}} \sim 1$ to $k_y\rho_{\mathrm{th,e}} \sim 1$ scales: entropy transfer analysis suggests that the nonadiabatic response of passing electrons mediates the backreaction of $k_y\rho_{\mathrm{th,e}} \sim 1$ eddies on $k_y\rho_{\mathrm{th,i}} \sim 1$ turbulence, via $k_r\rho_{\mathrm{th,i}} \gg 1$ narrow layers [6]. These observations suggest that theories of turbulence that attempt to capture the $(m_e/m_i)^{1/2} \to 0$ limit may need to be modified to include the effects of electrons in narrow radial layers on saturation: this includes theories of turbulence on $k_y\rho_{\mathrm{th,i}} \sim 1$ scales in isolation (cf. [29]) and theories of cross-scale interactions between $k_y\rho_{\mathrm{th,i}} \sim 1$ and $k_y\rho_{\mathrm{th,e}} \sim 1$ scales (cf. [28, 47]).

Finally, we note that whilst results presented here would appear to be specialised to an axisymmetric tokamak by virtue of using the identity (28), a similar theory to the one we present may be obtained for an omnigenous stellarator [48–53], providing that the departure from omnigeneity is small in the mass ratio expansion. Extended ETG-driven microinstabilities may well exist in linear simulations of current stellarators.

The authors are grateful for productive discussions with N. Christen, O. Beeke, B. Patel, J. Maurino-Alperovich, and S. Trinczek. The simulations were performed using the `GS2` *branch* `https://bitbucket.org/gyrokinetics/gs2/branch/ms_pgelres`*, with the latest revision at the time of writing being commit ade5780. This work has been carried out within the framework of the EUROfusion Consortium and has received funding from the Euratom research and training programme 2014-2018 and 2019-2020 under grant agreement No 633053, and from EPSRC [Grant Numbers EP/T012250/1 and EP/R034737/1]. The views and opinions expressed herein do not necessarily reflect those of the European Commission. The author acknowledges the the use of the EUROfusion High Performance Computer (Marconi-Fusion) under projects MULTEI and OXGK, ARCHER through the Plasma HEC Consortium EPSRC Grant Numbers EP/L000237/1 and EP/R029148/1 under the projects e281-gs2 and e607, the JFRS-1 supercomputer at IFERC-CSC in Rokkasho Fusion Institute of QST (Aomori, Japan), and software support through the Plasma-CCP Network under EPSRC Grant Number*

EP/M022463/1.

Appendix A. Classical perpendicular diffusion collisional terms

The collision integrals appearing in the definitions of the classical fluxes $\overline{\delta\Gamma}_{\rm C}$ and $\overline{\delta q}_{\rm C}$, equations (134) and (135), respectively, have the structural form

$$\int g(v)\boldsymbol{v}\cdot\boldsymbol{\tau}\,\mathcal{C}\left[H_{\rm e}^{(0)}(v)\boldsymbol{v}\cdot\boldsymbol{\sigma}\right]\,d^3\boldsymbol{v}, \tag{A.1}$$

with the isotropic function of $\boldsymbol{v}$, g, satisfying either $g=1$ or $g=v^2/v_{\rm th,e}^2-5/2$, and $\boldsymbol{\sigma}=\boldsymbol{k}_\perp^{(0)}\times\boldsymbol{b}/\Omega_{\rm e}$ and $\boldsymbol{\tau}={\rm i}\nabla r\times\boldsymbol{b}/\Omega_{\rm e}$ velocity independent vectors. We now proceed to evaluate the integral defined by equation (A.1). We first evaluate contributions from the electron Lorentz collision operator $\mathcal{L}[\cdot]$.

Appendix A.1. Lorentz collision operator contributions.

The Landau form of the Lorentz collision operator is given by equation (14). Inserting the definition (14) into equation (A.1), using the form of $H_{\rm e}^{(0)}$, equation (107), and integrating by parts, we find that

$$\int g(v)\boldsymbol{v}\cdot\boldsymbol{\tau}\,\mathcal{L}\left[H_{\rm e}^{(0)}(v)\boldsymbol{v}\cdot\boldsymbol{\sigma}\right]\,d^3\boldsymbol{v}=$$

$$\frac{3\sqrt{\pi}}{8}\nu_{\rm ei}v_{\rm th,e}^3\boldsymbol{\tau}\boldsymbol{\sigma}:\int\left\{g(v)\left(\frac{\delta n_{\rm e}^{(0)}}{n_{\rm e}}+\frac{\delta T_{\rm e}^{(0)}}{T_{\rm e}}\left(\frac{v^2}{v_{\rm th,e}^2}-\frac{3}{2}\right)\right)\frac{v^2\boldsymbol{I}-\boldsymbol{v}\boldsymbol{v}}{v^3}F_{0e}\right\}\,d^3\boldsymbol{v}. \tag{A.2}$$

To evaluate equation (A.2) for the appropriate functions g, we use the normalised velocity $\boldsymbol{w}=\boldsymbol{v}/v_{\rm th,e}$, and the identities

$$\int\left(1,w^2,w^4\right)\exp\left[-w^2\right]\frac{w^2\boldsymbol{I}-\boldsymbol{w}\boldsymbol{w}}{w^3}\,d^3\boldsymbol{w}=\frac{4\pi}{3}\boldsymbol{I}\left(1,1,2\right), \tag{A.3}$$

with $w=|\boldsymbol{w}|$. For the case of $g=1$, we find that

$$\int\boldsymbol{v}\cdot\boldsymbol{\tau}\,\mathcal{L}\left[H_{\rm e}^{(0)}(v)\boldsymbol{v}\cdot\boldsymbol{\sigma}\right]\,d^3\boldsymbol{v}=-n_{\rm e}\nu_{\rm ei}v_{\rm th,e}^2\frac{\boldsymbol{\tau}\cdot\boldsymbol{\sigma}}{2}\left(\frac{\delta n_{\rm e}^{(0)}}{n_{\rm e}}-\frac{1}{2}\frac{\delta T_{\rm e}^{(0)}}{T_{\rm e}}\right). \tag{A.4}$$

For the case of $g=v^2/v_{\rm th,e}^2-5/2$, we find that

$$\int\left(\frac{v^2}{v_{\rm th,e}^2}-\frac{5}{2}\right)\boldsymbol{v}\cdot\boldsymbol{\tau}\,\mathcal{L}\left[H_{\rm e}^{(0)}(v)\boldsymbol{v}\cdot\boldsymbol{\sigma}\right]\,d^3\boldsymbol{v}=$$

$$-n_{\rm e}\nu_{\rm ei}v_{\rm th,e}^2\frac{\boldsymbol{\tau}\cdot\boldsymbol{\sigma}}{2}\left(\frac{7}{4}\frac{\delta T_{\rm e}^{(0)}}{T_{\rm e}}-\frac{3}{2}\frac{\delta n_{\rm e}^{(0)}}{n_{\rm e}}\right). \tag{A.5}$$

Appendix A.2. Electron self-collision operator contributions.

In this section we evaluate the perpendicular-diffusion contributions from the electron self-collision operator $C_{\mathrm{ee}}[\cdot]$, following [54]. The electron self-collision operator is defined by equation (9) with $s = \mathrm{e}$. To perform the calculation, first, we substitute the definition (9) into the form (A.1) of the perpendicular-diffusion integral, noting that $2\pi e^4 \ln\Lambda/m_{\mathrm{e}}^2 = 3\sqrt{\pi}\nu_{\mathrm{ee}}v_{\mathrm{th,e}}^3/8n_{\mathrm{e}}$, with ν_{ee} defined by equation (12). Second, we integrate by parts, and symmetrise the resulting integral by relabelling the dummy variables $\boldsymbol{v}$ and $\boldsymbol{v}'$. Writing $f(v) = H_{\mathrm{e}}^{(0)}(v)/F_{0\mathrm{e}}$, we obtain the result

$$\int g(v)\boldsymbol{v}\cdot\boldsymbol{\tau}\, C_{\mathrm{ee}}\left[f(v)\boldsymbol{v}\cdot\boldsymbol{\sigma}F_{0\mathrm{e}}\right]\, d^3\boldsymbol{v} =$$

$$-\frac{3\sqrt{\pi}}{16}\frac{\nu_{\mathrm{ee}}v_{\mathrm{th,e}}^3}{n_{\mathrm{e}}}\int\int F_{0\mathrm{e}}F_{0\mathrm{e}}'\boldsymbol{\Psi}\cdot\boldsymbol{U}\cdot\boldsymbol{\Phi}\, d^3\boldsymbol{v}'\, d^3\boldsymbol{v}, \tag{A.6}$$

where the vectors

$$\boldsymbol{\Psi}(\boldsymbol{v},\boldsymbol{v}') = \boldsymbol{\tau}(g-g') + (\boldsymbol{v}\cdot\boldsymbol{\tau})\frac{\partial g}{\partial \boldsymbol{v}} - (\boldsymbol{v}'\cdot\boldsymbol{\tau})\frac{\partial g'}{\partial \boldsymbol{v}'}, \tag{A.7}$$

and

$$\boldsymbol{\Phi}(\boldsymbol{v},\boldsymbol{v}') = \frac{\partial f}{\partial \boldsymbol{v}}(\boldsymbol{v}\cdot\boldsymbol{\sigma}) - \frac{\partial f'}{\partial \boldsymbol{v}'}(\boldsymbol{v}'\cdot\boldsymbol{\sigma}) + \boldsymbol{\sigma}(f-f'), \tag{A.8}$$

respectively, with $g' = g(v')$, and $f' = f(v')$. The form of the vector $\boldsymbol{\Psi}$, defined in equation (A.7), shows that there is no self-collision operator contribution to the perpendicular-diffusion terms in the density equation, for which $g = 1$. To evaluate the self-collision operator contribution to the temperature equation, we take $g(v) = v^2/v_{\mathrm{th,e}}^2 - 3/2$ and use that

$$f(v) = \frac{H_{\mathrm{e}}^{(0)}}{F_{0\mathrm{e}}} = \frac{\delta n_{\mathrm{e}}^{(0)}}{n_{\mathrm{e}}} + \frac{\delta T_{\mathrm{e}}^{(0)}}{n_{\mathrm{e}}}\left(\frac{v^2}{v_{\mathrm{th,e}}^2} - \frac{3}{2}\right). \tag{A.9}$$

After substituting for g and f in equations (A.7) and (A.8), respectively, we find that

$$\boldsymbol{\Psi}(\boldsymbol{v},\boldsymbol{v}') = \boldsymbol{\tau}\frac{v^2 - v'^2}{v_{\mathrm{th,e}}^2} + \frac{2(\boldsymbol{v}(\boldsymbol{v}\cdot\boldsymbol{\tau}) - \boldsymbol{v}'(\boldsymbol{v}'\cdot\boldsymbol{\tau}))}{v_{\mathrm{th,e}}^2}, \tag{A.10}$$

and

$$\boldsymbol{\Phi}(\boldsymbol{v},\boldsymbol{v}') = \left(\boldsymbol{\sigma}\frac{v^2 - v'^2}{v_{\mathrm{th,e}}^2} + \frac{2(\boldsymbol{v}(\boldsymbol{v}\cdot\boldsymbol{\sigma}) - \boldsymbol{v}'(\boldsymbol{v}'\cdot\boldsymbol{\sigma}))}{v_{\mathrm{th,e}}^2}\right)\frac{\delta T_{\mathrm{e}}^{(0)}}{T_{\mathrm{e}}}. \tag{A.11}$$

To compute the velocity integrals in equation (A.6), we convert to the center-of-mass variables

$$\boldsymbol{s} = \frac{\boldsymbol{v}+\boldsymbol{v}'}{\sqrt{2}v_{\mathrm{th,e}}}, \quad \text{and} \quad \boldsymbol{w} = \frac{\boldsymbol{v}-\boldsymbol{v}'}{\sqrt{2}v_{\mathrm{th,e}}}, \tag{A.12}$$

with the result

$$\int\int F_{0\mathrm{e}}F_{0\mathrm{e}}'\boldsymbol{\Psi}\cdot\boldsymbol{U}\cdot\boldsymbol{\Phi}\, d^3\boldsymbol{v}'\, d^3\boldsymbol{v} = \frac{4n_{\mathrm{e}}^2}{\sqrt{2}\pi^3 v_{\mathrm{th,e}}}\frac{\delta T_{\mathrm{e}}^{(0)}}{T_{\mathrm{e}}} \times \tag{A.13}$$

$$\int\int \exp\left[-w^2 - s^2\right] (\boldsymbol{\tau}(\boldsymbol{s}\cdot\boldsymbol{w}) + (\boldsymbol{w}\cdot\boldsymbol{\tau})\boldsymbol{s}) \cdot \widehat{\boldsymbol{U}} \cdot (\boldsymbol{\sigma}(\boldsymbol{s}\cdot\boldsymbol{w}) + \boldsymbol{s}(\boldsymbol{w}\cdot\boldsymbol{\sigma}))\ d^3\boldsymbol{s}\ d^3\boldsymbol{w},$$

where we have used that the Jacobian $d^3\boldsymbol{v}'d^3\boldsymbol{v} = v_{\rm th,e}^6 d^3\boldsymbol{s}d^3\boldsymbol{w}$, the functions $v^2 - v'^2 = 2v_{\rm th,e}^2\boldsymbol{w}\cdot\boldsymbol{s}$, $\boldsymbol{v}\boldsymbol{v} - \boldsymbol{v}'\boldsymbol{v}' = v_{\rm th,e}^2(\boldsymbol{w}\boldsymbol{s} + \boldsymbol{s}\boldsymbol{w})$, $v^2 + v'^2 = v_{\rm th,e}^2(w^2 + s^2)$, and $\boldsymbol{U}(\boldsymbol{v} - \boldsymbol{v}') = \widehat{\boldsymbol{U}}(\boldsymbol{w})/(\sqrt{2}v_{\rm th,e})$, with

$$\widehat{\boldsymbol{U}}(\boldsymbol{w}) = \frac{w^2\boldsymbol{I} - \boldsymbol{w}\boldsymbol{w}}{w^3}. \tag{A.14}$$

Note as well that $\boldsymbol{w}\cdot\widehat{\boldsymbol{U}}(\boldsymbol{w}) = 0$. We first evaluate the integral in $\boldsymbol{s}$ using the identity

$$\int \exp\left[-s^2\right]\boldsymbol{s}\boldsymbol{s}\ d^3\boldsymbol{s} = \frac{\pi^{3/2}}{2}\boldsymbol{I}. \tag{A.15}$$

The result is

$$\int\int F_{0e}F'_{0e}\boldsymbol{\Psi}\cdot\boldsymbol{U}\cdot\boldsymbol{\Phi}\ d^3\boldsymbol{v}'\ d^3\boldsymbol{v} = \tag{A.16}$$

$$\frac{\sqrt{2}n_{\rm e}^2}{\pi^{3/2}v_{\rm th,e}}\frac{\delta T_{\rm e}^{(0)}}{T_{\rm e}}\boldsymbol{\tau}\boldsymbol{\sigma} : \int \exp\left[-w^2\right]\left(w^2\widehat{\boldsymbol{U}} + \boldsymbol{w}\boldsymbol{w}\ {\rm Tr}\left[\widehat{\boldsymbol{U}}\right]\right)\ d^3\boldsymbol{w}, \tag{A.17}$$

where ${\rm Tr}\left[\widehat{\boldsymbol{U}}\right] = 2/w$ is the trace of the tensor $\widehat{\boldsymbol{U}}(\boldsymbol{w})$. Finally, using equations (A.6) and (A.16), with the identities (A.3) and

$$\int \boldsymbol{w}\boldsymbol{w}{\rm Tr}\left[\widehat{\boldsymbol{U}}\right]\exp\left[-w^2\right]\ d^3\boldsymbol{w} = \frac{4\pi}{3}\boldsymbol{I}, \tag{A.18}$$

we can write down the result of the perpendicular-diffusion collision integral

$$\int\left(\frac{v^2}{v_{\rm th,e}^2} - \frac{3}{2}\right)\boldsymbol{v}\cdot\boldsymbol{\tau}\ C_{\rm ee}\left[H_{\rm e}^{(0)}(v)\boldsymbol{v}\cdot\boldsymbol{\sigma}\right]\ d^3\boldsymbol{v} = -\frac{1}{\sqrt{2}}\nu_{\rm ee}n_{\rm e}v_{\rm th,e}^2\boldsymbol{\tau}\cdot\boldsymbol{\sigma}\frac{\delta T_{\rm e}^{(0)}}{T_{\rm e}}. \tag{A.19}$$

Appendix B. Spitzer-Härm component of the parallel diffusion collisional terms

In order to evaluate the parallel flow and neoclassical perpendicular diffusion terms in equations (127) and (128), we need to solve equation (116) for $H_{\rm SH}$. To solve for $H_{\rm SH}$, we first note that the collision operators $C_{\rm ee}[\cdot]$ and $\mathcal{L}[\cdot]$, defined in equations, (9) and (14), respectively, are isotropic operators [27], and hence $H_{\rm SH}$ may be assumed to have the form given in equation (117). Second, we note that equation (116) is linear in $\delta n_{\rm e}^{(0)}$ and $\delta T_{\rm e}^{(0)}$. Third, we may express the ε dependence of $K_{\rm SH}$ in a convenient basis of polynomials. Hence, $K_{\rm SH}$ is given by

$$K_{\rm SH} = \boldsymbol{b}\cdot\nabla\theta\frac{\partial}{\partial\chi}\left(\frac{\delta n_{\rm e}^{(0)}}{n_{\rm e}}\right)f_{\rm SH}(\hat{x}) + \boldsymbol{b}\cdot\nabla\theta\frac{\partial}{\partial\chi}\left(\frac{\delta T_{\rm e}^{(0)}}{T_{\rm e}}\right)g_{\rm SH}(\hat{x}), \tag{B.1}$$

where

$$f_{\rm SH}(\hat{x}) = \sum_{p=0} a_p L_p^{3/2}(\hat{x}), \tag{B.2}$$

and

$$g_{\rm SH}(\hat{x}) = \sum_{p=0} c_p L_p^{3/2}(\hat{x}), \tag{B.3}$$

with $\hat{x} = \varepsilon/T_{\rm e} = v^2/v_{\rm th,e}^2$, $L_p^{3/2}(\hat{x})$ the $p^{\rm th}$ generalised Laguerre polynomial $L_p^j(\hat{x})$ of index $j = 3/2$, and a_p and c_p coefficients to be determined. The generalised Laguerre polynomials of index $j = 3/2$ are particularly convenient for this problem because we will be able to exploit the orthogonality relation [27]

$$\int_0^\infty L_p^j(\hat{x}) L_q^j(\hat{x}) \exp[-\hat{x}] \hat{x}^j \, d\hat{x} = \frac{\Gamma(p+j+1)}{p!} \delta_{p,q}, \tag{B.4}$$

where $\Gamma(j) = \int_0^\infty \hat{x}^{j-1} \exp[-\hat{x}] d\hat{x}$ is the Gamma function, and $\delta_{p,q}$ is the Kronecker delta. The polynomial $L_p^j(\hat{x})$ may be obtained from the generating function [27]

$$G(\hat{x}, z) = \frac{\exp[-\hat{x}z/(1-z)]}{(1-z)^{j+1}} = \sum_{p=0} z^p L_p^j(\hat{x}). \tag{B.5}$$

With the form of $K_{\rm SH}$ given by equation (B.1), the problem (116) may be cast into two seperate Spitzer problems for $f_{\rm SH}$ and $g_{\rm SH}$,

$$v_\parallel L_0^{3/2} F_{0e} = \mathcal{C}\left[v_\parallel f_{\rm SH} F_{0e} \right], \tag{B.6}$$

and

$$v_\parallel (L_0^{3/2} - L_1^{3/2}) F_{0e} = \mathcal{C}\left[v_\parallel g_{\rm SH} F_{0e} \right], \tag{B.7}$$

where we have used the first two generalised Laguerre polynomials, $L_0^{3/2}(\hat{x}) = 1$ and $L_1^{3/2}(\hat{x}) = 5/2 - \hat{x}$. We solve equations (B.6) and (B.7) by converting them into matrix equations for the coefficients a_p and c_p, respectively. To do this, we define an inner product $\langle \cdot | \cdot \rangle$ acting on velocity space functions $f = f(\boldsymbol{v})$ and $g = g(\boldsymbol{v})$ by

$$\langle f | g \rangle = \int \frac{f(\boldsymbol{v}) g(\boldsymbol{v})}{F_{0e}} \, d^3\boldsymbol{v}, \tag{B.8}$$

and we take the inner product of equations (B.6) and (B.7) with the function $v_\parallel L_q^{3/2} F_{0e}$. To perform the velocity integrals, we use the velocity coordinates $(\hat{x}, \xi, \gamma)$, where $\xi = v_\parallel / v$, and we recall that γ is the gyrophase. The velocity integral in these coordinates becomes

$$\int \cdot \, d^3\boldsymbol{v} = \int_0^{2\pi} \int_{-1}^{1} \int_0^\infty \cdot \, \frac{v_{\rm th,e}^3}{2} \sqrt{\hat{x}} \, d\hat{x} \, d\xi \, d\gamma. \tag{B.9}$$

Using the orthogonality relation (B.4), we find that the matrix form of equation (B.6) is

$$\sum_q \left(\nu_{\rm ee} C_{p,q} + \nu_{\rm ei} \mathcal{L}_{p,q} \right) a_q = -\delta_{0,p}, \tag{B.10}$$

where the matrix elements $C_{p,q}$ and $\mathcal{L}_{p,q}$ are defined by

$$C_{p,q} = -\frac{2}{n_{\rm e}\nu_{\rm ee}} \left\langle \hat{x}^{1/2} \xi F_{0e} L_p^{3/2} \middle| C_{\rm ee}\left[\hat{x}^{1/2} \xi F_{0e} L_q^{3/2} \right] \right\rangle \tag{B.11}$$

and

$$\mathcal{L}_{p,q} = -\frac{2}{n_{\mathrm{e}}\nu_{\mathrm{ei}}} \left\langle \hat{x}^{1/2}\xi F_{0e} L_p^{3/2} \middle| \mathcal{L}\left[\hat{x}^{1/2}\xi F_{0e} L_q^{3/2}\right]\right\rangle, \tag{B.12}$$

respectively. Similarly, we find that the matrix form of equation (B.7) is

$$\sum_q \left(\nu_{\mathrm{ee}} C_{p,q} + \nu_{\mathrm{ei}}\mathcal{L}_{p,q}\right) c_q = \frac{5}{2}\delta_{1,p} - \delta_{0,p}. \tag{B.13}$$

To solve the problem, we invert the matrix equations (B.10) and (B.13). In practice, we must include a finite number of polynomials, with the series truncated at a finite $p = N$. Velocity moments of H_{SH} will depend only on low-order coefficients a_p and c_p, and so only a few polynomials are required before convergence is reached. This same solution may be obtained using a variational method [27].

Although the calculation is tedious, it is relatively straightforward to calculate the matrix elements $C_{p,q}$ and $\mathcal{L}_{p,q}$ using the generating function $G(\hat{x}, z)$. Truncating the polynomial series at $N = 4$, we find the coefficient matrices (cf. [26, 27])

$$\boldsymbol{C} = \sqrt{2}\begin{pmatrix} 0 & 0 & 0 & 0 & 0 \\ 0 & 1 & 3/4 & 15/32 & 35/128 \\ 0 & 3/4 & 45/16 & 309/128 & 885/512 \\ 0 & 15/32 & 309/128 & 5657/1024 & 20349/4096 \\ 0 & 35/128 & 885/512 & 20349/4096 & 149749/16384 \end{pmatrix}, \tag{B.14}$$

and

$$\boldsymbol{\mathcal{L}} = \begin{pmatrix} 1 & 3/2 & 15/8 & 35/16 & 315/128 \\ 3/2 & 13/4 & 69/16 & 165/32 & 1505/256 \\ 15/8 & 69/16 & 433/64 & 1077/128 & 10005/1024 \\ 35/16 & 165/32 & 1077/128 & 2957/256 & 28257/2048 \\ 315/128 & 1505/256 & 10005/1024 & 28257/2048 & 288473/16384 \end{pmatrix}. \tag{B.15}$$

To illustrate the final result of the calculation for a simple case, we solve equations (B.10) and (B.13) for a hydrogenic plasma with $Z_{\mathrm{i}} = 1$, i.e., $\nu_{\mathrm{ei}} = \nu_{\mathrm{ee}}$. To three decimal places, we find that the coefficients $\{a_n\}$ and $\{c_n\}$ are

$$\begin{pmatrix} a_0 \\ a_1 \\ a_2 \\ a_3 \\ a_4 \end{pmatrix} = \frac{1}{\nu_{\mathrm{ei}}}\begin{pmatrix} -1.969 \\ 0.559 \\ 0.017 \\ 0.016 \\ 0.027 \end{pmatrix}, \tag{B.16}$$

and

$$\begin{pmatrix} c_0 \\ c_1 \\ c_2 \\ c_3 \\ c_4 \end{pmatrix} = \frac{1}{\nu_{\mathrm{ei}}}\begin{pmatrix} -3.366 \\ 2.226 \\ -0.635 \\ 0.095 \\ 0.003 \end{pmatrix}, \tag{B.17}$$

respectively.

To calculate the parallel flow and the neoclassical perpendicular diffusion terms, we need to evaluate velocity integrals of the form

$$\int v_\parallel H_{\rm SH}\, d^3\boldsymbol{v} = \frac{n_{\rm e} v_{\rm th,e}^2}{2}\boldsymbol{b}\cdot\nabla\theta\left(a_0\frac{\partial}{\partial\chi}\left(\frac{\delta n_{\rm e}^{(0)}}{n_{\rm e}}\right)+c_0\frac{\partial}{\partial\chi}\left(\frac{\delta T_{\rm e}^{(0)}}{T_{\rm e}}\right)\right), \tag{B.18}$$

and

$$\int v_\parallel\left(\frac{v^2}{v_{\rm th,e}^2}-\frac{5}{2}\right)H_{\rm SH}\, d^3\boldsymbol{v} \tag{B.19}$$

$$= -\frac{5 n_{\rm e} v_{\rm th,e}^2}{4}\boldsymbol{b}\cdot\nabla\theta\left(a_1\frac{\partial}{\partial\chi}\left(\frac{\delta n_{\rm e}^{(0)}}{n_{\rm e}}\right)+c_1\frac{\partial}{\partial\chi}\left(\frac{\delta T_{\rm e}^{(0)}}{T_{\rm e}}\right)\right).$$

Appendix C. Pfirsh-Schlüter parallel and perpendicular fluxes

In this section we compute the parallel flows and the perpendicular diffusion terms in the subsidiary limit of $qR_0\nu_{\rm ee}/v_{\rm th,e}\gg 1$. Following on from the results (151) and (152) in section 5.1.3, we explicitly evaluate $\mathcal{K}_n$ and $\mathcal{K}_T$ using the results (B.18) and (B.19) of Appendix B. We find that

$$\int \frac{v_\parallel}{B} H_{\rm e,(0)}^{(1/2)}\, d^3\boldsymbol{v} = \frac{n_{\rm e} v_{\rm th,e}^2}{2}\frac{\boldsymbol{B}\cdot\nabla\theta}{B^2}\left[a_0\left(\frac{\partial}{\partial\chi}\left(\frac{\delta n_{\rm e}^{(0)}}{n_{\rm e}}\right)+\frac{\partial}{\partial\theta}\left(\frac{\delta n_{\rm e,(-1)}^{(1/2)}}{n_{\rm e}}\right)\right)\right.$$

$$\left.+c_0\left(\frac{\partial}{\partial\chi}\left(\frac{\delta T_{\rm e}^{(0)}}{T_{\rm e}}\right)+\frac{\partial}{\partial\theta}\left(\frac{\delta T_{\rm e,(-1)}^{(1/2)}}{T_{\rm e}}\right)\right)\right]-\frac{n_{\rm e} v_{\rm th,e}^2}{2}\frac{{\rm i}k_\alpha q'\chi I}{\Omega_{\rm e} B}\left(\frac{\delta n_{\rm e}^{(0)}}{n_{\rm e}}+\frac{\delta T_{\rm e}^{(0)}}{T_{\rm e}}\right), \tag{C.1}$$

where $a_0=-1.969/\nu_{\rm ei}$, $c_0=-3.366/\nu_{\rm ei}$, and we have assumed $Z_{\rm i}=1$; and

$$\int \frac{v_\parallel}{B}\left(\frac{\varepsilon}{T_{\rm e}}-\frac{5}{2}\right) H_{\rm e,(0)}^{(1/2)}\, d^3\boldsymbol{v} = -\frac{5n_{\rm e} v_{\rm th,e}^2}{4}\frac{\boldsymbol{B}\cdot\nabla\theta}{B^2}\left[a_1\left(\frac{\partial}{\partial\chi}\left(\frac{\delta n_{\rm e}^{(0)}}{n_{\rm e}}\right)+\frac{\partial}{\partial\theta}\left(\frac{\delta n_{\rm e,(-1)}^{(1/2)}}{n_{\rm e}}\right)\right)\right.$$

$$\left.+c_1\left(\frac{\partial}{\partial\chi}\left(\frac{\delta T_{\rm e}^{(0)}}{T_{\rm e}}\right)+\frac{\partial}{\partial\theta}\left(\frac{\delta T_{\rm e,(-1)}^{(1/2)}}{T_{\rm e}}\right)\right)\right]-\frac{5n_{\rm e} v_{\rm th,e}^2}{4}\frac{{\rm i}k_\alpha q'\chi I}{\Omega_{\rm e} B}\frac{\delta T_{\rm e}^{(0)}}{T_{\rm e}}, \tag{C.2}$$

where $a_1=0.559/\nu_{\rm ei}$ and $c_1=2.226/\nu_{\rm ei}$. We obtain explicit expressions for $\mathcal{K}_n$ and $\mathcal{K}_T$ by multiplying equations (C.1) and (C.2) by B^2, and applying poloidal angle average $\langle\cdot\rangle^\theta$. The results are

$$\mathcal{K}_n(\chi) = \frac{n_{\rm e} v_{\rm th,e}^2}{2}\frac{\langle\boldsymbol{B}\cdot\nabla\theta\rangle^\theta}{\langle B^2\rangle^\theta}\left[a_0\frac{\partial}{\partial\chi}\left(\frac{\delta n_{\rm e}^{(0)}}{n_{\rm e}}\right)+c_0\frac{\partial}{\partial\chi}\left(\frac{\delta T_{\rm e}^{(0)}}{T_{\rm e}}\right)\right]$$

$$-\frac{n_{\rm e} v_{\rm th,e}^2}{2}\frac{{\rm i}k_\alpha q'\chi I\overline{B}}{\overline{\Omega}_{\rm e}}\frac{1}{\langle B^2\rangle^\theta}\left(\frac{\delta n_{\rm e}^{(0)}}{n_{\rm e}}+\frac{\delta T_{\rm e}^{(0)}}{T_{\rm e}}\right), \tag{C.3}$$

and

$$\mathcal{K}_T(\chi) = -\frac{5n_{\rm e} v_{\rm th,e}^2}{4}\frac{\langle\boldsymbol{B}\cdot\nabla\theta\rangle^\theta}{\langle B^2\rangle^\theta}\left[a_1\frac{\partial}{\partial\chi}\left(\frac{\delta n_{\rm e}^{(0)}}{n_{\rm e}}\right)+c_1\frac{\partial}{\partial\chi}\left(\frac{\delta T_{\rm e}^{(0)}}{T_{\rm e}}\right)\right]$$

$$-\frac{5n_{\rm e}v_{\rm th,e}^2}{4}\frac{{\rm i}k_\alpha q'\chi I\overline{B}}{\overline{\Omega}_{\rm e}}\frac{1}{\langle B^2\rangle^\theta}\frac{\delta T_{\rm e}^{(0)}}{T_{\rm e}}, \tag{C.4}$$

respectively. Finally, to obtain equations for $\delta n_{\rm e,(-1)}^{(1/2)}$ and $\delta T_{\rm e,(-1)}^{(1/2)}$, we subtract equation (C.3) from equation (C.1), and equation (C.4) from equation (C.2). The result is that

$$\begin{aligned}\frac{\boldsymbol{B}\cdot\nabla\theta}{B^2}&\left[a_0\frac{\partial}{\partial\theta}\left(\frac{\delta n_{\rm e,(-1)}^{(1/2)}}{n_{\rm e}}\right)+c_0\frac{\partial}{\partial\theta}\left(\frac{\delta T_{\rm e,(-1)}^{(1/2)}}{T_{\rm e}}\right)\right]=\\&\left(\frac{\langle\boldsymbol{B}\cdot\nabla\theta\rangle^\theta}{\langle B^2\rangle^\theta}-\frac{\boldsymbol{B}\cdot\nabla\theta}{B^2}\right)\left[a_0\frac{\partial}{\partial\chi}\left(\frac{\delta n_{\rm e}^{(0)}}{n_{\rm e}}\right)+c_0\frac{\partial}{\partial\chi}\left(\frac{\delta T_{\rm e}^{(0)}}{T_{\rm e}}\right)\right]\\&+\left(\frac{1}{B^2}-\frac{1}{\langle B^2\rangle^\theta}\right)\frac{{\rm i}k_\alpha q'\chi I\overline{B}}{\overline{\Omega}_{\rm e}}\left(\frac{\delta n_{\rm e}^{(0)}}{n_{\rm e}}+\frac{\delta T_{\rm e}^{(0)}}{T_{\rm e}}\right),\end{aligned} \tag{C.5}$$

and

$$\begin{aligned}\frac{\boldsymbol{B}\cdot\nabla\theta}{B^2}&\left[a_1\frac{\partial}{\partial\theta}\left(\frac{\delta n_{\rm e,(-1)}^{(1/2)}}{n_{\rm e}}\right)+c_1\frac{\partial}{\partial\theta}\left(\frac{\delta T_{\rm e,(-1)}^{(1/2)}}{T_{\rm e}}\right)\right]=\\&\left(\frac{\langle\boldsymbol{B}\cdot\nabla\theta\rangle^\theta}{\langle B^2\rangle^\theta}-\frac{\boldsymbol{B}\cdot\nabla\theta}{B^2}\right)\left[a_1\frac{\partial}{\partial\chi}\left(\frac{\delta n_{\rm e}^{(0)}}{n_{\rm e}}\right)+c_1\frac{\partial}{\partial\chi}\left(\frac{\delta T_{\rm e}^{(0)}}{T_{\rm e}}\right)\right]\\&-\left(\frac{1}{B^2}-\frac{1}{\langle B^2\rangle^\theta}\right)\frac{{\rm i}k_\alpha q'\chi I\overline{B}}{\overline{\Omega}_{\rm e}}\frac{\delta T_{\rm e}^{(0)}}{T_{\rm e}}.\end{aligned} \tag{C.6}$$

Inverting equations (C.5) and (C.6) for $\partial\left(\delta n_{\rm e,(-1)}^{(1/2)}\right)/\partial\theta$ and $\partial\left(\delta T_{\rm e,(-1)}^{(1/2)}\right)/\partial\theta$, we find that

$$\begin{aligned}\frac{\boldsymbol{B}\cdot\nabla\theta}{B^2}\frac{\partial}{\partial\theta}\left(\frac{\delta n_{\rm e,(-1)}^{(1/2)}}{n_{\rm e}}\right)&=\left(\frac{\langle\boldsymbol{B}\cdot\nabla\theta\rangle^\theta}{\langle B^2\rangle^\theta}-\frac{\boldsymbol{B}\cdot\nabla\theta}{B^2}\right)\frac{\partial}{\partial\chi}\left(\frac{\delta n_{\rm e}^{(0)}}{n_{\rm e}}\right)\\&+\left(\frac{1}{B^2}-\frac{1}{\langle B^2\rangle^\theta}\right)\frac{{\rm i}k_\alpha q'\chi I\overline{B}}{\overline{\Omega}_{\rm e}}\left(\frac{c_1}{a_0c_1-a_1c_0}\frac{\delta n_{\rm e}^{(0)}}{n_{\rm e}}+\frac{c_1+c_0}{a_0c_1-a_1c_0}\frac{\delta T_{\rm e}^{(0)}}{T_{\rm e}}\right),\end{aligned} \tag{C.7}$$

and

$$\begin{aligned}\frac{\boldsymbol{B}\cdot\nabla\theta}{B^2}\frac{\partial}{\partial\theta}\left(\frac{\delta T_{\rm e,(-1)}^{(1/2)}}{T_{\rm e}}\right)&=\left(\frac{\langle\boldsymbol{B}\cdot\nabla\theta\rangle^\theta}{\langle B^2\rangle^\theta}-\frac{\boldsymbol{B}\cdot\nabla\theta}{B^2}\right)\frac{\partial}{\partial\chi}\left(\frac{\delta T_{\rm e}^{(0)}}{T_{\rm e}}\right)\\&-\left(\frac{1}{B^2}-\frac{1}{\langle B^2\rangle^\theta}\right)\frac{{\rm i}k_\alpha q'\chi I\overline{B}}{\overline{\Omega}_{\rm e}}\left(\frac{a_0+a_1}{a_0c_1-a_1c_0}\frac{\delta T_{\rm e}^{(0)}}{T_{\rm e}}+\frac{a_1}{a_0c_1-a_1c_0}\frac{\delta n_{\rm e}^{(0)}}{n_{\rm e}}\right).\end{aligned} \tag{C.8}$$

To evaluate the effective electron parallel velocity $\overline{\delta u_\parallel}$, defined in equation (131), we compute the integral

$$\overline{\delta u_\parallel}=\frac{1}{\langle\boldsymbol{b}\cdot\nabla\theta\rangle^\theta}\left\langle\frac{\boldsymbol{b}\cdot\nabla\theta}{n_{\rm e}}\int v_\parallel\left(H_{\rm e,(-1)}^{(1/2)}+H_{\rm e,(0)}^{(1/2)}+{\rm i}\lambda_{\rm e}\chi H_{\rm e}^{(0)}\right)\,d^3\boldsymbol{v}\right\rangle^\theta, \tag{C.9}$$

where we have used the definition (129) and the expansion (140). With the solutions (143) and (147), and the integral (B.18), we find that

$$\overline{\delta u_{\parallel}} = \frac{v_{\rm th,e}^2/2}{\langle \boldsymbol{b}\cdot\nabla\theta\rangle^\theta}\left\langle \frac{(\boldsymbol{B}\cdot\nabla\theta)^2}{B^2}\right\rangle^\theta \left[a_0\frac{\partial}{\partial\chi}\left(\frac{\delta n_{\rm e}^{(0)}}{n_{\rm e}}\right) + c_0\frac{\partial}{\partial\chi}\left(\frac{\delta T_{\rm e}^{(0)}}{T_{\rm e}}\right)\right] \tag{C.10}$$

$$+\frac{v_{\rm th,e}^2/2}{\langle \boldsymbol{b}\cdot\nabla\theta\rangle^\theta}\left\langle \frac{(\boldsymbol{B}\cdot\nabla\theta)^2}{B^2}\left[a_0\frac{\partial}{\partial\theta}\left(\frac{\delta n_{\rm e,(-1)}^{(1/2)}}{n_{\rm e}}\right) + c_0\frac{\partial}{\partial\theta}\left(\frac{\delta T_{\rm e,(-1)}^{(1/2)}}{T_{\rm e}}\right)\right]\right\rangle^\theta.$$

Finally, using equations (C.7) and (C.8) to substitute for $\partial\left(\delta n_{\rm e,(-1)}^{(1/2)}\right)/\partial\theta$ and $\partial\left(\delta T_{\rm e,(-1)}^{(1/2)}\right)/\partial\theta$, we find that

$$\overline{\delta u_{\parallel}} = \frac{v_{\rm th,e}^2/2}{\langle \boldsymbol{b}\cdot\nabla\theta\rangle^\theta}\frac{(\langle\boldsymbol{B}\cdot\nabla\theta\rangle^\theta)^2}{\langle B^2\rangle^\theta} \left[a_0\frac{\partial}{\partial\chi}\left(\frac{\delta n_{\rm e}^{(0)}}{n_{\rm e}}\right) + c_0\frac{\partial}{\partial\chi}\left(\frac{\delta T_{\rm e}^{(0)}}{T_{\rm e}}\right)\right] \tag{C.11}$$

$$+{\rm i}\frac{v_{\rm th,e}}{2}\frac{k_\alpha q' I\chi\overline{\rho}_{\rm th,e}\overline{B}}{\langle \boldsymbol{b}\cdot\nabla\theta\rangle^\theta}\left(\left\langle\frac{\boldsymbol{B}\cdot\nabla\theta}{B^2}\right\rangle^\theta - \frac{\langle\boldsymbol{B}\cdot\nabla\theta\rangle^\theta}{\langle B^2\rangle^\theta}\right)\left(\frac{\delta n_{\rm e}^{(0)}}{n_{\rm e}} + \frac{\delta T_{\rm e}^{(0)}}{T_{\rm e}}\right).$$

Using the same techniques, and the integral (B.19), we obtain the effective electron parallel heat flux

$$\overline{\delta q_{\parallel}} = -\frac{5}{4}\frac{n_{\rm e}T_{\rm e}v_{\rm th,e}^2}{\langle \boldsymbol{b}\cdot\nabla\theta\rangle^\theta}\frac{(\langle\boldsymbol{B}\cdot\nabla\theta\rangle^\theta)^2}{\langle B^2\rangle^\theta} \left[a_1\frac{\partial}{\partial\chi}\left(\frac{\delta n_{\rm e}^{(0)}}{n_{\rm e}}\right) + c_1\frac{\partial}{\partial\chi}\left(\frac{\delta T_{\rm e}^{(0)}}{T_{\rm e}}\right)\right] \tag{C.12}$$

$$+{\rm i}\frac{5}{4}n_{\rm e}T_{\rm e}v_{\rm th,e}\frac{k_\alpha q' I\chi\overline{\rho}_{\rm th,e}\overline{B}}{\langle \boldsymbol{b}\cdot\nabla\theta\rangle^\theta}\left(\left\langle\frac{\boldsymbol{B}\cdot\nabla\theta}{B^2}\right\rangle^\theta - \frac{\langle\boldsymbol{B}\cdot\nabla\theta\rangle^\theta}{\langle B^2\rangle^\theta}\right)\frac{\delta T_{\rm e}^{(0)}}{T_{\rm e}}.$$

We now turn to the calculation of the neoclassical perpendicular diffusion terms appearing in equations (127) and (128). To evaluate the particle flux $\overline{\delta\Gamma}_{\rm N}$, defined in equation (136), we use equations (142) and (144) to show that

$$\overline{\delta\Gamma}_{\rm N} = -\left\langle\frac{I}{\Omega_{\rm e}}\frac{dr}{d\psi}\int v_\parallel^2\boldsymbol{b}\cdot\nabla\theta\frac{\partial}{\partial\theta}\left(H_{\rm e,(-1)}^{(1/2)}\right)\,d^3\boldsymbol{v}\right\rangle^\theta. \tag{C.13}$$

Substituting the solution (143) into equation (C.13), we find that

$$\overline{\delta\Gamma}_{\rm N} = -\frac{n_{\rm e}v_{\rm th,e}^2}{2}\frac{I\overline{B}}{\overline{\Omega}_{\rm e}}\frac{dr}{d\psi}\left\langle\frac{\boldsymbol{B}\cdot\nabla\theta}{B^2}\left(\frac{\partial}{\partial\theta}\left(\frac{\delta n_{\rm e,(-1)}^{(1/2)}}{n_{\rm e}}\right) + \frac{\partial}{\partial\theta}\left(\frac{\delta T_{\rm e,(-1)}^{(1/2)}}{T_{\rm e}}\right)\right)\right\rangle^\theta. \tag{C.14}$$

Finally, we substitute the results (C.7) and (C.8) into equation (C.14), to find the neoclassical particle flux

$$\frac{\overline{\delta\Gamma}_{\rm N}}{n_{\rm e}} = -\frac{v_{\rm th,e}^2}{2}\frac{I\overline{B}}{\overline{\Omega}_{\rm e}}\frac{dr}{d\psi}\left(\frac{\langle\boldsymbol{B}\cdot\nabla\theta\rangle^\theta}{\langle B^2\rangle^\theta} - \left\langle\frac{\boldsymbol{B}\cdot\nabla\theta}{B^2}\right\rangle^\theta\right)\left(\frac{\partial}{\partial\chi}\left(\frac{\delta n_{\rm e}^{(0)}}{n_{\rm e}}\right) + \frac{\partial}{\partial\chi}\left(\frac{\delta T_{\rm e}^{(0)}}{T_{\rm e}}\right)\right) \tag{C.15}$$

$$+{\rm i}k_\alpha\frac{dq}{dr}\chi\frac{v_{\rm th,e}^2}{2}\left(\frac{I\overline{B}}{\overline{\Omega}_{\rm e}}\frac{dr}{d\psi}\right)^2\left(\left\langle\frac{1}{B^2}\right\rangle^\theta - \frac{1}{\langle B^2\rangle^\theta}\right)\left[\frac{a_1-c_1}{a_0c_1-a_1c_0}\frac{\delta n_{\rm e}^{(0)}}{n_{\rm e}} + \frac{a_1+a_0-c_1-c_0}{a_0c_1-a_1c_0}\frac{\delta T_{\rm e}^{(0)}}{T_{\rm e}}\right].$$

Following identical steps, we find that the neoclassical heat flux $\overline{\delta q}_{\rm N}$, defined in equation (137), is

$$\frac{\overline{\delta q}_{\rm N}}{n_{\rm e}T_{\rm e}} = -\frac{5v_{\rm th,e}^2}{4}\frac{I\overline{B}}{\overline{\Omega}_{\rm e}}\frac{dr}{d\psi}\left(\frac{\langle \boldsymbol{B}\cdot\nabla\theta\rangle^\theta}{\langle B^2\rangle^\theta} - \left\langle\frac{\boldsymbol{B}\cdot\nabla\theta}{B^2}\right\rangle^\theta\right)\frac{\partial}{\partial\chi}\left(\frac{\delta T_{\rm e}^{(0)}}{T_{\rm e}}\right) \tag{C.16}$$

$$+{\rm i}k_\alpha\frac{dq}{dr}\chi\frac{v_{\rm th,e}^2}{2}\left(\frac{I\overline{B}}{\overline{\Omega}_{\rm e}}\frac{dr}{d\psi}\right)^2\left(\left\langle\frac{1}{B^2}\right\rangle^\theta - \frac{1}{\langle B^2\rangle^\theta}\right)\left[\frac{(5/2)(a_1+a_0)}{a_0c_1-a_1c_0}\frac{\delta T_{\rm e}^{(0)}}{T_{\rm e}} + \frac{5a_1/2}{a_0c_1-a_1c_0}\frac{\delta n_{\rm e}^{(0)}}{n_{\rm e}}\right].$$

Appendix D. The parallel flows and neoclassical perpendicular diffusion terms in the $\nu_* \ll 1$, $\epsilon \ll 1$ (banana) limit

In this section we calculate the electron distribution function $H_{\rm e,(0)}^{(1/2)}$ by solving equation (160) to leading-order in the expansion in inverse aspect ratio $\epsilon = r/R_0 \ll 1$, where we recall that r is the minor radial coordinate and R_0 is the major radius at the magnetic axis. We take the normalised electron collisionality $\nu_* = qR_0\nu_{\rm ee}/\epsilon^{3/2}v_{\rm th,e} \ll 1$. We assume that the equilibrium can be approximated by circular flux surfaces [25, 35]. Then we can use the fact that the 2π-periodic θ variation in geometric quantities is small by $\mathrm{O}(\epsilon)$. For example, the magnetic field strength

$$B \simeq B_0(1-\epsilon\cos\theta) = B_0 + \mathrm{O}(\epsilon B), \tag{D.1}$$

where $B_0 = I/R_0$ is a constant. As a consequence, the fraction of velocity space occupied by trapped particles become small. This can be seen from the definition of

$$v_\parallel = \sigma\left(\frac{2\varepsilon}{m_{\rm e}}\right)^{1/2}(1-\lambda B(\theta))^{1/2}: \tag{D.2}$$

passing particles occupy $0 \leq \lambda B_0 < B_0/B_{\max} \simeq 1-\epsilon$; and trapped particles occupy $B_0/B_{\max} \leq \lambda B_0 \leq B_0/B(\theta) \simeq 1+\epsilon\cos\theta$. We can identify two regions in the problem: there is a "deeply passing" region where $\lambda B_0 \sim 1 \sim 1-\lambda B_0 \gg \epsilon$, and also the trapped-passing boundary layer where $\lambda B_0 = 1-\mathrm{O}(\epsilon)$. In the deeply passing region, we can find the leading-order solution by taking $\lambda B_0 \sim 1 \sim 1-\lambda B_0$ and using $\epsilon \ll 1$ to approximate the geometric quantities. We find that

$$H_{\rm e,(0)}^{(1/2)} = H_{\rm SH,0} - {\rm i}\lambda_{\rm e}^0\chi H_{\rm e}^{(0)} + \mathrm{O}\left(\epsilon^{1/2}H_{\rm e,(0)}^{(1/2)}\right), \tag{D.3}$$

where

$$\lambda_{\rm e}^0 = \sigma\lambda_{\rm th,e}^0\sqrt{\frac{\varepsilon}{T_{\rm e}}}\sqrt{1-\lambda B_0}, \tag{D.4}$$

with $\lambda_{\rm th,e}^0 = k_\alpha q' I v_{\rm th,e}/\Omega_{\rm e}^0$, $\Omega_{\rm e}^0 = -eB_0/m_{\rm e}c$, and

$$H_{\rm SH,0} = \sigma\sqrt{\frac{\varepsilon}{T_{\rm e}}}\sqrt{1-\lambda B_0}v_{\rm th,e}K_{\rm SH}F_{0e}. \tag{D.5}$$

The $\mathrm{O}\left(\epsilon^{1/2}H_{\rm e,(0)}^{(1/2)}\right)$ correction in equation (D.3) arises from the presence of the trapped-passing boundary layer. To solve for the $\lambda B_0 = 1-\mathrm{O}(\epsilon)$ boundary layer, we note that the pitch-angle scattering components of of the collision operator, $\mathcal{C}_{\lambda\lambda}[\cdot]$ are larger than the other test-particle and field-particle terms by $\mathrm{O}\left(\epsilon^{-1}\right)$. In other words, we need only the pitch-angle scattering collision operator (cf. [25, 27])

$$\mathcal{C}_{\lambda\lambda}[\cdot] = \nu_{\mathrm{e}}(\varepsilon)\frac{\sqrt{1-\lambda B}}{B}\frac{\partial}{\partial\lambda}\left(\lambda\sqrt{1-\lambda B}\frac{\partial}{\partial\lambda}\left[\cdot\right]\right), \tag{D.6}$$

where

$$\nu_{\mathrm{e}}(\varepsilon) = \frac{3\sqrt{\pi}}{2}\left(\frac{T_{\mathrm{e}}}{\varepsilon}\right)^{3/2}\left(\nu_{\mathrm{ei}} + \nu_{\mathrm{ee}}\left(\mathrm{erf}\left(\sqrt{\varepsilon/T_{\mathrm{e}}}\right) - \Psi\left(\sqrt{\varepsilon/T_{\mathrm{e}}}\right)\right)\right), \tag{D.7}$$

with the error function $\mathrm{erf}(z)$ defined by equation (67), and the function $\Psi(z)$ defined by equation (68). We note the similarity of the forms of the collision frequencies ν_{e} and $\nu_{\perp,\mathrm{i}}$, defined in equation (66). This similarity arises because the terms involving these collision frequencies are due to the pitch-angle scattering pieces of the electron and ion collision operators, respectively. With these considerations, to leading-order in ϵ, equation (160) becomes

$$\frac{2}{B_0}\frac{\partial}{\partial\lambda}\left(\lambda\left\langle\sqrt{1-\lambda B(\theta)}\right\rangle^{\theta}\frac{\partial}{\partial\lambda}\left(H^{(1/2)}_{\mathrm{e},(0)}\right)\right)$$
$$+\sigma\sqrt{\frac{\varepsilon}{T_{\mathrm{e}}}}\left(v_{\mathrm{th,e}}K_{\mathrm{SH}}F_{0e} - \mathrm{i}\lambda^0_{\mathrm{th,e}}\chi H^{(0)}_{\mathrm{e}}\right) = 0, \tag{D.8}$$

where we have divided by the ε-dependent collision frequency pre-factors, we have used the identity

$$\mathcal{C}_{\lambda\lambda}[v_{\|}g(\varepsilon)] = -\frac{\nu_{\mathrm{e}}(\varepsilon)}{2}v_{\|}g(\varepsilon) \tag{D.9}$$

to simplify the terms proportional to $v_{\|}$, and we have employed the definitions of the transit average $\langle\cdot\rangle^{\mathrm{t}}$, and poloidal angle average $\langle\cdot\rangle^{\theta}$, equations (74) and (104), respectively, and finally we have expanded the geometrical factors to leading-order in $\epsilon \ll 1$. We note that $\sqrt{1-\lambda B(\theta)}$ may not be usefully expanded in ϵ because $\lambda B_0 = 1 + \mathrm{O}\left(\epsilon\right)$, and the θ dependence of $B(\theta)$ comes in at $\mathrm{O}\left(\epsilon\right)$. We also note that

$$H^{(1/2)}_{\mathrm{e},(0)} \sim \mathrm{O}\left(\epsilon^{1/2}\left(\frac{m_{\mathrm{e}}}{m_{\mathrm{i}}}\right)^{1/4}H^{(0)}_{\mathrm{e}}\right) \tag{D.10}$$

in the boundary layer. We can integrate equation (D.8) directly, with the boundary conditions $H^{(1/2)}_{\mathrm{e},(0)} = 0$ at $\lambda B_0 = B_0/B_{\max}$, and no divergence at $\lambda = 0$. The result is

$$H^{(1/2)}_{\mathrm{e},(0)} = -\sigma\sqrt{\frac{\varepsilon}{T_{\mathrm{e}}}}\left(v_{\mathrm{th,e}}K_{\mathrm{SH}}F_{0e} - \mathrm{i}\lambda^0_{\mathrm{th,e}}\chi H^{(0)}_{\mathrm{e}}\right)\int_{1/B_{\max}}^{\lambda}\frac{B_0 d\lambda/2}{\left\langle\sqrt{1-\lambda B(\theta)}\right\rangle^{\theta}}. \tag{D.11}$$

We can match to the deeply passing solution (D.3) by taking the solution (D.11), and evaluating the integral with $\epsilon \rightarrow 0$ and $1 - \lambda B_0 \gg \mathrm{O}\left(\epsilon\right)$.

Having evaluated the distribution function using the methods of neoclassical theory, we are now able to calculate the electron parallel velocity $\overline{\delta u}_{\|}$ and electron parallel heat flux $\overline{\delta q}_{\|}$, defined in equations (131) and (132), respectively. From the deeply passing solution, equation (D.3), we can see that the leading-order contributions will result from the response $H_{\rm SH,0}$ to the parallel gradients of density and temperature. As in the neoclassical calculation for the bootstrap current [27], we calculate the additional contribution arising from the interaction between passing and trapped electrons in the $\lambda B_0 = 1 - \mathrm{O}(\epsilon)$ boundary layer.

To evaluate the electron parallel velocity and the electron parallel heat flux, we need to compute an integral of the form

$$\Gamma = \frac{1}{\langle \boldsymbol{b}\cdot\nabla\theta\rangle^{\theta}} \left\langle \boldsymbol{b}\cdot\nabla\theta \int v_{\parallel} g(\varepsilon) \left(H^{(1/2)}_{\rm e,(0)} + {\rm i}\lambda_{\rm e}\chi H^{(0)}_{\rm e}\right)\, d^3\boldsymbol{v} \right\rangle^{\theta}, \tag{D.12}$$

where for $g(\varepsilon) = 1$ we obtain $\overline{\delta u}_{\parallel} = \Gamma/n_{\rm e}$, and where for $g = \varepsilon/T_{\rm e} - 5/2$ we obtain $\overline{\delta q}_{\parallel} = T_{\rm e}\Gamma$. First, we use that the result is expected to be close to the Spitzer-Härm flows obtained from $H_{\rm SH}$. We write

$$\Gamma = \Gamma_{\rm SH} + \Gamma_{\rm B}, \tag{D.13}$$

with $\Gamma_{\rm SH}$ defined by

$$\Gamma_{\rm SH} = \frac{1}{\langle \boldsymbol{b}\cdot\nabla\theta\rangle^{\theta}} \left\langle \boldsymbol{b}\cdot\nabla\theta \int v_{\parallel} g(\varepsilon) H_{\rm SH}\, d^3\boldsymbol{v} \right\rangle^{\theta}, \tag{D.14}$$

and

$$\Gamma_{\rm B} = \frac{1}{\langle \boldsymbol{b}\cdot\nabla\theta\rangle^{\theta}} \left\langle \boldsymbol{b}\cdot\nabla\theta \int v_{\parallel} g(\varepsilon) \left(H^{(1/2)}_{\rm e,(0)} - H_{\rm SH} + {\rm i}\lambda_{\rm e}\chi H^{(0)}_{\rm e}\right)\, d^3\boldsymbol{v} \right\rangle^{\theta}. \tag{D.15}$$

We can calculate $\Gamma_{\rm SH}$ using the results of Appendix B. To evaluate the leading nonzero component of $\Gamma_{\rm B}$ requires that we calculate the sub-leading corrections to $H^{(1/2)}_{\rm e,(0)}$ everywhere in λ. To avoid this, we convert the integral (D.15) into an integral where the dominant contribution comes from the trapped-passing boundary, and we can use the solution (D.11). We localise the integral to the trapped-passing boundary by introducing $\mathcal{C}[\cdot]$ into the integral. We do this by using the Spitzer-Härm problem (B.6) to replace $v_{\parallel}$ in equation (D.15), with the result

$$\Gamma_{\rm B} = \frac{1}{\langle \boldsymbol{b}\cdot\nabla\theta\rangle^{\theta}} \left\langle \boldsymbol{b}\cdot\nabla\theta \int g(\varepsilon) \frac{\mathcal{C}\left[v_{\parallel} f_{\rm SH} F_{0e}\right]}{F_{0e}} \left(H^{(1/2)}_{\rm e,(0)} - H_{\rm SH} + {\rm i}\lambda_{\rm e}\chi H^{(0)}_{\rm e}\right)\, d^3\boldsymbol{v} \right\rangle^{\theta}. \tag{D.16}$$

Now using the self-adjointness of $\mathcal{C}[\cdot]$ with respect to the inner product (B.8) [27], the integral becomes

$$\Gamma_{\rm B} = \frac{1}{\langle \boldsymbol{b}\cdot\nabla\theta\rangle^{\theta}} \left\langle \boldsymbol{b}\cdot\nabla\theta \int v_{\parallel} f_{\rm SH}\, \mathcal{C}\left[g(\varepsilon)(H^{(1/2)}_{\rm e,(0)} - H_{\rm SH} + {\rm i}\lambda_{\rm e}\chi H^{(0)}_{\rm e})\right]\, d^3\boldsymbol{v} \right\rangle^{\theta}. \tag{D.17}$$

Finally, we estimate the size of the contributions to $\Gamma_{\rm B}$ from the deeply passing region and the trapped-passing boundary. In the deeply passing region, we find that the contribution is of size

$$\Gamma_{\rm B} \sim \epsilon \left(\frac{m_{\rm e}}{m_{\rm i}}\right)^{1/4} v_{\rm th,e}\delta n^{(0)}_{\rm e}, \tag{D.18}$$

since $\mathcal{C}\left[H^{(1/2)}_{\mathrm{e},(0)} - H_{\mathrm{SH}} + \mathrm{i}\lambda_{\mathrm{e}}\chi H^{(0)}_{\mathrm{e}}\right]$ is small by $\mathrm{O}\left(\epsilon\right)$ in the deeply passing region. In the trapped-passing boundary layer, we find that the contribution is of size

$$\Gamma_{\mathrm{B}} \sim \epsilon^{1/2}\left(\frac{m_{\mathrm{e}}}{m_{\mathrm{i}}}\right)^{1/4} v_{\mathrm{th,e}}\delta n^{(0)}_{\mathrm{e}}, \tag{D.19}$$

since $H^{(1/2)}_{\mathrm{e},(0)} - H_{\mathrm{SH}} + \mathrm{i}\lambda_{\mathrm{e}}\chi H^{(0)}_{\mathrm{e}} \sim \epsilon^{1/2}\left(m_{\mathrm{e}}/m_{\mathrm{i}}\right)^{1/4} H^{(0)}_{\mathrm{e}}$ by the estimates (D.10) and $v_{\|} \sim \epsilon^{1/2} v_{\mathrm{th,e}}$, and $\mathcal{C}_{\lambda\lambda}[\cdot] d^3\boldsymbol{v}/v^3_{\mathrm{th,e}} \sim (\nu_{\mathrm{ei}}/\epsilon)\epsilon^{1/2} \sim \nu_{\mathrm{ei}}\epsilon^{-1/2}$. As the contribution from the trapped-passing boundary layer is larger than the contribution from the deeply passing region, we replace $\mathcal{C}\left[\cdot\right]$ by $\mathcal{C}_{\lambda\lambda}\left[\cdot\right]$ when we evaluate the integral in equation (D.17).

To evaluate the integral in equation, we insert the definition of $\mathcal{C}_{\lambda\lambda}\left[\cdot\right]$, equation (D.6), with $d^3\boldsymbol{v} = (B\varepsilon/m^2_{\mathrm{e}}|v_{\|}|)d\varepsilon d\lambda d\gamma$, and integrate by parts once in λ. The integrals in ε and λ are separable, and we find the intermediate result

$$\Gamma_{\mathrm{B}} = \frac{\pi v^4_{\mathrm{th,e}}}{3} f_{\mathrm{trap}} \int_0^\infty g(\varepsilon)\nu_{\mathrm{e}}(\varepsilon)\left(\frac{\varepsilon}{T_{\mathrm{e}}}\right)^{3/2} f_{\mathrm{SH}}\left(v_{\mathrm{th,e}} K_{\mathrm{SH}} F_{0e} - \mathrm{i}\lambda^0_{\mathrm{th,e}}\chi H^{(0)}_{\mathrm{e}}\right)\frac{d\varepsilon}{T_{\mathrm{e}}}, \tag{D.20}$$

where following [27] we have defined the fraction of trapped particles

$$f_{\mathrm{trap}} = \frac{3B_0^2}{4}\left\langle\left[\int_0^{1/B(\theta)} \frac{\lambda d\lambda}{\sqrt{1-\lambda B(\theta)}} - \int_0^{1/B_{\max}} \frac{\lambda d\lambda}{\left\langle\sqrt{1-\lambda B(\theta)}\right\rangle^\theta}\right]\right\rangle^\theta, \tag{D.21}$$

and taken $\epsilon \to 0$ in the other geometrical quantities appearing in equation (D.20). We note that the λ limits of the integrals in equation (D.21) are determined by the fact that $H^{(1/2)}_{\mathrm{e},(0)}$ is nonzero for passing particles only, whereas $K_{\mathrm{SH}}F_{0e}$ and $H^{(0)}_{\mathrm{e}}$ have both trapped and passing particle components. Standard manipulations can be used to simplify f_{trap} in the limit $\epsilon \to 0$. To leading order [27]

$$f_{\mathrm{trap}} = \frac{3\sqrt{2}}{2}\left[1 - \int_0^1 \left(\frac{\pi}{2E(z)} - 1\right)\frac{dz}{z^2}\right]\epsilon^{1/2} = 1.462\,\epsilon^{1/2}, \tag{D.22}$$

where

$$E(z) = \frac{1}{2}\int_0^\pi \sqrt{1 - z^2\sin^2\left(\frac{\theta}{2}\right)}d\theta \tag{D.23}$$

is the elliptic integral of the second kind. Finally, using the result in equation (D.20), we can calculate the "bootstrap" corrections to the electron parallel velocity and heat flux, $\overline{\delta u}_{\mathrm{B}}$, and $\overline{\delta q}_{\mathrm{B}}$, respectively. We find that

$$\overline{\delta u}_{\mathrm{B}} = v_{\mathrm{th,e}}\frac{f_{\mathrm{trap}}\nu_{\mathrm{ei}}}{2}\left[\frac{v_{\mathrm{th,e}}}{qR_0}\left(\sum_{p,q} a_p D_{p,q} a_q \frac{\partial}{\partial\chi}\left(\frac{\delta n^{(0)}_{\mathrm{e}}}{n_{\mathrm{e}}}\right) + \sum_{p,q} a_p D_{p,q} c_q \frac{\partial}{\partial\chi}\left(\frac{\delta T^{(0)}_{\mathrm{e}}}{T_{\mathrm{e}}}\right)\right)\right.$$
$$\left. -\mathrm{i}\lambda^0_{\mathrm{th,e}}\chi\left(\sum_p a_p D_{p,0}\frac{\delta n^{(0)}_{\mathrm{e}}}{n_{\mathrm{e}}} + \sum_p a_p (D_{p,0} - D_{p,1})\frac{\delta T^{(0)}_{\mathrm{e}}}{T_{\mathrm{e}}}\right)\right], \tag{D.24}$$

with the matrix element

$$D_{p,q} = \int_0^\infty \exp\left[-\hat{x}\right] L^{3/2}_p(\hat{x}) L^{3/2}_q(\hat{x})\hat{\nu}(\hat{x})\,d\hat{x}, \tag{D.25}$$

and the function

$$\hat{\nu}(\hat{x}) = 1 + \mathrm{erf}(\hat{x}^{1/2}) - \Psi(\hat{x}^{1/2}). \tag{D.26}$$

Similarly, we find that

$$\overline{\delta q}_{\mathrm{B}} = v_{\mathrm{th,e}} n_{\mathrm{e}} T_{\mathrm{e}} \frac{f_{\mathrm{trap}} \nu_{\mathrm{ei}}}{2} \left[\frac{v_{\mathrm{th,e}}}{qR_0} \left(\sum_{p,q} a_p Q_{p,q} a_q \frac{\partial}{\partial \chi} \left(\frac{\delta n_{\mathrm{e}}^{(0)}}{n_{\mathrm{e}}} \right) + \sum_{p,q} a_p Q_{p,q} c_q \frac{\partial}{\partial \chi} \left(\frac{\delta T_{\mathrm{e}}^{(0)}}{T_{\mathrm{e}}} \right) \right) \right.$$
$$\left. - \mathrm{i} \lambda_{\mathrm{th,e}}^{0} \chi \left(\sum_{p} a_p Q_{p,0} \frac{\delta n_{\mathrm{e}}^{(0)}}{n_{\mathrm{e}}} + \sum_{p} a_p (Q_{p,0} - Q_{p,1}) \frac{\delta T_{\mathrm{e}}^{(0)}}{T_{\mathrm{e}}} \right) \right], \tag{D.27}$$

with the matrix element

$$Q_{p,q} = \int_0^{\infty} \exp\left[-\hat{x}\right] \left(\hat{x} - \frac{5}{2} \right) L_p^{3/2}(\hat{x}) L_q^{3/2}(\hat{x}) \hat{\nu}(\hat{x}) \, d\hat{x}. \tag{D.28}$$

The numerical coefficients appearing in equations (D.24) and (D.27) may be evaluated by using the $N = 4$ truncated polynomial solution obtained in Appendix B. We use the values of $\{a_p\}$ and $\{c_p\}$ given in equations (B.16) and (B.17), respectively. We compute the matrix elements $D_{p,q}$ and $Q_{p,q}$, with the results (to two decimal places)

$$\boldsymbol{D} = \begin{pmatrix} 1.53 & 2.12 & 2.53 & 2.85 & 3.13 \\ 2.12 & 4.64 & 5.88 & 6.78 & 7.53 \\ 2.53 & 5.88 & 9.25 & 11.15 & 12.61 \\ 2.85 & 6.78 & 11.15 & 15.34 & 17.91 \\ 3.13 & 7.53 & 12.61 & 17.91 & 22.88 \end{pmatrix}, \tag{D.29}$$

and

$$\boldsymbol{Q} = - \begin{pmatrix} 2.12 & 4.64 & 5.88 & 6.78 & 7.53 \\ 4.64 & 7.79 & 13.07 & 15.87 & 17.98 \\ 5.88 & 13.07 & 17.03 & 25.14 & 29.65 \\ 6.78 & 15.87 & 25.14 & 29.80 & 40.79 \\ 7.53 & 17.98 & 29.65 & 40.79 & 46.09 \end{pmatrix}, \tag{D.30}$$

respectively. Combining these results, we find that

$$\overline{\delta u}_{\mathrm{B}} = v_{\mathrm{th,e}} \frac{f_{\mathrm{trap}}}{2} \left[\frac{v_{\mathrm{th,e}}}{qR_0 \nu_{\mathrm{ei}}} \left(2.55 \frac{\partial}{\partial \chi} \left(\frac{\delta n_{\mathrm{e}}^{(0)}}{n_{\mathrm{e}}} \right) + 3.51 \frac{\partial}{\partial \chi} \left(\frac{\delta T_{\mathrm{e}}^{(0)}}{T_{\mathrm{e}}} \right) \right) \right.$$
$$\left. + \mathrm{i} \lambda_{\mathrm{th,e}}^{0} \chi \left(1.66 \frac{\delta n_{\mathrm{e}}^{(0)}}{n_{\mathrm{e}}} + 0.47 \frac{\delta T_{\mathrm{e}}^{(0)}}{T_{\mathrm{e}}} \right) \right], \tag{D.31}$$

and

$$\overline{\delta q}_{\mathrm{B}} = v_{\mathrm{th,e}} n_{\mathrm{e}} T_{\mathrm{e}} \frac{f_{\mathrm{trap}}}{2} \left[\frac{v_{\mathrm{th,e}}}{qR_0 \nu_{\mathrm{ei}}} \left(2.98 \frac{\partial}{\partial \chi} \left(\frac{\delta T_{\mathrm{e}}^{(0)}}{T_{\mathrm{e}}} \right) - 0.07 \frac{\partial}{\partial \chi} \left(\frac{\delta n_{\mathrm{e}}^{(0)}}{n_{\mathrm{e}}} \right) \right) \right.$$
$$\left. - \mathrm{i} \lambda_{\mathrm{th,e}}^{0} \chi \left(1.19 \frac{\delta n_{\mathrm{e}}^{(0)}}{n_{\mathrm{e}}} - 2.63 \frac{\delta T_{\mathrm{e}}^{(0)}}{T_{\mathrm{e}}} \right) \right]. \tag{D.32}$$

Including both the Spitzer-Härm and the bootstrap contributions, the results for the flows are (to $\mathrm{O}\left(\epsilon^{1/2}\right)$)

$$\frac{\overline{\delta u}_{\parallel}}{v_{\mathrm{th,e}}} = \mathrm{i}\frac{q\hat{s}k_y\rho^0_{\mathrm{th,e}}\chi}{2\epsilon^{1/2}}\left(2.43\frac{\delta n_{\mathrm{e}}^{(0)}}{n_{\mathrm{e}}} + 0.69\frac{\delta T_{\mathrm{e}}^{(0)}}{T_{\mathrm{e}}}\right) \tag{D.33}$$

$$-\frac{v_{\mathrm{th,e}}}{2qR_0\nu_{\mathrm{ei}}}\left[1.97\left(1-1.90\epsilon^{1/2}\right)\frac{\partial}{\partial\chi}\left(\frac{\delta n_{\mathrm{e}}^{(0)}}{n_{\mathrm{e}}}\right) + 3.37\left(1-1.52\epsilon^{1/2}\right)\frac{\partial}{\partial\chi}\left(\frac{\delta T_{\mathrm{e}}^{(0)}}{T_{\mathrm{e}}}\right)\right],$$

and

$$\frac{\overline{\delta q}_{\parallel}}{v_{\mathrm{th,e}}n_{\mathrm{e}}T_{\mathrm{e}}} = -\mathrm{i}\frac{5q\hat{s}k_y\rho^0_{\mathrm{th,e}}\chi}{4\epsilon^{1/2}}\left(0.70\frac{\delta n_{\mathrm{e}}^{(0)}}{n_{\mathrm{e}}} - 1.54\frac{\delta T_{\mathrm{e}}^{(0)}}{T_{\mathrm{e}}}\right) \tag{D.34}$$

$$-\frac{5v_{\mathrm{th,e}}}{4qR_0\nu_{\mathrm{ei}}}\left[0.56\left(1+0.07\epsilon^{1/2}\right)\frac{\partial}{\partial\chi}\left(\frac{\delta n_{\mathrm{e}}^{(0)}}{n_{\mathrm{e}}}\right) + 2.23\left(1-0.78\epsilon^{1/2}\right)\frac{\partial}{\partial\chi}\left(\frac{\delta T_{\mathrm{e}}^{(0)}}{T_{\mathrm{e}}}\right)\right],$$

respectively, where we have defined $\rho^0_{\mathrm{th,e}} = v_{\mathrm{th,e}}/\Omega^0_{\mathrm{e}}$, and used that, for $\epsilon \ll 1$ and circular flux surfaces, $f_{\mathrm{trap}} = 1.46\epsilon^{1/2}$, $\hat{\kappa} \simeq 1$, $\boldsymbol{b}\cdot\nabla\theta \simeq 1/qR_0$ and $I dr/d\psi \simeq q/\epsilon$. We note that $\lambda^0_{\mathrm{th,e}} = \hat{s}k_y\rho^0_{\mathrm{th,e}}q/\epsilon$.

Having calculated the parallel flows and fluxes, we now turn to the calculation of the transport due to perpendicular diffusion via the neoclassical fluxes $\overline{\delta\Gamma}_{\mathrm{N}}$ and $\overline{\delta q}_{\mathrm{N}}$, defined in equations (136) and (137). To evaluate these fluxes, we need to compute integrals of the form

$$\Gamma_\perp = -\left\langle \frac{I}{\Omega_{\mathrm{e}}}\frac{dr}{d\psi}\int v_\parallel g(\varepsilon)\mathcal{C}\left[H^{(1/2)}_{\mathrm{e},(0)} + \mathrm{i}\lambda_{\mathrm{e}}\chi H^{(0)}_{\mathrm{e}} - H_{\mathrm{SH}}\right]\, d^3\boldsymbol{v}\right\rangle^{\theta}. \tag{D.35}$$

We note that the form of the integral (D.35) is structurally similar to the integral defined in equation (D.17). To be precise, we can use the estimates (D.18) and (D.19) to justify replacing $\mathcal{C}\left[\cdot\right]$ with $\mathcal{C}_{\lambda\lambda}\left[\cdot\right]$ when evaluating (D.35). Again, since the integrals in ε and λ are separable in (D.35), we find the intermediate result

$$\Gamma_\perp = -\frac{I}{\Omega^0_{\mathrm{e}}}\frac{dr}{d\psi}\frac{\pi v^4_{\mathrm{th,e}}}{3}f_{\mathrm{trap}}\int_0^\infty g(\varepsilon)\nu_{\mathrm{e}}(\varepsilon)\left(\frac{\varepsilon}{T_{\mathrm{e}}}\right)^{3/2}\left(v_{\mathrm{th,e}}K_{\mathrm{SH}}F_{0e} - \mathrm{i}\lambda^0_{\mathrm{th,e}}\chi H^{(0)}_{\mathrm{e}}\right)\frac{d\varepsilon}{T_{\mathrm{e}}}, \tag{D.36}$$

where we note the similarity to (D.20). To compute the neoclassical particle flux, we set $g(\varepsilon) = 1$ in equation (D.36), and obtain the result (correct to $\mathrm{O}\left(\epsilon^{1/2}\right)$)

$$\frac{\overline{\delta\Gamma}_{\mathrm{N}}}{n_{\mathrm{e}}} = -\rho^0_{\mathrm{th,e}}\frac{q}{\epsilon}\frac{f_{\mathrm{trap}}\nu_{\mathrm{ei}}}{2}\left[\frac{v_{\mathrm{th,e}}}{qR_0}\left(\sum_q D_{0,q}a_q\frac{\partial}{\partial\chi}\left(\frac{\delta n_{\mathrm{e}}^{(0)}}{n_{\mathrm{e}}}\right) + \sum_q D_{0,q}c_q\frac{\partial}{\partial\chi}\left(\frac{\delta T_{\mathrm{e}}^{(0)}}{T_{\mathrm{e}}}\right)\right)\right.$$

$$\left. -\mathrm{i}k_y\rho^0_{\mathrm{th,e}}\hat{s}\chi\frac{q}{\epsilon}\left(D_{0,0}\frac{\delta n_{\mathrm{e}}^{(0)}}{n_{\mathrm{e}}} + (D_{0,0}-D_{0,1})\frac{\delta T_{\mathrm{e}}^{(0)}}{T_{\mathrm{e}}}\right)\right].$$

Similarly, to compute the neoclassical heat flux, we set $g(\varepsilon) = \varepsilon/T_{\mathrm{e}} - 5/2$ in equation (D.36), and obtain the result (correct to $\mathrm{O}\left(\epsilon^{1/2}\right)$)

$$\frac{\overline{\delta q}_{\mathrm{N}}}{n_{\mathrm{e}}T_{\mathrm{e}}} = -\rho^0_{\mathrm{th,e}}\frac{q}{\epsilon}\frac{f_{\mathrm{trap}}\nu_{\mathrm{ei}}}{2}\left[\frac{v_{\mathrm{th,e}}}{qR_0}\left(\sum_q Q_{0,q}a_q\frac{\partial}{\partial\chi}\left(\frac{\delta n_{\mathrm{e}}^{(0)}}{n_{\mathrm{e}}}\right) + \sum_q Q_{0,q}c_q\frac{\partial}{\partial\chi}\left(\frac{\delta T_{\mathrm{e}}^{(0)}}{T_{\mathrm{e}}}\right)\right)\right.$$

$$-\mathrm{i}k_y\rho^0_{\mathrm{th,e}}\hat{s}\chi\frac{q}{\epsilon}\left(Q_{0,0}\frac{\delta n_{\mathrm{e}}^{(0)}}{n_{\mathrm{e}}}+\left(Q_{0,0}-Q_{0,1}\right)\frac{\delta T_{\mathrm{e}}^{(0)}}{T_{\mathrm{e}}}\right)\Bigg].$$

Inserting the numerical coefficients, we find that

$$\frac{\overline{\delta\Gamma}_{\mathrm{N}}}{n_{\mathrm{e}}}=\rho^0_{\mathrm{th,e}}\frac{q}{\epsilon}\frac{f_{\mathrm{trap}}}{2}\frac{v_{\mathrm{th,e}}}{qR_0}\left(1.66\frac{\partial}{\partial\chi}\left(\frac{\delta n_{\mathrm{e}}^{(0)}}{n_{\mathrm{e}}}\right)+1.75\frac{\partial}{\partial\chi}\left(\frac{\delta T_{\mathrm{e}}^{(0)}}{T_{\mathrm{e}}}\right)\right)$$
$$+\mathrm{i}\nu_{\mathrm{ei}}k_y\hat{s}\chi(\rho^0_{\mathrm{th,e}})^2\left(\frac{q}{\epsilon}\right)^2\frac{f_{\mathrm{trap}}}{2}\left(1.53\frac{\delta n_{\mathrm{e}}^{(0)}}{n_{\mathrm{e}}}-0.59\frac{\delta T_{\mathrm{e}}^{(0)}}{T_{\mathrm{e}}}\right),$$

and

$$\frac{\overline{\delta q}_{\mathrm{N}}}{n_{\mathrm{e}}T_{\mathrm{e}}}=\rho^0_{\mathrm{th,e}}\frac{q}{\epsilon}\frac{f_{\mathrm{trap}}}{2}\frac{v_{\mathrm{th,e}}}{qR_0}\left(0.11\frac{\partial}{\partial\chi}\left(\frac{\delta T_{\mathrm{e}}^{(0)}}{T_{\mathrm{e}}}\right)-1.19\frac{\partial}{\partial\chi}\left(\frac{\delta n_{\mathrm{e}}^{(0)}}{n_{\mathrm{e}}}\right)\right)$$
$$+\mathrm{i}\nu_{\mathrm{ei}}k_y\hat{s}\chi(\rho^0_{\mathrm{th,e}})^2\left(\frac{q}{\epsilon}\right)^2\frac{f_{\mathrm{trap}}}{2}\left(2.51\frac{\delta T_{\mathrm{e}}^{(0)}}{T_{\mathrm{e}}}-2.12\frac{\delta n_{\mathrm{e}}^{(0)}}{n_{\mathrm{e}}}\right).$$

Appendix E. A detailed analysis of the ion response for large θ

In this appendix, we give a more detailed analysis of the nonadiabatic ion response at large ballooning θ. This discussion will illustrate in more detail how the hyperbolic ion gyrokinetic equation, equation (3) with $s = \mathrm{i}$, reduces to the local algebraic equations (64) and (96) in the electron-dominated tail of the ballooning mode.

We begin this analysis by noting that, for large θ, the leading-order ion gyrokinetic equation has the form

$$\sigma\frac{\partial h_{\mathrm{i}}}{\partial\theta}+P(\theta)h_{\mathrm{i}}=S(\theta), \tag{E.1}$$

where we have emphasised the θ dependence of the source

$$S=\mathrm{i}\left(\omega_{*,\mathrm{i}}-\omega\right)J_{0\mathrm{i}}F_{0i}\frac{Z_{\mathrm{i}}e\phi}{T_{\mathrm{i}}}, \tag{E.2}$$

and the factor $P \gg 1$. We argue, in section 4.2.1, that in the collisionless limit

$$P=\frac{1}{|v_\|||\boldsymbol{b}\cdot\nabla\theta}\left(\frac{k_\alpha^2q'^2|\nabla\psi|^2\theta^2v^2}{4\Omega_{\mathrm{i}}^2}\left(\nu_{\|,\mathrm{i}}\lambda B+\frac{\nu_{\perp,\mathrm{i}}}{2}\left(2-\lambda B\right)\right)-\mathrm{i}k_\alpha q'\theta\boldsymbol{v}_{\mathrm{M,i}}\cdot\nabla\psi\right), \tag{E.3}$$

whereas, in section 5.1.1, we argue that in the collisional limit

$$P=\frac{k_\alpha^2q'^2|\nabla\psi|^2\theta^2v^2}{4\Omega_{\mathrm{i}}^2|v_\||\boldsymbol{b}\cdot\nabla\theta}\left(\nu_{\|,\mathrm{i}}\lambda B+\frac{\nu_{\perp,\mathrm{i}}}{2}\left(2-\lambda B\right)\right), \tag{E.4}$$

i.e., we can neglect the term due to the radial magnetic drift. In solving for the ion response, we have no need to distinguish between θ and χ – this distinction is only a requirement for solving for the electron response. For simplicity, in the subsequent algebra we drop the usage of χ. In writing equation (E.1), we have neglected the differential terms of the ion gyrokinetic collision operator, and the terms due to the time derivative of h_{i}, and the precessional magnetic drift. These terms can be neglected because $\theta \gg 1$, $k_y \rho_{\rm th,i} \sim 1$ and $\omega \sim v_{\rm th,i}/a$, and hence the leading terms are large, i.e., $P \gg 1$. Note that the real part of P is positive, i.e., $\Re\left[P\right] > 0$.

We consider the solution of equation (E.1) for $\theta > 0$. Integrating equation (E.1) directly, we find that, for forward going particles ($\sigma = 1$),

$$h_{\rm i} = \int_0^\theta S(\theta'') \exp\left[-\int_{\theta''}^{\theta} P(\theta')d\theta'\right] d\theta'' + h_{\rm i}(\theta = 0, \sigma = 1) \exp\left[-\int_0^\theta P(\theta')d\theta'\right]. \quad \text{(E.5)}$$

For backward-going particles ($\sigma = -1$), we find that

$$h_{\rm i} = \int_\theta^\infty S(\theta'') \exp\left[-\int_\theta^{\theta''} P(\theta')d\theta'\right] d\theta'', \quad \text{(E.6)}$$

where we have used $h_{\rm i}(\theta = \infty, \sigma = -1) = 0$ as a boundary condition. Inspecting the solutions (E.5) and (E.6), we note that there are two components: a "local" solution involving S, and an exponentially decaying solution (proportional to $h_{\rm i}(\theta = 0, \sigma = 1)$) due to the outgoing particles from $\theta = 0$. The exponentially decaying part of the solution gives rise to the logarithmic boundary layer referred to in section 5.2.2. In this discussion, we can neglect the exponentially decaying part of the ion response, because the electron tail at large θ generates its own potential that drives the ions via the "local" response.

We now consider the form of the local solution when $P \gg 1$ and $\Re[P] > 0$, and the integrals can be treated using the standard Laplace method [55]. We treat the case of $\sigma = 1$ explicitly. First, we note that the dominant contributions to the integrals in equation (E.5) come from where $\theta \simeq \theta''$. In this region, we write

$$\exp\left[-\int_{\theta''}^{\theta} P(\theta')d\theta'\right] = \exp\left[-P(\theta)(\theta - \theta'')\right] \left(1 + \mathrm{O}\left(\frac{1}{P}\frac{\partial P}{\partial \theta}(\theta - \theta'')\right)\right), \quad \text{(E.7)}$$

which is accurate provided that $(\theta - \theta'')/\theta \ll 1$. We introduce a parameter δ, so that we can write

$$h_{\rm i} = I_0 + I_\delta \quad \text{(E.8)}$$

with

$$I_0 = \int_{\theta-\delta}^{\theta} S(\theta'') \exp\left[-\int_{\theta''}^{\theta} P(\theta')d\theta'\right] d\theta'', \quad \text{(E.9)}$$

and

$$I_\delta = \int_0^{\theta-\delta} S(\theta'') \exp\left[-\int_{\theta''}^{\theta} P(\theta')d\theta'\right] d\theta''. \quad \text{(E.10)}$$

We can use the appoximation (E.7) in I_0 provided $\delta/\theta \ll 1$. Using (E.7), the leading contribution to I_0 is given by

$$I_0 = \int_{\theta-\delta}^{\theta} S(\theta) \exp\left[-P(\theta)(\theta - \theta'')\right] d\theta''. \quad \text{(E.11)}$$

Evaluating the integral, we find that

$$I_0 = \frac{S(\theta)}{P(\theta)} \left(1 - \exp\left[-P(\theta)\delta\right]\right). \quad \text{(E.12)}$$

Taking δ such that $\Re[P]\delta \gg 1$ (consistent with $\delta/\theta \ll 1$), we find that, to leading order,

$$h_{\rm i} = \frac{S(\theta)}{P(\theta)}, \tag{E.13}$$

where we have used the smallness of $\exp\left[-P(\theta)\delta\right]$ to neglect I_δ. An analogous calculation can be performed for $\sigma = -1$, with the result that $h_{\rm i}$ satisfies (E.13) for both signs of the velocity. The result (E.13) is identical in form to equations (64) and (96). We have demonstrated that, although the ion gyrokinetic equation is hyperbolic, the fact that $P \gg 1$ means that parallel streaming is unable to effectively propagate information at large θ, and hence, the nonadiabatic response of ions is local in ballooning angle.

References

[1] Dorland W, Jenko F, Kotschenreuther M and Rogers B N 2000 *Phys. Rev. Lett.* **85** 5579–5582

[2] Jenko F, Dorland W, Kotschenreuther M and Rogers B N 2000 *Physics of Plasmas* **7** 1904–1910

[3] Jenko F and Dorland W 2002 *Phys. Rev. Lett.* **89** 225001

[4] Roach C M, Abel I G, Akers R J, Arter W, Barnes M, Camenen Y, Casson F J, Colyer G, Connor J W, Cowley S C, Dickinson D, Dorland W, Field A R, Guttenfelder W, Hammett G W, Hastie R J, Highcock E, Loureiro N F, Peeters A G, Reshko M, Saarelma S, Schekochihin A A, Valovic M and Wilson H R 2009 *Plasma Physics and Controlled Fusion* **51** 124020

[5] Maeyama S, Idomura Y, Watanabe T H, Nakata M, Yagi M, Miyato N, Ishizawa A and Nunami M 2015 *Physical review letters* **114** 255002

[6] Maeyama S, Watanabe T H, Idomura Y, Nakata M, Ishizawa A and Nunami M 2017 *Nuclear Fusion* **57** 066036

[7] Howard N T, Holland C, White A E, Greenwald M and Candy J 2014 *Physics of Plasmas* **21** 112510

[8] Howard N T, Holland C, White A E, Greenwald M and Candy J 2016 *Nuclear Fusion* **56** 014004

[9] Howard N T, Holland C, White A E, Greenwald M, Candy J and Creely A J 2016 *Physics of Plasmas* **23** 056109

[10] Maeyama S, Watanabe T H and Ishizawa A 2017 *Phys. Rev. Lett.* **119** 195002

[11] Bonanomi N, Mantica P, Citrin J, Goerler T and and B T 2018 *Nuclear Fusion* **58** 124003

[12] Hallatschek K and Dorland W 2005 *Phys. Rev. Lett.* **95** 055002

[13] Dominski J, Brunner S, Görler T, Jenko F, Told D and Villard L 2015 *Physics of Plasmas* **22** 062303

[14] Connor J W, Hastie R J and Taylor J B 1979 *Proceedings of the Royal Society of London. A. Mathematical and Physical Sciences* **365** 1–17

[15] Parisi J F, Parra F I, Roach C M, Giroud C, Dorland W, Hatch D R, Barnes M, Hillesheim J C, Aiba N, Ball J, Ivanov P G and contributors J 2020 *Nuclear Fusion* **60** 126045

[16] Applegate D J, Roach C M, Connor J W, Cowley S C, Dorland W, Hastie R J and Joiner N 2007 *Plasma Physics and Controlled Fusion* **49** 1113–1128

[17] Dickinson D, Roach C M, Saarelma S, Scannell R, Kirk A and Wilson H R 2013 *Plasma Physics and Controlled Fusion* **55** 074006

[18] Moradi S, Pusztai I, Guttenfelder W, Fülöp T and Mollén A 2013 *Nuclear Fusion* **53** 063025

[19] Cowley S C, Kulsrud R M and Sudan R 1991 *Phys. Fluids B* **3** 2767

[20] Romanelli F 1989 *Physics of Fluids B: Plasma Physics* **1** 1018–1025

[21] Adam J C, Tang W M and Rutherford P H 1976 *The Physics of Fluids* **19** 561–566

[22] Beer M A and Hammett G W 1996 *Physics of Plasmas* **3** 4018–4022

[23] Kotschenreuther M, Rewoldt G and Tang W 1995 *Computer Physics Communications* **88** 128 – 140

[24] Catto P J 1978 *Plasma Phys.* **20** 719

[25] Hazeltine R D and Meiss J D 2003 *Plasma Confinement* (New York: Dover)

[26] Braginskii S I 1957 *J. Exptl. Theoret. Phys. (U.S.S.R.)* **33** 459–472

[27] Helander P and Sigmar D J 2002 *Collisional transport in magnetized plasmas* (Cambridge: Cambridge University Press)

[28] Hardman M R, Barnes M, Roach C M and Parra F I 2019 *Plasma Physics and Controlled Fusion* **61** 065025

[29] Abel I G and Cowley S C 2013 *New Journal of Physics* **15** 023041

[30] Catto P J and Tsang K T 1977 *The Physics of Fluids* **20** 396–401

[31] Abel I G, Barnes M, Cowley S C, Dorland W, Hammett G W and Schekochihin A A 2008 *Phys. Plasmas* **15** 122509 arXiv:0806.1069

[32] Barnes M, Abel I G, Dorland W, Ernst D R, Hammett G W, Ricci P, Rogers B N, Schekochihin A A and Tatsuno T 2009 *Phys. Plasmas* **16** 072107

[33] Hinton F L and Hazeltine R D 1976 *Rev. Mod. Phys.* **25** 239–308

[34] Spitzer L and Härm R 1953 *Phys. Rev.* **89** 977–981

[35] Freidberg J 2014 *Ideal MHD* (Cambridge: Cambridge University Press)

[36] Dimits A M, Bateman G, Beer M A, Cohen B I, Dorland W, Hammett G W, Kim C, Kinsey J E, Kotschenreuther M, Kritz A H, Lao L L, Mandrekas J, Nevins W M, Parker S E, Redd A J, Shumaker D E, Sydora R and Weiland J 2000 *Physics of Plasmas* **7** 969–983

[37] Miller R L, Chu M S, Greene J M, Lin-Liu Y R and Waltz R E 1998 *Physics of Plasmas* **5** 973–978

[38] Barnes M, Dorland W and Tatsuno T 2010 *Phys. Plasmas* **17** 032106

[39] CJ A, Brunner S, McMillan B, Ball J, Dominski J and Merlo G 2020 *Journal of Plasma Physics* **86** 905860504

[40] CJ A, Ball J and Brunner S 2020 *arXiv:2104.12585*

[41] Patel B 2021 Ph.D. thesis University of York

[42] Belli E A, Candy J and Waltz R E 2019 *Phys. Plasmas* **26** 082305

[43] Belli E A, Candy J and Waltz R E 2020 *Phys. Rev. Lett.* **125** 015001

[44] Waltz R E, Austin M E, Burrell K H and Candy J 2006 *Physics of Plasmas* **13** 052301

[45] Ball J, Brunner S and CJ A 2020 *Journal of Plasma Physics* **86** 905860207

[46] Parisi J F, Parra F I, Roach C M, Hardman M R, Barnes M, Dorland W, St-Onge D, Ball J, Hatch D R, Dickinson D, Abel I G, Saarelma S, Chapman B, Giroud C, Hillesheim J C, Aiba N and JET Contributors 2021 *In preparation*

[47] Hardman M R, Barnes M and Roach C M 2020 *J. Plasma Phys.* **86** 905860601

[48] Hall L S and McNamara B 1975 *The Physics of Fluids* **18** 552–565

[49] Cary J R and Shasharina S G 1997 *Phys. Rev. Lett.* **78** 674–677

[50] Cary J R and Shasharina S G 1997 *Physics of Plasmas* **4** 3323–3333

[51] Helander P 2014 *Reports on Progress in Physics* **77** 087001

[52] Parra F I, Calvo I, Helander P and Landreman M 2015 *Nuclear Fusion* **55** 033005

[53] Calvo I, Parra F I, Velasco J L and Alonso J A 2017 *Plasma Physics and Controlled Fusion* **59** 055014

[54] Newton S L, Cowley S C and Loureiro N F 2010 *Plasma Physics and Controlled Fusion* **52** 125001

[55] Bender C M and Orszag S A 1999 *Advanced Mathematical Methods for Scientists and Engineers I: Asymptotic Methods and Perturbation Theory.* (New York: Springer)